



Slovak Biophysical Society

Department of Biophysics and

Center for Interdisciplinary Biosciences

Faculty of Science, P. J. Šafárik University in Košice



Book of Contributions

7th Slovak Biophysical Symposium

April 6 – 8, 2016

Nový Smokovec, Slovakia

Book of Contributions, 7th Slovak Biophysical Symposium, April 6-8, 2016, Nový Smokovec, Slovakia

Editors: D. Jancura, G. Fabriciová
Reviewers: M. Fabian, A. Musatov

© Department of Biophysics, Institute of Physics, Faculty of Science, P. J. Šafárik University in Košice

ISBN: 978-80-972284-0-8
EAN: 9788097228408

ORGANIZATION

SCIENTIFIC COMMITTEE

Ján Jakuš (JLF UK Martin)
Daniel Jancura (PF UPJŠ Košice)
Tibor Hianik (FMFI UK Bratislava)
Pavol Miškovský (PF UPJŠ Košice)
Alexandra Zahradníková (UMFG SAV Bratislava)

ORGANIZING COMMITTEE

from Department of Biophysics and Center for Interdisciplinary Biosciences, P. J. Šafárik University in Košice

Daniel Jancura
Gabriela Fabriciová
Zuzana Jurašeková
Zuzana Naďová
Mária Stehlíková
Zuzana Paulíny

CONFERENCE VENUE

Hotel Atrium, Nový Smokovec 42, High Tatras, Slovakia

REVIEWERS

M. Fabian
A. Musatov

EDITORS

D. Jancura
G. Fabriciová

ACKNOWLEDGEMENTS

The Organizing Committee of the 7th Slovak Biophysical Symposium would like to express appreciations and thanks to the following companies for their generous support.



We make it visible.



CONTENTS

Program	8
List of plenary lectures	11
List of short communications	12
List of posters	14
Plenary lectures	19
Short communications	27
Posters	55
Author index	97
List of participants	101





SCIENTIFIC PROGRAM



PROGRAM

WEDNESDAY, April 6, 2016

12:00 – 14:00 **Registration**

14:00 – 14:10 **Opening ceremony**

14:10 – 16:00 **Session I**

Chair: J. Jakuš

14:10 – 15:00

PL1 A. Faltinová, J. Sevčík, **A. Zahradníková:**
Interaction of the RyR2 channel with its domain peptide

15:00 – 15:20

SC1 **J. Gaburjaková**, M. Gaburjaková:
Luminal regulation of cardiac ryanodine receptor by alkaline earth metal cations

15:20 – 15:40

SC2 **M. Gaburjaková**, J. Gaburjaková:
Cardiac ryanodine receptor: Looking for luminal Ca²⁺ binding sites

15:40 – 16:00

SC3 **E. Urbániková**
Structural research of beta-D-glucosidase from *Zea mays*

16:00 – 16:30 **Poster section – Coffee break**

16:30 – 17:30 **Meeting of Slovak BioImaging section**

THURSDAY, April 7, 2016

9:00 – 10:30 **Session II**

Chair: A. Zahradníková

9:00 – 9:50

PL2 **K. Štroffeková**, V. Huntošová, L. Koptašíková, M. Novotova, Z. Nichtová, T. Kožár:
Dark hypericin effects in cells depend on cell metabolism

9:50 – 10:10

SC4 **M. Klacsová**, D. Uhríková, P. Balgavý, J.C. Martínez, Ch. Kamma-Lorger:
Hexosomal and cubosomal CnOH+DOPE+DOPC liquid crystals as potential drug delivery system



10:10 – 10:30

SC5 **A. Poturnayova**, M. Snejdarkova, L. Babelova, M. Burikova, I. Karpisova, J. Bizik, A. Ebner, M. Leitner, T. Hianik:
Detection of the cancer markers at Jurkat cells using DNA aptamers

10:30 – 10:50 **Coffee break**

10:50 – 11:50 **Session III.**

Chair: M. Gaburjaková

10:50 – 11:10

SC6 **M. Fabian**, K. Kopčová:
Reaction of cyanide inhibited cytochrome oxidase with oxygen

11:10 – 11:30

SC7 **M. Grman**, M. M. Cortese-Krott, M. Feelisch, P. Nagy, A. Berényiová, S. Čačányiová, K. Ondriaš:
Interaction of hydrogen sulfide with S-nitrosothiols – from chemistry to biological effects of products

11:30 – 11:50

SC8 M. Karmažínová, K. Ondáčová, E. Perez-Reyes, **Ľ. Lacinová**:
Activation of a single voltage sensor of the T-type calcium channel may be sufficient for pore opening

12:00 – 14:00 **Lunch Break**

14:00 – 15:40 **Session IV**

Chair: K. Štroffeková

14:00 – 14:20

SC9 M. Hořka, A. Zahradníková, Jr., **I. Zahradník**:
Age Dependent Capacitive Membrane Activity in Rat Cardiac Myocytes

14:20 – 14:40

SC10 **B. Hoffmannová**, E. Poláková, A. Zahradníková, I. Zahradník, A. Zahradníková Jr.:
Inactivation of calcium current by local calcium release events

14:40 – 15:00

SC11 **K. Macková**, M. Hořka, A. Zahradníková, I. Zahradník, A. Zahradníková Jr.:
Postnatal development of calcium signalling in rat ventricular cardiomyocytes

15:00 15:20

SC12 **B. Čunderlíková**, A. Mateašík:
Fluorescence bioimaging in native 3D cell cultures

15:20 – 15:40

SC13 **J. Mísek**, D. Spiguthova, H. Habinakova, M. Veternik, M. Kohan, O. Osina, J. Jakus:
Heart rate variability during short-term exposure in teenage students



15:40 – 16:00 **Poster section – Coffee break**

16:00 – 17:00 **Winners of the SKBS prizes**

Chair: P. Miškovský

16:00 – 16:20

M. Fabian

Biophysics without borders

16:20 – 17:00

PL3 V. Huntošová

Drug delivery systems and oxygen detection in photodynamic therapy and photo-diagnostics

17:30 – 18:30 **General Assembly of the Slovak Biophysical Society**

18:45 **Conference dinner**

FRIDAY, April 8, 2016

9:00 – 10:50 **Session V**

Chair: D. Jancura

9:30 – 10:10

PL4 J. Uličný:

Toward an understanding of cell DNA structure – from modeling to X-ray imaging experiments

10:10 – 10:30

SC14 J. Uličný, T. Kožár:

All-atoms versus „coarse-grained“ approaches for biomacromolecular and nanoparticle modeling

10:30 – 10:50

SC15 S. Hrivňak, L. Mikeš, J. Uličný, P. Vagovič:

Reconstruction of diffractograms in X-ray imaging of biological objects using Bragg Magnifier Microscope

10:50 **Concluding remarks**



LIST OF PLENARY LECTURES

PL1 Interaction of the RyR2 channel with its domain peptide

A. FALTINOVÁ¹, J. SEVČÍK², A. ZAHRADNÍKOVÁ¹

¹ *Institute of Molecular Physiology and Genetics, Slovak Academy of Sciences, Bratislava, Slovakia*

² *Institute of Molecular Biology, Slovak Academy of Sciences, Bratislava, Slovakia*

PL2 Dark hypericin effects in cells depend on cell metabolism.

K. ŠTROFFEKOVÁ¹, V. HUNTOŠOVÁ³, L. KOPTAŠÍKOVÁ¹, M. NOVOTOVA², Z. NICHTOVÁ², T. KOŽÁR³

¹ *Department of Biophysics, Faculty of Natural Sciences, P. J. Šafárik University in Košice, Košice, Slovakia*

² *Department of Muscle Cell Research, Institute of Molecular Physiology and Genetics, Slovak Academy of Sciences, Bratislava, Slovakia*

³ *Center for Interdisciplinary Biosciences, P. J. Šafárik University in Košice, Slovakia*

PL3 Drug delivery systems and oxygen detection in photodynamic therapy and photo-diagnostics

V. HUNTOSOVA

Center for Interdisciplinary Biosciences, Faculty of Science, P. J. Šafárik University in Košice, Košice, Slovakia

PL4 Toward an understanding of cell DNA structure – from modeling to X-ray imaging experiments

J. ULIČNÝ^{1,2}

¹ *Department of Biophysics, Institute of Physics, P. J. Šafárik University in Košice, Košice, Slovakia*

² *Center for Interdisciplinary Biosciences, P. J. Šafárik University in Košice, Košice, Slovakia*



LIST OF SHORT COMMUNICATIONS

SC1 Luminal regulation of cardiac ryanodine receptor by alkaline earth metal cations

J. GABURJÁKOVÁ, M. GABURJÁKOVÁ

Institute of Molecular Physiology and Genetics, Slovak Academy of Sciences, Bratislava, Slovakia

SC2 Cardiac ryanodine receptor: Looking for luminal Ca²⁺ binding sites

M. GABURJÁKOVÁ, J. GABURJÁKOVÁ

Institute of Molecular Physiology and Genetics, Slovak Academy of Sciences, Bratislava, Slovakia

SC3 Structural research of beta-D-glucosidase from *Zea mays*

Ľ. URBÁNIKOVÁ

Institute of Molecular Biology, Slovak Academy of Sciences, Bratislava, Slovak Republic

SC4 Hexosomal and cubosomal CnOH+DOPE+DOPC liquid crystals as potential drug delivery systems

M. KLACSOVÁ¹, D. UHRÍKOVÁ¹, P. BALGAVÝ¹, J. C. MARTÍNEZ², CH. KAMMA-LORGER²

¹ *Department of Physical Chemistry of Drugs, Faculty of Pharmacy, Comenius University in Bratislava, Bratislava, Slovakia*

² *BL-11 NCD beamline, ALBA Synchrotron, Cerdanyola del Vallès, Barcelona, Spain*

SC5 Detection of the cancer markers at Jurkat cells using DNA aptamers

A. POTURNAYOVA^{1,2}, M. SNEJDARKOVA¹, L. BABELOVA¹, M. BURIKOVA¹,
I. KARPISOVA², J. BIZIK³, A. EBNER⁴, M. LEITNER⁵, T. HIANIK²

¹ *Institute of Animal Biochemistry and Genetics, Slovak Academy of Sciences, Ivanka pri Dunaji, Slovakia*

² *Department of Nuclear Physics and Biophysics, FMFI UK, Bratislava, Slovakia*

³ *Institute of Experimental Oncology of the Slovak Academy of Science, Bratislava, Slovakia*

⁴ *Institute of Biophysics, Johannes Kepler University Linz, Linz, Austria*

⁵ *Center for Advanced Bioanalysis GmbH, Linz, Austria*

SC6 Reaction of cyanide inhibited cytochrome oxidase with oxygen

K. KOPCOVA¹, M. FABIAN²

¹ *Department of Biophysics, Faculty of Science, Safarik University in Kosice, Kosice, Slovakia*

² *Center for Interdisciplinary Biosciences, Faculty of Science, Safarik University in Kosice, Kosice, Slovakia*

SC7 Interaction of hydrogen sulfide with S-nitrosothiols – from chemistry to biological effects of products

M. GRMAN^{1,2}, M. M. CORTESE-KROTT³, M. FEELISCH⁴, P. NAGY⁵, A. BERÉNYIOVÁ⁶,
S. ČAČANYIOVÁ⁶, K. ONDRIAS^{1,2}

¹ *Institute of Clinical and Translational Research, Biomedical Research Center, Slovak Academy of Sciences, Bratislava, Slovakia*

² *Institute of Molecular Physiology and Genetics, Bratislava, Slovak Republic*

³ *Medical Faculty, Heinrich Heine University of Düsseldorf, Düsseldorf, Germany*

⁴ *Faculty of Medicine, University of Southampton, Southampton General Hospital and Institute for Life Sciences, Southampton, United Kingdom*

⁵ *National Institute of Oncology, Budapest, Hungary*

⁶ *Institute of Normal and Pathological Physiology, Bratislava, Slovakia*



SC8 Activation of a single voltage sensor of the T-type calcium channel may be sufficient for pore opening.

M. KARMAŽINOVÁ¹, K. ONDÁČOVÁ¹, E. PEREZ-REYES², L. LACINOVÁ¹

¹ *Institute of Molecular Physiology and Genetics, Slovak Academy of Sciences, Bratislava, Slovakia*

² *Department of Pharmacology, University of Virginia, Charlottesville, USA*

SC9 Age Dependent Capacitive Membrane Activity in Rat Cardiac Myocytes

M. HOŤKA, A. ZAHRADNÍKOVÁ, JR., I. ZAHRADNÍK

Department of Muscle Cell Research, Institute of Molecular Physiology and Genetics, Slovak Academy of Sciences, Bratislava, Slovak Republic

SC10 Inactivation of calcium current by local calcium release events

B. HOFFMANNOVÁ¹, E. POLÁKOVÁ², A. ZAHRADNÍKOVÁ², I. ZAHRADNÍK², A. ZAHRADNÍKOVÁ JR.²

¹ *Faculty of Mathematics, Physics and Informatics, Comenius University, Bratislava, Slovakia*

² *Institute of Molecular Physiology and Genetics, Slovak Academy of Sciences, Bratislava, Slovakia*

SC11 Postnatal development of calcium signalling in rat ventricular cardiomyocytes

K. MACKOVÁ, M. HOŤKA, A. ZAHRADNÍKOVÁ, I. ZAHRADNÍK, A. ZAHRADNÍKOVÁ JR.

Institute of Molecular Physiology and Genetics, Slovak Academy of Sciences, Bratislava, Slovakia

SC12 Fluorescence bioimaging in native 3D cell cultures

B. ČUNDERLÍKOVÁ^{1,2}, A. MATEAŠÍK¹

¹ *International Laser Centre, Bratislava, Slovakia*

² *Institute of Medical Physics, Biophysics, Informatics and Telemedicine, Faculty of Medicine, Comenius University, Bratislava, Slovakia*

SC13 Heart rate variability during short-term exposure in teenage students

J. MISEK¹, D. SPIGUTHOVA¹, H. HABINAKOVA¹, M. VETERNIK¹, M. KOHAN¹, O. OSINA², J. JAKUS¹

¹ *Department of Medical Biophysics, Jessenius Faculty of Medicine in Martin, Comenius University, Martin, Slovakia*

² *Clinic of Occupational Medicine and Toxicology, Jessenius Faculty of Medicine in Martin, Comenius University, Martin, Slovakia*

SC14 All-atoms versus „coarse-grained“ approaches for biomacromolecular and nanoparticle modeling

J. ULICNY¹, T. KOZAR²

¹ *Department of Biophysics, P. J. Šafárik University in Košice, Košice, Slovakia*

² *Centrum for Interdisciplinary Biosciences, P. J. Šafárik University in Košice, Košice, Slovakia*

SC15 Reconstruction of diffractograms in X-ray imaging of biological objects using Bragg Magnifier Microscope

S. HRIVŇAK¹, L. MIKEŠ², J. ULIČNÝ¹, P. VAGOVIČ^{3,4}

¹ *Department of Biophysics, Faculty of Science, P. J. Šafárik University in Košice, Košice, Slovakia*

² *Department of Computer Science, Faculty of Science, P. J. Šafárik University in Košice, Košice, Slovakia*

³ *Center for Free Electron Laser Science, DESY, Hamburg, Germany*

⁴ *European XFEL, Hamburg, Germany*

LIST OF POSTERS

- PO1 Catalytic properties of trypsin and chymotrypsin in the presence of salts**
E. DUŠEKOVÁ¹, K. GARAJOVÁ², R. YAVASER³, A. KAŇUKOVÁ², S. HAMADEJOVÁ², E. SEDLÁK^{2,4}
¹ Department of Biophysics, P. J. Šafárik University in Košice, Košice, Slovakia
² Department of Biochemistry, P. J. Šafárik University in Košice, Košice, Slovakia
³ Department of Chemistry, Adnan Menderes University, Aydin, Turkey
⁴ Centre for Interdisciplinary Biosciences, P. J. Šafárik University in Košice, Košice, Slovakia
- PO2 On a quest to finding the most effective method for glucose oxidase deflavination**
K. GARAJOVÁ¹, E. DUŠEKOVÁ², E. SEDLÁK^{1,3}
¹ Department of Biochemistry, P. J. Šafárik University in Košice, Moyzesova 11, 040 01 Košice, Slovakia
² Department of Biophysics, P. J. Šafárik University in Košice, Jesenná 5, 040 01 Košice, Slovakia
³ Centre for Interdisciplinary Biosciences, P. J. Šafárik University in Košice, Jesenná 5, 040 01 Košice, Slovakia
- PO3 Correlation between perturbation of heme region and peroxidase-like activity of cytochrome c**
N. TOMÁŠKOVÁ¹, R. VARHAČ¹, K. GARAJOVÁ¹, E. SEDLÁK^{1,2}
¹ Department of Biochemistry, Faculty of Sciences, P. J. Šafárik University in Košice, Košice, Slovakia
² Centre for interdisciplinary biosciences, Faculty of Sciences, P. J. Šafárik University in Košice, Košice, Slovakia
- PO4 Targeted mutagenesis of the gene KCNJ2 for the potassium channel Kir 2.1**
M. PETREŇČÁKOVÁ
Department of Biochemistry, Faculty of Sciences, P. J. Šafárik University in Košice, Košice, Slovakia
Institute of molecular biology and biotechnology, Faculty of Pharmaceutics, VFU Brno
- PO5 Kinetics of the interaction between intrinsically disordered protein tau and antibody Fab fragment against its C-terminus**
O. CEHLÁR^{1,2}, M. JANUBOVÁ², R. ŠKRABANA^{1,2}, M. NOVÁK^{1,2}
¹ Institute of Neuroimmunology, Slovak Academy of Sciences, Bratislava, Slovakia
² Axon Neuroscience SE, Bratislava, Slovakia
- PO6 Influenza haemagglutinin fusion peptide: a story of three aminoacids that matter**
A. FILIPEK, J. KRUPA, R. WORCH
Institute of Physics Polish Academy of Science, Warsaw, Poland
- PO7 The shape of mitochondria and its changes during oxidative stress**
L. LENKAŤSKÁ¹, A. FRAGOLA², F. SURREAU³, P. MISKOVSKÝ^{4,5}, S. BONNEAU³, Z. NADOVA^{1,4}
¹ Department of Biophysics, P. J. Šafárik University in Košice, Košice, Slovakia
² Laboratoire Physique et d'Etude de Matériaux, Université Pierre et Marie Curie, Paris, France
³ Laboratoire Jean Perrin, Université Pierre et Marie Curie, Paris, France
⁴ Center for Interdisciplinary Biosciences, P. J. Šafárik University in Košice, Košice, Slovakia
⁵ SAFTRA Photonics, Košice, Slovakia



PO8 Activation and relocalization of Protein kinase C- α and Protein kinase C- δ in U-87MG glioma cells after hypericin treatment

M. MISUTH¹, Z. NADOVA^{1,2}, P. MISKOVSKY^{1,2}, V. HUNTOSOVA^{1,2}

¹ Department of Biophysics, Faculty of Science, P. J. Safarik University in Kosice, Kosice, Slovakia

² Center for Interdisciplinary Biosciences, Faculty of Science, P. J. Safarik University in Kosice, Kosice, Slovakia

PO9 Singlet Oxygen Photosensitized by Hypericin in Dimethyl-Sulfoxide

J. VARCHOLA, K. ŽELONKOVÁ, D. JANCURA, P. MIŠKOVSKÝ, G. BÁNÓ

Department of Biophysics, P. J. Šafárik University in Košice, Košice, Slovakia

PO10 Nuclear targeting via selective photo-activation and by regulation of P-glycoprotein

V. VEREBOVÁ¹, D. BELEJ², J. JONIOVÁ², Z. JURAŠEKOVÁ^{2,3}, P. MIŠKOVSKÝ^{2,3}, T. KOŽÁR³, D. HORVÁTH³, J. STANIČOVÁ^{1,4}, V. HUNTOŠOVÁ³

¹ Institute of Biophysics, University of Veterinary Medicine and Pharmacy, Košice, Slovakia

² Department of Biophysics, Faculty of Science, P. J. Šafárik University in Košice, Košice, Slovakia

³ Center for Interdisciplinary Biosciences, Faculty of Science, P. J. Šafárik University in Košice, Košice, Slovakia

⁴ Institute of Biophysics and Informatics, First Faculty of Medicine, Charles University in Prague, Prague, Czech Republic

PO11 In vitro regeneration system of selected *Hypericum* species

Z. DIČÁKOVÁ^{1,2}, E. ČELLÁROVÁ²

¹ Department of Biophysics, P. J. Šafárik University in Košice, Košice, Slovakia

² Department of Genetics, P. J. Šafárik University in Košice, Košice, Slovakia

PO12 Study of the NIR light induced effects on neuroblastoma N2A cells with Parkinson's-like feature

L. KOPTASIKOVA¹, V. HUNTOSOVA^{2,3}, E. GERELLI³, G. WAGNIERES³, K. STROFFEKOVA¹

¹ Department of Biophysics, P. J. Safarik University in Kosice, Kosice, Slovakia

² Center for Interdisciplinary Biosciences, P. J. Safarik University in Kosice, Kosice, Slovakia

³ Laboratory of Organometallic and Medical Chemistry, ISIC, EPFL, Lausanne, Switzerland

PO13 Ability of nanoparticles coated with different types of dextran to inhibit amyloid aggregation of lysozyme

Z. BEDNARIKOVA^{1,2}, E. DEMJEN², S. DUTZ³, M. M. MOCANU⁴, K. ULICNA^{1,5}, P. KOPČANSKÝ², Z. GAZOVA^{2,6}

¹ Department of Biochemistry, Faculty of Sciences, P. J. Šafárik University in Košice, Košice, Slovakia

² Department of Biophysics, Institute of Experimental Physics, Slovak Academy of Sciences, Košice, Slovakia

³ Institute of Biomedical Engineering and Informatics, Technische Universität Ilmenau, Ilmenau, Germany

⁴ Department of Biophysics, "Carol Davila" University of Medicine and Pharmacy, Bucharest, Romania

⁵ Institute of Biology and Ecology, Faculty of Science, Safarik University in Kosice, Kosice, Slovakia

⁶ Department of Medical and Clinical Biochemistry, Faculty of Medicine, Safarik University in Kosice, Kosice, Slovakia



PO14 Destabilization and fibrillization of proteins in ionic liquids – anion vs. cation role

D. FEDUNOVÁ¹, Z. BEDNÁRIKOVÁ^{1,2}, E. DEMJÉN¹, J. MAREK¹, D. SEDLÁKOVÁ¹,
Z. GAŽOVÁ¹

¹ *Institute of Experimental Physics, Slovak Academy of Sciences, Košice, Slovakia*

² *Department of Biochemistry, Institute of Chemistry, Faculty of Science, Košice, Slovakia*

PO15 Lysozyme amyloid species and their influence on neural cell viability

E. BYSTRENOVA¹, Z. BEDNARIKOVA^{2,3}, M. BARBALINARDO¹, C. ALBONETTI¹,
F. VALLE¹, Z. GAZOVA^{2,4}

¹ *C.N.R. - I.S.M.N., Bologna, Italy*

² *Department of Biophysics, Institute of Experimental Physics Slovak Academy of Sciences, Košice, Slovakia.*

³ *Department of Biochemistry, Faculty of Sciences, P. J. Šafárik University in Košice, Košice, Slovakia*

⁴ *Department of Medical and Clinical Biochemistry, Faculty of Medicine, Safarik University in Košice, Kosice, Slovakia*

PO16 Structure-activity relationship of acridine derivates to amyloid aggregation of A β peptide

J. KUBACKOVÁ¹, K. ULIČNÁ^{1,2}, Z. BEDNÁRIKOVÁ^{1,3}, Z. GAŽOVÁ^{1,4}

¹ *Department of Biophysics, Institute of Experimental Physics, Slovak Academy of Sciences, Kosice, Slovakia*

² *Institute of Biology and Ecology, Faculty of Science, P. J. Safarik University in Kosice, Kosice, Slovakia*

³ *Department of Biochemistry, Faculty of Science, P. J. Safarik University in Kosice, Kosice, Slovakia*

⁴ *Department of Medical and Clinical Biochemistry, Faculty of Medicine, P. J. Safarik University in Kosice, Kosice, Slovakia*

PO17 Fragments from human lysozyme affect lysozyme amyloid fibrillization

K. ULICNA^{1,2}, Z. BEDNARIKOVA^{1,3}, A. BHUNIA⁴, Z. GAZOVA^{1,5}

¹ *Department of Biophysics, Institute of Experimental Physics, Slovak Academy of Sciences, Kosice, Slovakia*

² *Institute of Biology and Ecology, Faculty of Science, Safarik University in Kosice, Kosice, Slovakia*

³ *Department of Biochemistry, Institute of Chemistry, Faculty of Science, Safarik University in Kosice, Kosice, Slovakia*

⁴ *Department of Biophysics, Bose Institute, Kolkata, India*

⁵ *Department of Medical and Clinical Biochemistry Faculty of Medicine, Safarik University in Kosice, Slovakia*

PO18 Study of the thermal unfolding of human serum albumin

M. NEMERGUT¹, E. SEDLÁK², D. BELEJ¹ AND D. JANCURA¹

¹ *Department of Biophysics, P. J. Šafárik University in Košice, Košice, Slovakia*

² *Center for Interdisciplinary Biosciences, P. J. Šafárik University in Košice, Košice, Slovakia*

PO19 Kinetic Monte-Carlo simulation of hypericin aggregation in bilayer lipid membranes

M. REBIČ¹, J. JONIOVÁ¹, A. STREJČKOVÁ², V. HUNTOSOVA³, J. STANIČOVÁ²,
D. JANCURA^{1,3}, P. MISKOVSKY^{1,3}, G. BÁNÓ^{1,3}

¹ *Department of Biophysics, P. J. Šafárik University in Košice, Košice, Slovakia*

² *Department of Chemistry, Biochemistry and Biophysics, University of Veterinary Medicine and Pharmacy, Košice, Slovakia*

³ *Center for Interdisciplinary Biosciences, P. J. Šafárik University in Košice, Košice, Slovakia*



PO20 Transfer of lipophilic molecules into water solutions of the natural surfactant saponin

L. BLASCAKOVA¹, A. FILIPEK¹, K. KOPCOVA¹, D. JANCURA^{1,2}, M. FABIAN²

¹ Department of Biophysics, Faculty of Science, Šafárik University in Kosice, Kosice;

² Center for Interdisciplinary Biosciences, Faculty of Science, Šafárik University in Kosice, Kosice

PO21 Aptamer conjugation of polymer based nanoparticles – a possible strategy for cancer treatment

Z. GARAIÓVÁ¹, Y. MØRCH², C. DE LANGE DAVIES³, T. HIANIK¹

¹ Department of Nuclear Physics and Biophysics, Faculty of Mathematics, Physics and Informatics, Comenius University, Bratislava, Slovakia

² Department of Biotechnology and Nanomedicine, SINTEF Materials and Chemistry, Trondheim, Norway

³ Department of Physics, Norwegian University of Science and Technology, Trondheim, Norway

PO22 Polymeric nanoparticles as potential drug carriers for cancer treatment – a cytotoxicity study.

V. SUBJAKOVA¹, Y. MØRCH², Z. GARAIÓVÁ¹, C. DE LANGE DAVIES³, T. HIANIK¹

¹ Department of Nuclear Physics and Biophysics, Faculty of Mathematics, Physics and Informatics, Comenius University, Bratislava, Slovakia

² Department of Biotechnology and Nanomedicine, SINTEF Materials and Chemistry, Trondheim, Norway

³ Department of Physics, Norwegian University of Science and Technology, Trondheim, Norway

PO23 Complex formation between photosensitizer hypericin and high-density lipoproteins (HDL)

A. JUTKOVA¹, Ľ. BLAŠČÁKOVÁ¹, D. JANCURA¹, P. MIŠKOVSKÝ^{1,2}, J. KRONEK³

¹ Department of Biophysics, P. J. Šafárik University in Košice, Košice, Slovakia

² International Laser Center, Ilkovičova 3, 841 04 Bratislava 4, Slovakia

³ Polymer Institute of the Slovak Academy of Sciences, Bratislava, Slovakia

PO24 Anionic liposomes in gene therapy

G. LISKAYOVÁ, L. HUBČÍK, A. BÚCSI, D. UHRÍKOVÁ

Faculty of Pharmacy, Comenius University in Bratislava, Bratislava, Slovakia

PO25 Formation of ABTS radical cation in the presence of silver nanoparticles as revealed by UV-visible and Raman spectroscopy

Z. JURAŠEKOVÁ^{1,2}, A. GARCÍA-LEIS³, S. SÁNCHEZ-CORTÉS³, D. JANCURA^{1,2}

¹ Department of Biophysics, P. J. Šafárik University, Košice, Slovakia

² Center for Interdisciplinary Biosciences, P. J. Šafárik University, Košice

³ Instituto de Estructura de la Materia, Madrid, Spain

PO26 Development of biosensor for detection proteases activity by means of thickness shear mode transducer with immobilized casein

A. POTURNAYOVA^{1,2}, M. TATARKO¹, I. KARPISOVA¹, G. CASTILLO¹, Z. KERESZTES³, T. HIANIK¹

¹ Faculty of Mathematics, Physics and Informatics, Comenius University in Bratislava, Bratislava, Slovakia

² Institute of Animal Biochemistry and Genetics, Slovak Academy of Sciences, Ivanka pri Dunaji, Slovakia

³ Research Centre for Natural Sciences, Hungarian Academy of Sciences, Budapest, Hungary





PLENARY LECTURES

Interaction of the RyR2 channel with its domain peptide

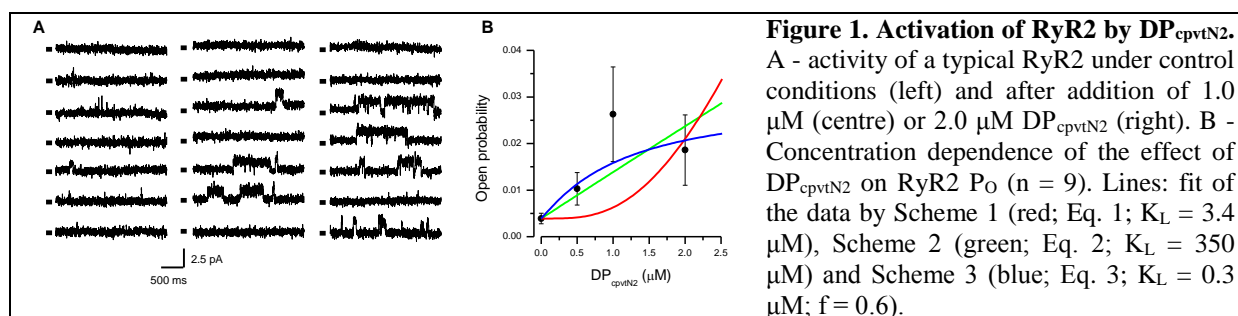
A. FALTINOVÁ¹, J. SEVČÍK², AND A. ZAHRADNÍKOVÁ¹

¹ Institute of Molecular Physiology and Genetics, Slovak Academy of Sciences, Dúbravská cesta 9, 840 05 Bratislava, Slovakia

² Institute of Molecular Biology, Slovak Academy of Sciences, Dúbravská cesta 21, 845 51 Bratislava, Slovakia
e-mail: alexandra.zahradnikova@savba.sk

Cardiac ryanodine receptor (RyR2) is a calcium release channel containing several domains where arrhythmogenic mutations tend to be clustered. One of them, the N-terminal domain [2], contains a central helix, important for structural stability, in which five amino acids are prone to such mutations [3]. Therefore it has been proposed that in RyR channels the N-terminal region allosterically regulates channel activity by interacting with the central part of the protein. It is assumed that the domains participate in intramolecular interactions regulating the stability of the resting (closed) state of the RyR2; that mutations cause defects in these interactions; and that peptides from mutation-prone regions compete in these interactions mimicking the situation caused by arrhythmogenic mutations [1]. The aim of this study was to test the effect of the peptide DP_{cpvtN2}, corresponding to the central helix of the N-terminal domain of human RyR2 (amino acids 410-438), on single channel activity of RyR2.

Activity of single RyR2 channels from rat myocardium was monitored in planar lipid bilayers [4]. Addition of DP_{cpvtN2} induced long openings within a minute (Figure 1A). Open probabilities varied strongly within one channel (Figure 1A) and among individual RyR2 channels (Figure 1B), which precluded unambiguous determination of DP_{cpvtN2} binding affinity to RyR2.



We compared the observed open probabilities with the calcium dependence of three gating schemes: In Scheme 1, long channel openings correspond to periods of peptide binding. Binding of one peptide molecule to the ryanodine receptor tetramer is sufficient for channel opening. The equilibrium open probability P_O is then defined as

$$P_O = P_{O0} + (P_{Omax} - P_{O0}) c_L^4 / (c_L + K_L)^4, \quad (\text{Eq. 1})$$

where P_{O0} is open probability in the absence of the ligand, c_L is ligand concentration, and K_L is ligand dissociation constant.

Scheme 2 differs from Scheme 1 by requiring all four binding sites of the tetramer to be occupied in the open state. The equilibrium open probability P_O is then defined as

$$P_O = P_{O0} + (1 - P_{O0}) c_L (c_L + 2K_L) (c_L^2 + 2c_L K_L + 2K_L^2) / (c_L + K_L)^4. \quad (\text{Eq. 2})$$

In Scheme 3, the peptide increases RyR2 open probability allosterically, as previously observed for the peptide DP_{cpvtC} [4]. That is, when the peptide is bound to the channel, the free energy necessary for channel opening is decreased. In this scheme, the concentration dependence of open probability (P_O) is described by the equation

$$P_O = (c_L + f_L K_L)^4 / ((c_L + f_L K_L)^4 + f_L^4 (c_L + K_L)^4 (1/P_{O0} - 1)), \quad (\text{Eq. 3})$$

where f_L is the allosteric factor coupling ligand binding to channel opening.

Both Scheme 2 and Scheme 3 but not Scheme 1 provided acceptable description of experimental data (Figure 1B). To determine, which of Schemes 2 and 3 is more plausible, we modelled complex formation of the peptide with the N-terminal region of RyR2 with the *GRAMM-X* public web server [5]. The resulting molecular models were further energy-optimized [6]. The resulting three plausible models of the complex are shown in Figure 2. In all three cases the peptide binds to the N-terminal domain at the top face of the RyR2 and its binding does not interfere with the remainder of the RyR2 molecule. The energies of the studied molecules after energy minimization are compared in Table 1.

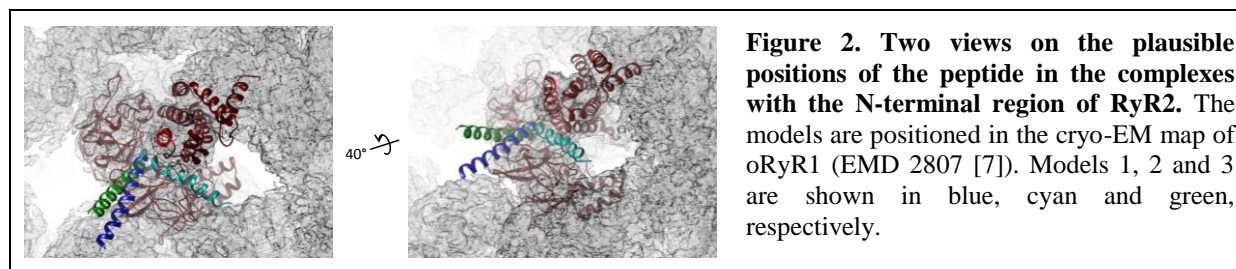


Table 1. Energies of the studied molecules and their complexes

Compound	Energy (kJ/mol)				
	free hRyR2 ¹⁻⁶⁰⁶	DP _{cpvtN2}	Model 1	Model 2	Model 3
Closed state	-51180	-4000	-54860	-57710	-54790
Open state	-49600	-4000	-55450	-56850	-56490
$\Delta\Delta G_{\text{binding}}^{\text{closed}}$			320	-2530	380
$\Delta\Delta G_{\text{binding}}^{\text{open}}$			-1850	-3250	-2890
$\Delta\Delta G_{\text{opening}}$	+1580		-590	+860	-1690

The transition from the closed to the open conformation of the isolated N-terminal region is energetically highly unfavourable. In Model 1 and Model 3, formation of the complex is energetically unfavourable in the closed state but favourable in the open state of hRyR2¹⁻⁶⁰⁶, and opening of the ligand-bound hRyR2¹⁻⁶⁰⁶ is energetically favourable. This is consistent with the gating model depicted in Schemes 1 and 2. In contrast, in Model 2 the energy of complex formation is highly favourable in both, open and closed states of hRyR2¹⁻⁶⁰⁶, while the opening of both ligand-free and ligand-bound hRyR2¹⁻⁶⁰⁶ is energetically unfavourable, consistent with the gating model depicted in Scheme 3. These data show that complex formation between DP_{cpvtN2} and hRyR2¹⁻⁶⁰⁶ is energetically plausible; Model 2, consistent with Scheme 3, is energetically the most favourable.

Acknowledgement

This work was supported by research grants from the Agency for Support of Research and Development (APVV-0628-10 and APVV-0721-10) and from the Slovak Grant Agency (VEGA 2/0148/14).

References

- [1] L Borko, V Bauerova-Hlinkova, E Hostinova *et al.*, *Acta Cryst*, D70 (2014) 2897–2912.
- [2] <http://triad.fsm.it/cardmoc/>
- [3] N Ikemoto, T Yamamoto, *Front Biosci* 7 (2002) d671-683.
- [4] A Faltinova, A Zahradnikova, *Centr Eur J Biol* 8 (2013) 1164-1171.
- [5] A Tovchigrechko, IA Vakser, *Nucleic Acids Res* 34 (2006) W310-314.
- [6] K Hinsén, *J Comput Chem* 21 (2000) 79-85.
- [7] Z Yan, XC Bai, C Yan *et al.*, 2015 #77

Dark hypericin effects in cells depend on cell metabolism

KATARÍNA ŠTROFFEKOVÁ¹, VERONIKA HUNTOŠOVÁ³, LENKA KOPTAŠÍKOVÁ¹, MARTA NOVOTOVÁ², ZUZANA NICHTOVÁ², AND TIBOR KOŽÁR³

¹ Department of Biophysics, Faculty of Natural Sciences, PJ Safarik University, Jesenna 5, Kosice, Slovakia

² Department of Muscle Cell Research, Institute of Molecular Physiology and Genetics, Slovak Academy of Science, Bratislava, Slovakia

³ Center for Interdisciplinary Biosciences, PJ Safarik University in Kosice, Slovakia
e-mail: katarina.stroffekova@upjs.sk

Photosensitizers (PSs) in photodynamic therapy (PDT) are administered systemically with preferential accumulation in malignant cells; however, exposure of non-malignant cells to PS may be clinically relevant if PS molecules affect the pro-apoptotic cascade without illumination. The important PS characteristic is low dark cytotoxicity. Originally, Hypericin (Hyp) as PS displayed minimal dark cytotoxicity and preferential accumulation in tumor cells [1], however recently, evidence to contrary appeared [2]. The molecular mechanisms underlying Hyp dark toxicity are not understood in detail. They may be due to its interaction with different molecules at the Hyp accumulation sites including mitochondria, ER and Golgi apparatus. Our previous work demonstrated that in human glioma U87 MG [3] and human coronary artery endothelial HCAEC cells [4], presence of Hyp in the dark resulted in translocation of anti-apoptotic Bcl2 and pro-apoptotic Bax, from Bcl2 family of proteins that are key regulators of apoptosis and mitogenesis. To understand the mechanisms underlying Hyp dark toxicity better, we investigated the Hyp in the dark effect on mitochondrial function and cell metabolism, and on cell ultrastructure in U87 MG and HCAEC cells. We have found that Hyp in HCAEC resulted in significant dark cytotoxicity in contrast to U87 MG cells, which could be due to different locations of Bcl2 and Bax after Hyp treatment in these cells. In both cell types, Hyp in the dark triggered morphological changes in mitochondria, the endoplasmic reticulum (ER) and Golgi apparatus (GA). The treatment with Hyp in the dark led to mild swelling of mitochondria and cisterns of GA, and to decreased incidence of ribosomes at the ER surface. In addition, changes in size and shape of mitochondria in HCAEC cells indicated altered mitogenesis. All ultrastructure effects indicate a possibility of altered protein synthesis. Hyp in the dark significantly affected mitochondria function in U87 MG), but it did not have the same effect in HCAEC. In U87 MG cells, which have high participation of oxidative phosphorylation (OXPHOS) in cell metabolism, Hyp turn mitochondria to the more quiescent state (less oxidative phosphorylation and less glycolysis). In HCAEC cells with glycolysis as prevailing metabolism type, Hyp did not have an effect. At the same time, Hyp in the dark resulted in slight hyperpolarization of mitochondrial potential ΔY_m in both cell types. All our findings so far indicate that outcomes of Hyp treatment strongly depend on cell metabolism and proliferation rate. Lastly, we investigated further our hypothesis that Hyp affected the distribution of Bcl2 and Bax proteins via hydrophobic interaction at their BH1-BH3 domains. We have tested the interactions between BH1 and BH3 domain peptides, respectively, and either Bcl2 inhibitor ABT 263 or Hyp. We performed fluorescence measurements of Tryptophan (BH1 domain) and Tyrosin (BH3 domain) *in vitro* in PBS and DMSO, respectively. In addition, we have used the Schrodinger suite of programs [5] to compute the docking poses of ABT-263 and Hyp into the BH3-BH1 domains of Bcl-2 (PDB code 4IEH). The calculated binding preferences between BH domains peptides and either ABT 263 or Hyp are in a good agreement with the fluorescence interaction experiments. Our results strongly suggest that Hyp affects the distribution of Bcl2 and Bax proteins via hydrophobic interaction at their BH1-BH3 domains.

In conclusion, all our results indicates that Hyp in the dark affects cells at the several levels: organelle ultrastructure and function, protein synthesis and distribution. The Hyp impact depends on cell metabolism and proliferation. Hyp acts similar to other small mitochondria targeting molecules (mitocans) [6], and therefore Hyp can be explored as mitocan.

Acknowledgement: This work was supported by EU 7FP PIRG06-GA-2009-256580, CELIM 316310; EU SF ITMS 26240120040; VEGA -1-0111-12, VEGA 1-0425-15 and VEGA 2-0110-15, APVV-0134-11 and APVV-0242-11

References

- [1] Almeida et al. *Biochimica Et Biophysica Acta-Reviews on Cancer* 2004, **1704**(2): 59-86.
- [2] Gyenge et al *Photochemistry and Photobiology* 2013, **89**(1): 150-162.
- [3] Balogová et al (2013) *Gen. Physiol. Biophys.* 32: 179–187.
- [4] Štroffeková et al (2014) *Biophys. J.* 106_Issue 2, 187A.
- [5] Schrödinger Release 2013-3. 2013, Schrödinger, LLC: New York, NY.
- [6] Biasutto et al. *Mitochondrion* 2010, **10**(6): 670-681.

Drug delivery systems and oxygen detection in photodynamic therapy and photo-diagnostics

V. HUNTOSOVA

Center for Interdisciplinary Biosciences, Faculty of Science, P. J. Safarik University in Kosice, Jesenna 5, 041 54 Kosice, Slovakia

e-mail: veronika.huntosova@upjs.sk

Photodynamic therapy (PDT) is a modern treatment modality for cancerous and several non-cancerous diseases, which employs photosensitive drugs (photosensitizers), oxygen and light together. The main advantage of such approach is selective destruction of treated (cancerous) area. This selectivity is partially achieved by controlled photosensitive drug delivery to non-healthy (cancer) cells. Intravenously injected photosensitive drugs are transported in the blood stream and demonstrate promiscuous leak into extra-vascular space both healthy and diseased tissues. Due to detoxification processes and drugs redistribution between serum proteins in the blood stream, the effective drug dose received by cancer tissues is often only fraction of the administered doses. In our studies we developed new possibility how to overcome these problems by construction (native) lipid-based transport system that is covered by protection layer [1, 2]. Such transport system loaded with a photosensitive drug can be targeted to cancer cells, where PDT is consequently applied. By understanding of the mechanism of cell death induced by PDT one can identify intracellular targets [3, 4, 5]. The major role of cell destruction in PDT plays singlet oxygen and other reactive oxygen species [6, 7, 8]. For the purpose to precisely define PDT dosimetry (drug/light doses), it is very important to detect level of oxygen in treated tissues before and during PDT [9]. Furthermore, measuring oxygen partial pressure provides valuable information for the early diagnosis of various conditions associated with changes in tissue metabolism. The luminescence lifetime measurement of oxygen-sensitive molecules is a very promising, non-invasive approach to determine oxygen partial pressure *in vivo* and can be performed shortly before PDT [10, 11]. A water soluble dichlorotris(1,10-phenanthroline)-ruthenium(II)hydrate ($[\text{Ru}(\text{Phen})_3]^{2+}$) is a sensor of molecular oxygen presenting a minimal phototoxicity. We have demonstrated that $[\text{Ru}(\text{Phen})_3]^{2+}$ luminescence lifetime in various microenvironments present linear Stern-volmer oxygen dependences. Reliable and easy oxygen partial pressure prediction was illustrated not only in the intra/extravascular space of chicken chorioallantoic membrane model (CAM), but also in CAM tumors with this approach [10].

Acknowledgement

This work was funded by the EU 7FP grant CELIM 316310, by the Slovak Research and Development Agency VEGA 1-0425-15 and by the Swiss National Science Foundation, Project: CR32I3_159746.

References

- [1] V. Huntosova, L. Alvarez, L. Bryndzova et al., *Int.J Pharm*, 389 (2010) 32
- [2] V. Huntosova, D. Buzova, D. Petrovajova et al., *Int J Pharm*, 436 (2012) 463
- [3] S. Kascakova, Z. Nadova, A. Mateasik et al., *Photochem Photobiol*, 84 (2008) 120
- [4] V. Huntosova, Z. Nadova, L. Dzurova et al., *Photochem Photobiol Sci*, 11 (2012) 1428
- [5] L. Dzurova, D. Petrovajova, Z. Nadova et al., *Photodiagn Photodyn*, 11 (2014) 213
- [6] P. Gbur, R. Dedic, D. Chorvat Jr. et al., *Photochem Photobiol*, 85 (2009) 816
- [7] D. Petrovajova, D. Jancura, P. Miskovsky et al., *Laser Phys Letter*, 10 (2013) 075609
- [8] J. Varchola, V. Huntosova, D. Jancura et al., *Photochem Photobiol Sci*, 13 (2014) 1781
- [9] F. Piffaretti, A.M. Novello, R.S. Kumar et al., *J Biomed Opt*, 17 (2012) 115007
- [10] V. Huntosova, S. Gay, P. Nowak-Sliwinska et al., *J Biomed Opt*, 19 (2014) 077004
- [11] V. Huntosova, K. Stroffekova, G. Wagnieres et al., *Metallomics*, 6 (2014) 2279

Toward an understanding of cell DNA structure – from modeling to X-ray imaging experiments

J. ULIČNÝ^{1,2}

¹ Department of Biophysics, Institute of Physics, P. J. Šafárik University, Jesenná 5, 041 54 Košice, Slovakia

² Center for Interdisciplinary Biosciences, P. J. Šafárik University, Jesenná 5, 041 54 Košice, Slovakia
e-mail: jozef.ulicny@upjs.sk

In June 2017, the first „friendly users“ will have an access to breakthrough X-ray (bio)imaging modality at European XFEL, 1250+ million EUR project, considered by many to be a flagship European Research Infrastructure. In my talk I will summarise our long term project to take advantage of the XFEL for direct cell DNA imaging and provide an actual information about the experimental progress and opportunities (but also limitations) of diffract-before-destroy X-ray bioimaging for Slovak bioimaging community. Slovak scientists can benefit not only from the Slovak Republic being one of the shareholders of XFEL, but also due to our participation in SFX and XBI user consortia at XFEL have an early adopter advantage of this exciting technology.

The ultimate bioimaging experiment aims at atomistic resolution imaging of living matter at native physiological conditions. While conventional imaging methods face Rose criterium [1] limiting severely the achievable resolution due to unavoidable damage caused by image-forming interaction of photons (or electrons) with matter, diffract-before-destroy experiments, allow – at least in principle - subnanometer resolution limited by our ability to spend whole coherent X-ray photon budget within first few femtoseconds. For actual experiments feasible at Single Particles and Biomolecules (SPB) and Serial Femtosecond Crystallography (SFX) experimental stations, nanocrystals, single small but reproducible bioparticles and large (up to 3 μm) nonrepeatable particles can be displayed and its shape reconstructed from diffract-before-destroy pattern [2].



- near field diffractogram of model organism Echiniscus (tardigrada) obtained by synchrotron microtomography
- Single U87MG cell prepared for hard X-ray ptychography and tomography imaging experiment and contrasted using functionalised gold nanoparticles
- Full space diffractogram of human quadruplex DNA motif evaluated from our coarse-grain representation

Our scientific interest is in developing methodology for direct imaging of cell DNA approaching native conditions, due to suspected role of 3D DNA architecture at mesoscopic scale on cell programming and encoding of epigenomic information [4,5]. Due to limitations in current technical possibilities (even for XFEL record parameters) we are focusing on following areas – development of coarse grain modeling schemes suitable for data processing

of mesoscale DNA structures [3], start-to-end simulations of diffraction experiments at SPB/SFX stations, development of new imaging techniques based on differential phase-contrast principles and cell-state specific contrasting technologies using functionalised nanoparticles with suitable bioimaging properties. While the primary experimental target is XFEL diffract-before-destroy experiment, tests can be (and are) done on variety of available X-ray sources (synchrotrons and free-electron lasers) and our results can be utilised also in less demanding and elusive experimental setups. Contrasting techniques and data processing methods we are developing are also of practical interest for biomedical imaging using X-ray and gamma-ray, such as computational tomography and SPECT.

Acknowledgement

The research leading to these results has received funding from the European Community's Seventh Framework Programme FP7-REGPOT-2012-2013-1 call - Proposal 316310 - CELIM, (FP7/2007-2013) under grant agreement n.°312284 (CALIPSO), ASFEU - SR program ITMS 26110230088 (SOFOS), ASFEU - SR ITMS 26220220182 (TECHNIKOM), ASFEU - SR ITMS 26110230084 (KVARK).

References

- [1] M.R. Howells, T. Beetz, H.N. Chapman, C. Cui, J.M. Holton, C.J. Jacobsen, J. Kirz, et al. *J. Electron Spectr.* 170, 4 (2009)
- [2] XFEL.EU TR-2013-004, doi:10.3204/XFEL.EU/TR-2013-004
- [3] M.Rebič, F. Mocci, A. Laaksonen, and J. Uličný. *J. Phys. Chem. B*, 2014. doi:10.1021/jp5103274.
- [4] Lieberman-Aiden, Erez, Nynke L. van Berkum, Louise Williams, Maxim Imakaev, Tobias Ragoczy, Agnes Telling, Ido Amit, et al. *Science* 326, no. 5950 (2009) 289–93.
- [5] Rao, Suhas S. P., Miriam H. Huntley, Neva C. Durand, Elena K. Stamenova, Ivan D. Bochkov, James T. Robinson, Adrian L. Sanborn, et al. *Cell* 159, no. 7 (2014): 1665–80.



SHORT COMMUNICATIONS

Luminal regulation of cardiac ryanodine receptor by alkaline earth metal cations

J. GABURJÁKOVÁ, AND M. GABURJÁKOVÁ

Institute of Molecular Physiology and Genetics, Slovak Academy of Sciences, Health Sciences Pavilion, Dúbravská cesta 9, 840 05 Bratislava, Slovakia
e-mail: jana.gaburjakova@savba.sk

Contraction event in cardiomyocytes is tightly coupled with the transient elevation of cytosolic Ca^{2+} that activates the muscle contractile apparatus. Ca^{2+} ions are mobilized from the intracellular store (the sarcoplasmic reticulum, SR) through the cardiac ryanodine receptor (RYR2). The main regulatory part of the RYR2 channel is a gigantic cytosolic domain that comprises well-characterized Ca^{2+} activation/inhibition sites. A much smaller pore-forming region embedded in the SR membrane holds not intensively characterized Ca^{2+} binding sites that are accessible from the RYR2 luminal face and are involved into the luminal regulation. Importantly, the luminal dysregulation of the RYR2 channel has been linked to several cardiac disease states, including familial catecholaminergic polymorphic ventricular tachycardia (CPVT) [1]. It is commonly believed that RYR2 auxiliary protein calsequestrin (CSQ2) serves as a key luminal Ca^{2+} sensor of the RYR2 channel [2]. However, several studies highlighted the growing importance of the CSQ2-independent luminal regulation [3,4] that is likely mediated by RYR2-resident luminal Ca^{2+} binding sites. Since now, localizations as well as detailed functional profiles of these sites have not been reported.

The aim of our study was to characterize the RYR2 luminal Ca^{2+} binding sites by studying the functional effects of various alkaline earth metal divalents (M^{2+} : Mg^{2+} , Sr^{2+} , Ca^{2+} or Ba^{2+}) on the channel response to cytosolic caffeine in light of function-structure relationships. Native RYR2 channels were isolated from the adult rat heart ventricle using differential centrifugation and reconstituted into a planar lipid membrane (BLM) [5]. Since the SR microsomes yielded a detectable amount of CSQ2 [4], this protein was removed using two methods, depending on the luminal conditions in the BLM experiments. The interaction of luminal M^{2+} with the RYR2 channel was monitored by fitting the caffeine dose-response curve to the Hill equation and determining the EC_{50} values. Figure 1A shows representative current recordings of the caffeine-activated RYR2 channel obtained at 8 mM luminal M^{2+} to illustrate the RYR2 behaviour at the channel activity of ~ 0.5 . We adopted 8 mM concentration of luminal M^{2+} as our standard. Although even 8 mM luminal M^{2+} is out of the physiological range (~ 1 mM), this concentration could be reached under some pathological conditions, such as ischemia/reperfusion [6]. Thus, the RYR2 luminal regulation at 8 mM luminal M^{2+} could account for some pathophysiological components of heart failure.

We observed that the RYR2 channel was the most sensitive to cytosolic caffeine when luminal Ca^{2+} was present, luminal Sr^{2+} displayed a moderate ability to increase the apparent affinity for caffeine, and luminal Ba^{2+} and Mg^{2+} were the weakest players in this regard (Figure 1, B and C). The apparent heterogeneity in the RYR2 response might be explained by existence of distinct M^{2+} binding sites on the RYR2 luminal face [7]. To test this idea, we conducted three series of competition experiments when Ca^{2+} was gradually replaced by Mg^{2+} , Sr^{2+} or Ba^{2+} at the RYR2 luminal face. The concentration of luminal Ca^{2+} was fixed to the physiological level (1 mM) and concentration of luminal M^{2+} was varied from 8 mM to 53 mM. The RYR2 dose-responses for caffeine were collected for each M/Ca mixture. To evaluate M/Ca competition, we focused on the EC_{50} for caffeine, for which we found a M^{2+} -specific effect. In all data sets, the dose-response curve shifted from that obtained for pure 1 mM luminal Ca^{2+} to the right, toward the dose-response curves collected for pure luminal M^{2+} (Mg^{2+} , Sr^{2+} or Ba^{2+}) when M/Ca competition was absent. Competition experiments

documented that all tested luminal M^{2+} compete for the same binding sites located on the RYR2 luminal face with relative RYR2/M binding affinities in the order: $Ca^{2+} > Sr^{2+} > Mg^{2+} \sim Ba^{2+}$.

Our experimental results collectively demonstrate that there exists only one type of RYR2 luminal binding sites that specifically interact with all tested luminal divalents. What is more, these binding regions display characteristics reminiscent of the EF-hand motif, the most common sequence associated with Ca^{2+} binding in proteins. So, our findings provide a clue for us to hypothesize that RYR2 luminal face is EF-hand positive.

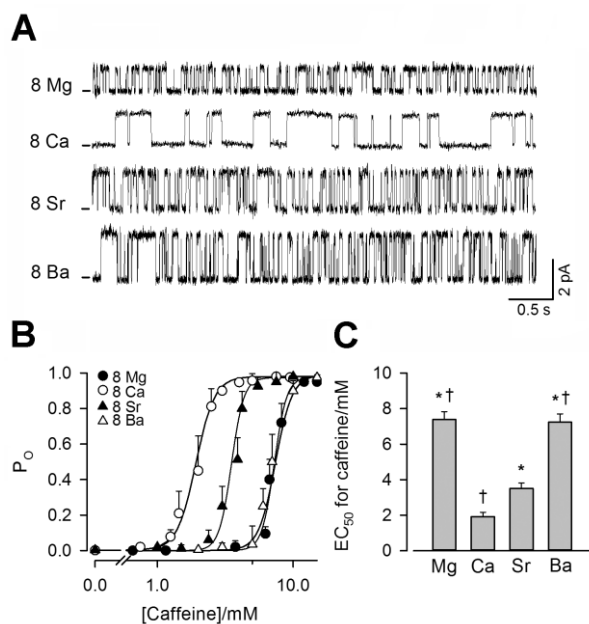


Figure 1: Effects of luminal M^{2+} on the RYR2 activation by cytosolic caffeine.

(A) Representative current traces of the RYR2 channel activated by cytosolic caffeine to open probability $P_o \sim 0.5$ in the presence of 8 mM luminal M^{2+} (Mg^{2+} , Ca^{2+} , Sr^{2+} or Ba^{2+}). Channel openings are in the upward direction. (B) Caffeine dependence of P_o for 8 mM luminal M^{2+} . The solid lines are the best fits to the Hill equation. (C) EC_{50} values for tested luminal M^{2+} . (*) versus luminal Ca^{2+} and (†) versus luminal Sr^{2+} ; $n \geq 7$ per condition.

Acknowledgement

This work was supported by the research grant from the Slovak Grant Agency VEGA No. 2/0006/15 (J.G.) and No. 2/0003/14 (M.G.).

References

- [1] A. Leenhardt, V. Lucet, I. Denjoy, F. Grau, D.D. Ngoc and P. Coumel, *Circulation* 91 (1995), 1512-1519.
- [2] I. Gyöke, N. Hester, L.R. Jones and S. Györke, *Biophys. J.* 86 (2004), 2121-2128.
- [3] W. Chen, R. Wang, B. Chen, X. Zhong, H. Kong, Y. Bai, Q. Zhou, C. Xie, J. Zhang, A. Guo, X. Tian, P.P. Jones, M.L. O'Mara, Y. Liu, T. Mi, L. Zhang, J. Bolstad, L. Semeniuk, H. Cheng, J. Zhang, J. Chen, D.P. Tieleman, A.M. Gillis, H.J. Duff, M. Fill, L.S. Song and S.R. Wayne Chen, *Nat. Med.* 20 (2014), 184-192.
- [4] B. Tencerova, A. Zahradnikova, J. Gaburjakova and M. Gaburjakova, *J. Gen. Physiol.* 140 (2012), 93-108.
- [5] J. Gaburjakova and M. Gaburjakova, *J. Membr. Biol.* 212 (2006), 17-28.
- [6] A.F. Dulhunty, N.A. Beard and A.D. Hanna, *J. Gen. Physiol.* 140 (2012), 87-92.
- [7] P.L. Diaz-Sylvester, M. Porta and J.A. Copello, *PLoS One* 6 (2011), e26693.

Cardiac ryanodine receptor: Looking for luminal Ca²⁺ binding sites

M. GABURJÁKOVÁ, AND J. GABURJÁKOVÁ

Institute of Molecular Physiology and Genetics, Slovak Academy of Sciences, Health Sciences Pavilion, Dúbravská cesta 9, 840 05 Bratislava, Slovakia
e-mail: marta.gaburjakova@savba.sk

In cardiac muscle, Ca²⁺ release from the intracellular Ca²⁺ store (sarcoplasmic reticulum, SR) through the ryanodine receptor (RYR2) channel plays an essential role in mediating the muscle contraction. The RYR2 structure possesses two major domains. Whereas, a volume dominant cytosolic domain comprises Ca²⁺ activation/inhibition sites with fairly well-defined selectivity for alkaline earth metal divalent cations (Mg²⁺, Ca²⁺, Sr²⁺ and Ba²⁺), a much smaller pore-forming region embedded in the SR membrane holds less characterized Ca²⁺ binding sites. It is well known that the RYR2 activation by cytosolic Ca²⁺ plays a central role in cardiac excitation-contraction coupling. For luminal Ca²⁺, its stimulation effect on the RYR2 channel is still not fully understood; however, this process has been linked to various cardiac disease states [1]. Although Ca²⁺ ions are critical for cardiac excitation-contraction coupling, the precise positions of the RYR2 Ca²⁺ binding sites are still unknown, mainly because the complete RYR2 crystal structure is currently not available. To overcome this, we have recently tackled the issue of RYR2 luminal Ca²⁺ binding sites using a non-standard strategy based on function-structure relationships [2]. At the single channel level, we reported that M²⁺ affinities of RYR2 luminal Ca²⁺ binding sites show a strong correlation with the M²⁺ affinity of the EF-hand motif known to bind Ca²⁺ with high affinity and selectivity. This indicates that the RYR2 luminal binding regions and the EF-hand motif likely share some structural similarities.

In the helix-loop-helix topology of the EF-hand motif, only the loop composed of 12 amino acids plays a critical role in Ca²⁺ coordination. Various patterns (motif signatures) have been generated for EF-hand loop identification even in the primary sequence of proteins [3, 4]. In the present study, we combined this concept with the near-atomic resolution 3D model of the skeletal RYR isoform [5-7] to identify the most feasible spots where RYR2 luminal Ca²⁺ binding regions could be localized. As the first step, we used a tryptic digestion method to separate potential luminal loop-resident and channel pore-resident binding sites. Trypsin at a concentration of 1 mg/ml was added to the RYR2 luminal face when the channel was almost fully activated by 4.5 mM cytosolic caffeine. Tryptic digestion was allowed to proceed and after approximately 20 minutes we observed a drop in the RYR2 activity. Since trypsin is too big (26 kDa) to enter the RYR2 pore, its luminal action was only limited to the freely accessible luminal loops (Fig. 1A).

According to the topology model generated for the RYR2 transmembrane domain [7], three luminal loops with unresolved 3D structure could harbor Ca²⁺ binding sites, namely, the S1-S2, S3-S4 and S5-S6 loops (Fig. 1A). The S3-S4 loop was excluded from our analysis because it consists of only three residues; thus, it is too short to coordinate Ca²⁺. Furthermore, we were only interested in the hairpin loop between S5 and the pore helix because only this small part of the longer S5-S6 loop projects into the SR lumen [7]. To identify the EF-hand motif, first, we highlighted all Asp, Asn and Ser as start points in primary sequences of selected RYR2 luminal loops because the position 1 in the EF-hand loop displayed strong residue conservation. Afterward, we compared the subsequent 11 amino acids with the extended EF-hand signature [4]. To select regions that fit the best to the EF-hand consensus, we considered three different attributes with ascending order of importance, and for each attribute, we calculated the identity score. We began by determining how many of the 12

Structural research of beta-D-glucosidase from *Zea mays*

L. URBÁNIKOVÁ

Institute of Molecular Biology, Slovak Academy of Sciences, Dúbravská cesta 21, 845 51 Bratislava, Slovakia
e-mail: lubica.urbanikova@savba.sk

Glucosidases hydrolyze a broad variety of carbohydrate glycosides as well as aryl- and alkyl- D-glucosides. Catalyzing the cleavage of individual glucosyl residues from various glycoconjugates they accomplish important functions in essential biological processes like glycolipid and exogenous glycoside metabolism in animals, developmental regulation and chemical defense against pathogen attack in plants. Glucosidase can be used in a number of industrial applications, e.g. biomass conversion. Beta-1,4-D-glucosidase Zm-p60.1 was isolated from maize coleoptils (*Zea mays*). The enzyme was cloned and its crystal structure was solved at 2.05-Å resolution [1] pdb code 1hxj. It has been shown that the enzyme is involved in regulation of plant development by the targeted release of free cytokinins from cytokinin-*O*-glucosides, their inactive storage forms. The mechanism by which beta-D-glucosidase recognizes and hydrolyzes substrates with different specificities remains an area of intense study. It has been shown that the enzyme specificity toward substrates with aryl aglycones is determined by the interactions of aglycone aromatic system with W373, F193, F200, and F461 which form a slot-like aglycone-binding site. Substrate specificity and enzyme activity were also studied [2,3].

Our study was focused on the crystallization and X-ray structure determination of the complexes of the enzyme with inhibitors rutin (flavonoid inhibitor) and p-nitrophenyl-beta-d-thioglucoside (pNPTG - substrate analog). At present, three structures were solved, wt and mutant W373K in the complex with rutin and triple mutant P372T, W373K, M376L with pNPTG at the resolution of 2.10, 2.16 and 1.6 Å, respectively. Beta glucosidase consists of 507 amino-acid residues and functional unit is a dimer. Decomposition of dimer led to inactivation of the enzyme. Crystals of all three complexes were prepared by soaking the crystals in the solution containing the inhibitors and then in the solution of glycerol which was used as a cryo-protectant. The crystals were flash cooled in the stream of nitrogen and the data were measured at 100 K. The crystals of all complexes belonged to P21 space group with 2 to 6 protein molecules in the asymmetric unit, i.e. 1 dimer in W373K-rutin, 2 in triple mutant-pNPTG and 3 dimers in wt-rutin structure. Crystals were very fragile and a special procedure for soaking was elaborated. Tips and tricks used in protein-inhibitor complex preparation and crystallization as well as some features of beta-D-glucosidase tertiary structure revealed at 1.6 Å resolution structure will be discussed.

Acknowledgement

This work was supported by the Slovak Grant Agency VEGA grants No. 2/0189/10 and 2/0190/14 and by the Ministry of Education, Science, Research and Sport of the Slovak Republic within the Research and Development Operational Programme for the project "Establishment of Competence center for research and development in molecular medicine", ITMS 26240220071, co-funded by the European Regional Development Fund.

References

- [1] Zouhar J., Vévodová J., Marek J., Damborský J., Su X.-D. and Brzobohatý B. *Plant Physiology*, 127 (2001), 973–985.
- [2] Dopitová R., Mazura P., Janda L., Chaloupková R., Jeřábek P., Damborský J., Filipi T., Kiran N.S. and Brzobohatý B. *FEBS J.*, 275 (2008), 6123–6135.
- [3] Filipi T., Mazura P., Janda L., Kiran N.-S. and Brzobohatý B. *Phytochemistry* 74 (2011), 40-42.

Hexosomal and cubosomal CnOH+DOPE+DOPC liquid crystals as potential drug delivery systems

M. KLACSOVÁ¹, D. UHRÍKOVÁ¹, P. BALGAVÝ¹, J.C. MARTÍNEZ², AND CH. KAMMA-LORGER²

¹ Department of Physical Chemistry of Drugs, Faculty of Pharmacy, Comenius University in Bratislava, Odbojárov 10, 832 32 Bratislava, Slovakia

² BL-11 NCD beamline, ALBA Synchrotron, Carrer de la Llum 2-26, 08290 Cerdanyola del Vallès, Barcelona, Spain

e-mail: klacsova@pharm.uniba.sk

The thermotropic phase behavior of lyotropic lipid-based liquid crystals is very diverse, ranging from 1D fluid lamellar L_α phase to more complex mesophases with increasing negative curvature, such as 2D inverse hexagonal H_{II} or 3D cubic Q phase. Non-lamellar lipid structures perform a number of key roles in biological processes [1] and play an important role for applications in food science and pharmacology, e.g. lipidic nanoscale systems for drug delivery (cubosomes and hexosomes) [2]. Many factors influence the phase behavior of H_{II} and Q liquid crystals, e.g. molecular structure of lipids, hydration, temperature and/or addition of a third substance. Primary aliphatic alcohols (CnOHs) are substances of choice for topical drug delivery systems thanks to their transdermal penetration enhancing effect. This effect increases with alcohol chain length up to C10OH and decreases for longer chains [3,4], i.e. a cut-off in the penetration enhancing potency is present.

We have followed the structural polymorphism of the dioleoylphosphatidylcholine (DOPC) and dioleoylphosphatidylethanolamine (DOPE) mixture depending on hydration and addition of CnOHs. Synthetic lipids were purchased from Avanti Polar Lipids (Alabaster), CnOHs from Sigma (St. Luis), organic solvents from Slavus (Bratislava). Stock solutions of DOPE, DOPC and CnOHs, respectively, were prepared in methanol+chloroform mixture. Samples were prepared at CnOH:(DOPE+DOPC) = 0.4:1 mol/mol. The solvent was evaporated under a stream of gaseous nitrogen and by an oil vacuum pump. Deionized MilliQ water was added at H₂O:(DOPE+DOPC) = 100:1-500:1 mol/mol. Measurements were performed at NCD-BL11 beamline (ALBA Synchrotron). Temperature was changed in the range 20-80 °C with the heating rate of 1°C/min.

Control DOPE+DOPC samples showed at lowest temperatures two sharp reflections corresponding to lamellar L_α phase. On heating, a superposition of lamellar and inverse hexagonal H_{II} reflections occurred. With further increase of temperature three reflections, characteristic for pure H_{II} phase were observed (Fig. 1 left). At highest temperatures studied further low-intensity reflections appeared after completion of the L_α to H_{II} phase transition. These reflections were identified as a superposition of two cubic phases of Pn3m and Im3m space group (inset at Fig. 1). The presence of Q phases became more pronounced at higher hydration, what might indicate that increasing hydration stimulates formation of Q phases in the studied DOPE+DOPC system.

By evaluation of positions and intensities of observed L_α and H_{II} diffraction peaks, L_α to H_{II} phase transition temperatures t_{LH} and lattice parameters of respective phases were estimated [5] (Fig.2). For control samples $t_{LH\text{on}}$ and $t_{LH\text{end}}$ systematically decreases with hydration, whereas structure parameters of the L_α and H_{II} phase do not change significantly. CnOHs were found to decrease t_{LH} in a chain length dependent manner. In comparison with the control sample, the lattice parameter of the L_α phase, d_{20} , is decreased in the presence of C8OH and C10OH and slightly increased when longer CnOHs were intercalated. The lattice parameter of the H_{II} phase a_{80} is decreased for all CnOHs studied. All dependences were fitted with a linear function for C8-C12 data points. Deviations from these dependences obtained for $n \geq 16$ are caused by alcohol crystallization within the system [5].

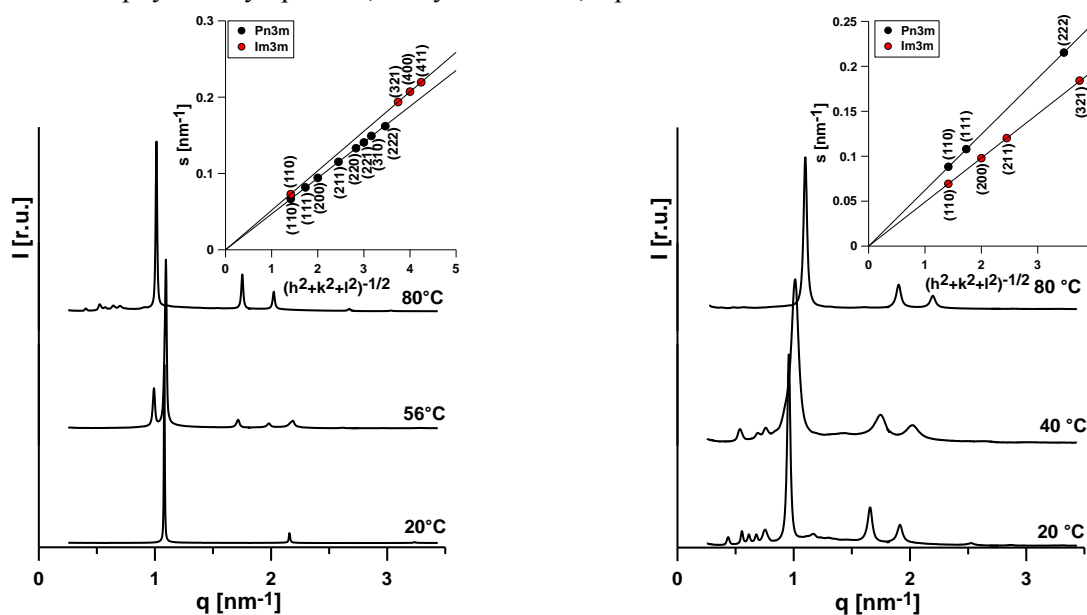


Fig.1 Typical SAX diffractograms obtained on heating for DOPE+DOPC control sample (left) and C14OH+DOPE+DOPC sample (right), at H₂O:(DOPE+DOPC)=500:1 mol/mol hydration. Insets depict the Q phase space group identification.

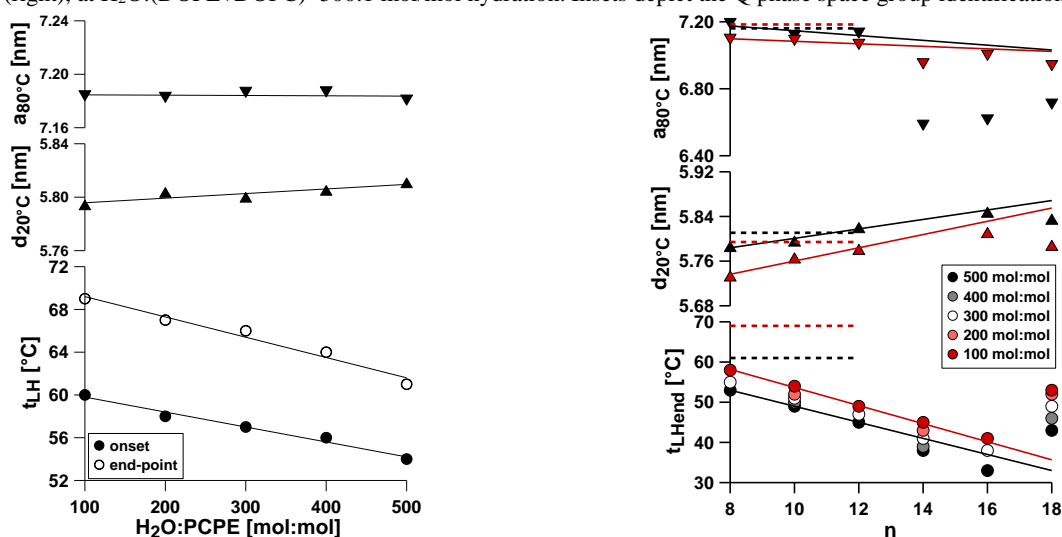


Fig.2 Dependence of the L_α to H_{II} phase transition temperature onset and end-point and the structure parameters of the L_α and H_{II} phase at 20°C and 80°C for the DOPE+DOPC (left) and C_nOH+DOPE+DOPC system (right), as a function of hydration and C_nOH chain length (legend denotes hydration). Lines represent the best linear fits of respective data points.

Further we found, that short C_nOHs ($n \leq 12$) promote formation of Q phase at high temperatures, i.e. within the H_{II} matrix (as observed for control samples), whereas in presence of longer C_nOHs the Q phase is formed in coexistence with the L_α phase and disappears after L_α to H_{II} phase transition completion (Fig.1 right). Interestingly, no reflections of the cubic phase were detected for the C18OH+DOPE+DOPC system, what might suggest that bulk crystallization of alcohols suppress formation of the Q phase.

Differences in liquid crystal nanostructure are used to improve drug diffusion and release. Our experiments revealed that C_nOH+DOPE+DOPC system might be used as stimuli responsive drug delivery system.

Acknowledgement

Grants under JINR project 04-4-1121-2015/2017, VEGA 1/0855/16 and VEGA 1/0916/16 are acknowledged.

References

- [1] V. Luzzati, *Curr Struct Biol* 7 (1997), 661-668.
- [2] Y. Chen, P. Ma and S. Gui, *BioMed Res Int* ID 815981 (2014), 1-12.
- [3] S. Andega, N. Kanikkannan and M. Singh, *J Con Rel* 77 (2001), 17-25.
- [4] K. Vávrová, J. Zbytovská and A. Hrabálek, *Curr Med Chem* 12 (2005), 2273-2291.
- [5] M. Klacsová, J. Karlovská, D. Uhríková, S.S. Funari and P. Balgavý, *Soft Matter* 10 (2014), 5842-5848.

Detection of the cancer markers at Jurkat cells using DNA aptamers

A. POTURNAYOVA^{1,2}, M. SNEJDARKOVA¹, L. BABELOVA¹, M. BURIKOVA¹, I. KARPISOVA², J. BIZIK³, A. EBNER⁴, M. LEITNER⁵, AND T. HIANIK²

¹Institute of Animal Biochemistry and Genetics, Slovak Academy of Sciences, 900 28 Ivanka pri Dunaji, Slovakia

²Department of Nuclear Physics and Biophysics, FMFI UK, Mlynska dolina F1, 842 48 Bratislava, Slovakia

³Institute of Experimental Oncology of the Slovak Academy of Science, Vlarska 7, 833 91 Bratislava, Slovakia

⁴Institute of Biophysics, Johannes Kepler University Linz, Gruberstrasse 40, 4020 Linz, Austria

⁵Center for Advanced Bioanalysis GmbH, Gruberstrasse 40, 4020 Linz, Austria

e-mail: alexandra.poturnayova@savba.sk

Leukemia is one of the most malignant tumor induced death. Early diagnosis and screening are two major components of fast detection of cancer. The new trends in the diagnosis of cancer include the identification of particular markers using specific antibodies. An alternative to antibodies are single stranded oligonucleotides called “aptamers”. Aptamers are group of promising recognition units that can specifically bind to target molecules and cells. Due to their excellent specificity and high affinity to targets, aptamers have attracted great attention in various fields in which selective receptors are required. They have been used in biosensing, drug delivery, disease diagnosis and therapy (especially for cancer treatment).

In this work we used atomic force microscopy (AFM) and acoustic thickness shear mode method (TSM) for study interaction between DNA aptamers and tyrosine kinase 7 (PTK7) receptors on the leukemic Jurkat cells. Using the TSM method, we studied the kinetics of changes of the series resonant frequency, f_s , and the motional resistance, R_m , of the quartz crystal transducer. The TSM method is sensitive to the surface viscosity of the layer, which changed following addition of cells. We used two concepts of the gold support coating: namely by neutravidine with biotinylated aptamer or the second, by the thiol group labeled aptamer, where the vacancies were blocked by dodecanethiol (DDT). Addition of Jurkat cells in concentration 5×10^6 /ml caused the decay of resonant frequency by about 95 Hz for biotinylated system and about 84 Hz for thiol system, respectively. The aptamer specificity were verified using non-specific aptamer or control cells U266. Non-specific interactions with neutravidine and DDT were excluded.

Using special PEG linker we immobilised DNA aptamer sensitive to PTK7 on the AFM tips to determine the specificity of the interaction between aptamers and the PTK7. Single molecule force spectroscopy (SMFS) experiments demonstrated the addressability and allowed to determine kinetic parameters rate of dissociation k_{off} ($5.16 \pm 0.19 \text{ s}^{-1}$) and energy landscape $x\beta$ ($0.65 \pm 0.01 \text{ \AA}$). The specificity was proven in a surface-blocked by addition of DNA aptamers to the surface prior SMFS experiments. The binding probability in blocked experiment was significantly reduced by about ~77%. Moreover, this experiment proved that even after cell fixation there are still undamaged PTK7 receptors on the cell surface able to interact with target molecules. This finding allows us to design new experimental setups to investigate these model cell lines by the reason of proper and detail understanding, which may help in future target cancer therapy.

Acknowledgments

This work was supported by the Slovak Research and Development Agency under the contracts No. APVV-14-0267 and SK-AT-2015-0004 and by Science Grant Agency VEGA (project No. 2/0055/14).

Reaction of cyanide inhibited cytochrome oxidase with oxygen

K. KOPCOVA¹, AND M. FABIAN²

¹Department of Biophysics, Faculty of Science, Safarik University, Jesenna 5, Kosice

²Center for Interdisciplinary Biosciences, Faculty of Science, Safarik University, Jesenna 5, Kosice
email: fabian@rice.edu

The final step of respiration in aerobic organisms is a reduction of molecular oxygen to water. In mitochondria, the respiratory enzyme cytochrome c oxidase (CcO) catalyzes the oxidation of ferrocytochrome *c* with O₂. The reaction is inhibited by small ligands among which cyanide is the most famous. The inhibition of respiration by cyanide is accomplished by binding of ligand directly to the catalytic binuclear center, composed of heme *a*₃ and ion of copper, Cu_B. The ligand is bound so strongly that CcO remains in the complex with cyanide (CcO.CN) even after the removal of free HCN from solution [1].

We observed that this CcO.CN, if it is partially reduced, is able to react with O₂. The reaction slowly regenerate the oxidized form of CcO.CN with the bound ligand. Surprisingly, the addition of low amount of cyanide (~1 mM) to the buffer during the oxidation of CcO.CN does not inhibit the process. In contrast, this additional cyanide enhances the rate of oxidation. It appears that under these conditions cyanide is very likely one of the substrates in this reaction. Based on the obtained data we assume that the redox reaction catalyzed by partially reduced CcO.CN may be analogous to the reactions performed by bacterial cyanide monooxygenases or dioxygenases.

Acknowledgement

This work was supported by FP7 EU project CELIM 316310.

References

1. D. Jancura, J. Stanicova, G. Palmer, M. Fabian *Biochemistry*, **53** (2014), 3564-3575.

Interaction of hydrogen sulfide with S-nitrosothiols – from chemistry to biological effects of products

M. GRMAN^{1,2}, M. M. CORTESE-KROTT³, M. FEELISCH⁴, P. NAGY⁵, A. BERÉNYIOVÁ⁶, S. ČAČANYIOVÁ⁶, AND K. ONDRIAS^{1,2}

¹ Institute of Clinical and Translational Research, Biomedical Research Center, Slovak Academy of Sciences, Dúbravská cesta 9, 845 05 Bratislava 4, Slovakia

² Institute of Molecular Physiology and Genetics, Dúbravská cesta 9, 840 05 Bratislava, Slovakia

³ Medical Faculty, Heinrich Heine University of Düsseldorf, Moorenstrasse 5, 40225 Düsseldorf

⁴ Faculty of Medicine, University of Southampton, Southampton General Hospital and Institute for Life Sciences, Tremona Road SO16 6YD, Southampton, United Kingdom

⁵ National Institute of Oncology, Ráth György utca 7-9, 1122 Budapest, Hungary

⁶ Institute of Normal and Pathological Physiology, Sienkiewiczova 1, 813 71 Bratislava, Slovakia
e-mail: grman.marian@gmail.com

Hydrogen sulfide (H₂S) and nitric oxide (NO) are two the most studied gaseous signaling molecules endogenously produced in human body by specific enzymes. They are involved in many (patho)physiological functions. S-nitrosothiols (RSNO) are molecules resulting from binding of NO to thiol group of cysteine and they serve as a bioreservoir of NO in cells. Numerous cross-talks between NO/RSNO and H₂S signaling pathways have been reported [1-3]. For example, an application of mixture of S-nitroso-N-acetyl-DL-penicillamine (SNAP) and excess of H₂S led to higher activity of soluble guanylyl cyclase (sGC) in comparison to SNAP alone [4]. We showed that the interaction of RSNO with H₂S resulted to generation of four major products - polysulfides (HS_x⁻), nitrosopersulfide (SSNO⁻), dinitrososulfite (SULFI/NO) and nitroxyl (HNO) [5]. Polysulfides increased a reaction rate of RSNO decomposition and SSNO⁻ formation, what pointed out to an autocatalytic effect of polysulfides. SSNO⁻, as one of the major product, was resistant to general used disulfide bond reductant - dithiotreitol, KCN, reduced glutathione and cysteine. Decomposition of SSNO⁻ was slow and homolytical process and led to generation of disulfide radical SS^{•-} and NO[•]. Using methylene blue method, cold cyanolysis and extraction of elemental sulfur into chloroform we quantified amount of SSNO⁻ generated in the mixture of 500 μM SNAP with 5 mM H₂S. We found that SSNO⁻ accounts only for 25-30% of SNAP concentration. Application of interaction mixture of 50/500 and 100/1000 nM GSNO/H₂S (GSNO – S-nitrosoglutathione) relaxed precontracted aorta rings much faster than GSNO alone [6]. Our results indicate that nitrosopersulfide, as the product of NO-H₂S interaction, is both donor of sulfane sulfur and donor of nitric oxide and therefore it can represent cross-talk molecule of H₂S-NO signaling pathway.

Acknowledgement

This work was supported by the research grant from the Slovak Grant Agency VEGA/2/0146/16, VEGA/2/0019/15 and VEGA/2/0050/13.

References

- [1] B. King, *Free Radic. Biol. Med.* 55 (2013): 1-7
- [2] B. V. Nagpure, J. S. Bian, *Oxid. Med. Cell. Longev.* (2016): 6904327.
- [3] G. K. Kolluru, S. Juan, X. Shen, C. G. Kevil, *Methods Enzymol.* 554 (2015): 271-297
- [4] M. M. Cortese-Krott, B. O. Fernandez, J. L. Santos, E. Mergia, M. Grman, P. Nagy, M. Kelm, A. Butler, M. Feelisch, *Redox Biol.* 2 (2014): 233-244.
- [5] M. M. Cortese-Krott, G. G. Kuhnle, A. Dyson, B. O. Fernandez, M. Grman, J. F. DuMond, M. P. Barrow, G. McLeod, H. Nakagawa, K. Ondrias, P. Nagy, S. B. King, J. E. Saavedra, L. K. Keefer, M. Singer, M. Kelm, A. R. Butler, M. Feelisch, *Proc. Natl. Acad. Sci. U S A* 112 (2015): E4651-E4660
- [6] A. Berenyiova, M. Grman, A. Mijuskovic, A. Stasko, A. Misak, P. Nagy, E. Ondriasova, S. Cacanyiova, M. Feelisch, K. Ondrias, *Nitric Oxide* 46 (2015): 123-130

Activation of a single voltage sensor of the T-type calcium channel may be sufficient for pore opening

M. KARMAŽINOVÁ¹, K. ONDÁČOVÁ¹, E. PEREZ-REYES², AND L. LACINOVA¹

¹ Institute of Molecular Physiology and Genetics, Slovak Academy of Sciences, Dubravská cesta 9, 840 05 Bratislava, Slovakia

² Department of Pharmacology, University of Virginia, Charlottesville, VA 22908, USA.

e-mail: lubica.lacinoval@savba.sk

Low-voltage activated T-type calcium channels, i.e., Cav3.1, Cav3.2 and Cav3.3 channels, are best recognized for their negative voltage of activation and inactivation thresholds [1], which is more than 30 mV lower than the activation threshold of closely related high-voltage activated (HVA) calcium channels. It is possible that gating and kinetics of T-type channels are regulated by mechanisms distinct from that regulating HVA channels.

Activation of voltage-gated calcium channels (VGCC) proceeds in two steps. First step represents an activation of the channel voltage-sensor (presumably formed by the S1-S4 segments), which is manifested in an upward motion of S4 segments. Opening of the ionic pore follows in the second step (Figure 1). The outward movement of S4 segments produces the charge movement (Q) measurable as gating currents [2]. Consequent opening of the pore generates the ionic current (I). The voltage-dependence of the pore opening, i.e., current-voltage (I-V) dependence, is virtually identical among all three Cav3 channel isoforms.

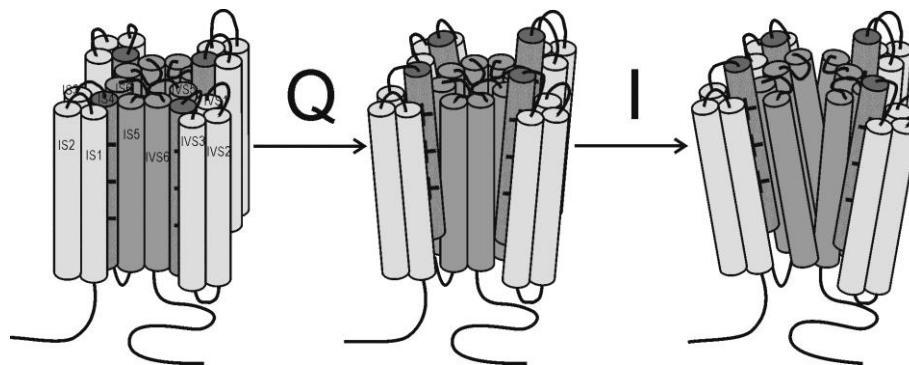


Figure 1. Depolarization of the cell membrane activates upward movement of voltage sensors resulting in a charge movement Q, which is followed by a pore opening resulting in an ionic current I. Adapted from [3].

The time constant of current activation, which reflects the transition kinetic between closed and open states of the channel, is similar between Cav3.1 and Cav3.2 channels, but of one order magnitude slower for Cav3.3 channel. Analysis of the charge movement revealed intriguing feature of Cav3 gating. In contrast to other VGCC, only a minor fraction of total charges is moved when maximal inward current is reached [2,4-5]. This fraction differs between Cav3 channel isoforms being approximately 40 % for the Cav3.1 channel, 50 % for the Cav3.2 channel, and less than 20 % for the Cav3.3 channel suggesting that pore may open before all S4 segments are activated.

Voltage dependence of the ON-charge movement occurs at significantly more positive voltages for Cav3.3 channel compared to Cav3.1 channel [4-5]. This suggests that more energy is needed to mobilize the voltage-sensor of Cav3.3 channels than of Cav3.1 channels. On the other hand, because the voltage-dependences of pore opening are nearly identical, it implies that even less charge transfer is needed to open the pore of Cav3.3 channels than of

Cav3.1 channels suggesting a more efficient coupling between the activation of the voltage-sensor and the pore opening.

Structural and functional analyses have revealed the presence of a helix-loop-helix structure, so-called *gating brake*, located within the proximal 62 amino acids region of the intracellular I-II linker of the Cav3 subunit, and highly conserved among virtually all T-type channels including mammals and their invertebrate orthologs [6]. Deletion of this molecular determinant results in a hyperpolarizing shift of the activation threshold and accelerated activation and inactivation kinetics [7]. Interestingly, upon deletion of the *gating brake*, intrinsic differences between Cav3.3 and Cav3.1 channels were abolished and the Cav3.3 deletion mutant presented a similar behavior as the Cav3.1 channel [4].

The coupling between the activation of the voltage-sensor and the pore opening was improved by the removal of the *gating brake* in Cav3 channels, as documented by a doubled slope of G_{\max} - $Q_{ON\max}$ relationship [4-5]. In addition, removing the gating brake in Cav3.1 and Cav3.3 channels resulted in a hyperpolarized shift of the voltage-dependence of the charge movement, indicating that less energy is required to move the voltage-sensor and that the *gating brake* regulates not only the pore opening but also the activation of the voltage sensor. Shift caused by the deletion of the *gating brake* in Cav3.3 channels was of much greater magnitude, suggesting that the *gating brake* in Cav3.3 channels is “braking” more than in Cav3.1 channels [4-5]. In addition, the kinetics of the ON-charge movement were found significantly accelerated upon deletion of the *gating brake* in the Cav3.3 channel, suggesting an increased mobility of the voltage-sensor.

Altogether, we suggest that pore of Cav3 channels may open after activation of a single voltage sensor and that S4 segment in the domain I is a likely candidate.

Acknowledgement

This work was supported by the research grant from the Slovak Grant Agency Vega No. 2/0044/13.

References

- [1] E. Perez-Reyes, *Physiol Rev* 83 (2003), 117-161.
- [2] L. Lacinová, N. Klugbauer and F. Hofmann *FEBS Lett* 531 (2002) 235-240.
- [3] N. Weiss and L. Lacinová *Channels (Austin)* (2015) doi 10.1080/19336950.2015.1106655
- [4] M. Karmažínová, J. P. Baumgart, E. Perez-Reyes and L. Lacinová, *Pflugers Arch* 461 (2011) 461-468.
- [5] M. Karmažínová, K. Jašková, P. Griac, E. Perez-Reyes and L. Lacinová, *Pflugers Arch* (2015) 467: 2519-2527.
- [6] E. Perez-Reyes, *Channels (Austin)* 4 (2010), 453-458.
- [7] J. P. Baumgart, I. Vitko, I. Bidaud, A. Kondratskyi, P. Lory, E. Perez-Reyes, *PLoS One* 3 (2008) e2976.

Age Dependent Capacitive Membrane Activity in Rat Cardiac Myocytes

M. HOŤKA, A. ZAHRADNÍKOVÁ, JR., AND I. ZAHRADNÍK

Department of Muscle Cell Research, Institute of Molecular Physiology and Genetics, Slovak Academy of Sciences, Dúbravská cesta 9, P.O. Box 63, 840 05 Bratislava, Slovak Republic
e-mail: ivan.zahradnik@savba.sk

Cardiac myocytes are cells with complex surface membrane system that changes during postnatal development. The smooth plasmalemma of embryonic myocytes transforms within a few weeks postpartum into an intricate 3D network of tubules invading the whole volume of myocytes. The purpose behind is to facilitate spreading of action potential excitation closer to the contractile myofibrils where it triggers calcium release and contraction. High-resolution membrane capacitance measurements, instrumental in disclosing secretory and endocytotic mechanisms in specific cell types, allow recording membrane capacitance changes as small as 1 fF, corresponding to a membrane vesicle of about 100 nm in radius. We speculated that this sensitivity could be sufficient to study the dynamics of membrane events related to development of plasmalemma also in cardiac myocytes.

We used our new method of high resolution membrane capacitance recording, optimized for isolated cardiac myocytes [1], to record spontaneous and stimulated membrane capacitance changes. In parallel experiments we followed the development of calcium release using inactivation of calcium current as a specific indicator. Cardiac myocytes, isolated from newborn rats at various days postpartum, were whole-cell voltage clamped by the standard patch clamp method.

Continuous recordings of membrane capacitance revealed variable discrete capacitance changes (Fig. 1). The most frequent were random events of 1 – 20 fF in amplitude, occurring 0.1 – 2 times per second. These might correspond to attachment and

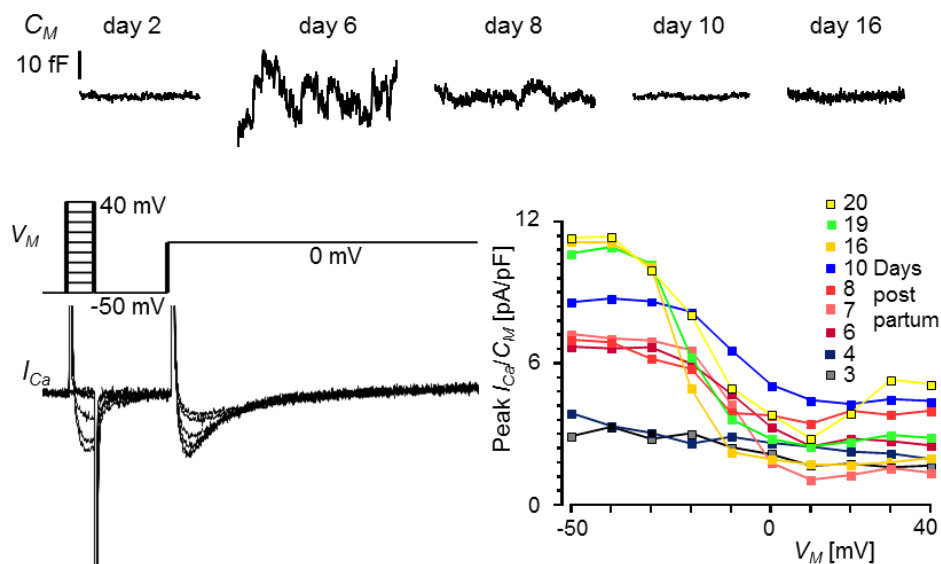


Fig. 1. Membrane activity is age-dependent. *Upper panel* - changes in spontaneous variation of membrane capacitance during postnatal development. *Lower panels* - postnatal development of calcium release-dependent inactivation of I_{Ca} . A typical family of recorded I_{Ca} with the stimulation protocol (left) and the dependence of peak I_{Ca} inactivation on the pre-pulse voltage at various stages of postnatal development (right).

detachment of membrane bodies or vesicles of 180 – 800 nm in diameter to the plasmalemma. In addition, large and spontaneous stepwise increases of membrane capacitance of 80 – 250 fF in amplitude were also occasionally observed. The large discrete capacitance increases were also observed after stimulation of myocytes by a train of calcium currents (Fig. 2). In these experiments, the discrete capacitance increases of 50 – 160 fF occurred 3 to 20 seconds after stimulation. This might reflect calcium-induced fusion of intracellular membrane bodies with the surface membrane. These large capacitance increases were preceded by transient opening of a fusion pore with a conductance of several hundreds of pS that lasted for a few hundred milliseconds. Such large stepwise changes of membrane capacitance might be related to the opening of the mouth of transversal tubules.

The small and frequent fluctuations of membrane capacitance culminated between days 6 – 10 postpartum. In the same age period we have observed transformation of the calcium current inactivation mechanism (Fig. 1). The inactivation kinetics changed from slow to fast, and the extent of fast inactivation increased. As we have shown previously [2], the rate and extent of the fast inactivation process reflect the rate and extent of calcium release from the sarcoplasmic reticulum. In adult myocytes these takes place solely at dyadic junctions of plasmalemmal and sarcoplasmic reticulum membranes.

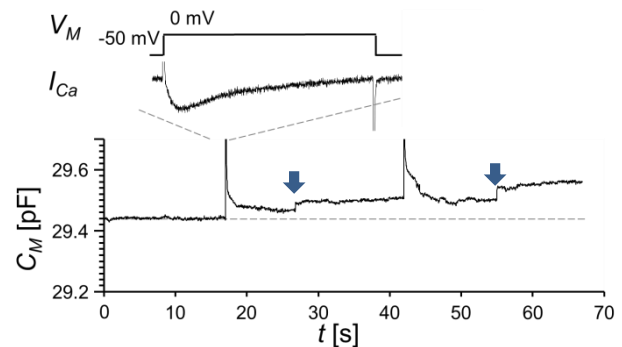


Fig. 2. Calcium current-induced large step increases of membrane capacitance. *Upper panel* – an example I_{Ca} during a single voltage pulse from a train of 10. *Lower panel* – an example of C_M responses to 2 trains of stimuli in the record. The large step increases are marked by arrows.

We suppose that the high capacitive membrane activity in postnatal myocytes is related to maturation of the structure of plasmalemma and formation of dyads at the sites of calcium entry where L-type calcium channels reside. In this function, the intracellular calcium that stimulates membrane dynamics in cardiac myocytes may play a role. Altogether, these findings provide the first evidence of vesicle fusion events related to physiologically relevant membrane activity in cardiac myocytes.

Acknowledgement

This work was supported by research grants from the Agency for Support of Research and Development (APVV-0721-10) and from the Slovak Grant Agency VEGA– (2/0147/14).

References

- [1] MAT-MECAS: <https://sourceforge.net/projects/mat-mecas/>
- [2] A Zahradníková, Z Kubalová, J Pavelková, S Györke and I Zahradník, *Am J Physiol Cell Physiol* 286 (2004) 330-341

Inactivation of calcium current by local calcium release events

B. HOFFMANNOVÁ¹, E. POLÁKOVÁ², A. ZAHRADNÍKOVÁ², I. ZAHRADNÍK², AND A. ZAHRADNÍKOVÁ JR.²

¹ Faculty of Mathematics, Physics and Informatics, Comenius University, Bratislava, Slovakia

² Institute of Molecular Physiology and Genetics, Slovak Academy of Sciences, Bratislava, Slovakia
e-mail: basa132@gmail.com

Proper function of cardiac myocytes requires a reliable mechanism for regulation of calcium influx during the contraction-relaxation cycle to prevent calcium overload and minimize energetic costs. Calcium release activation by L-type calcium current elicits rapid and extensive inactivation of the calcium current and thus provides an effective negative feedback based on the calcium-dependent inactivation mechanism of calcium channels. The aim of this study was to characterize the effect of local calcium release on the extent of calcium release-dependent inactivation (RDI) using rapid confocal detection of local calcium release events – calcium spikes.

Calcium release was induced in isolated rat ventricular myocytes in the whole-cell patch-clamp configuration either by single depolarization to 0 mV (Figure 1A), or, using a two pulse protocol [1], by a short pre-pulse of varying length or voltage that was followed by a standard test-pulse (0 mV, 80 ms; Figure 2A). The extent of RDI was obtained either by fitting the time course of calcium current recorded by the single pulse protocol [2] by the equation

$$I_{Ca}(t) = I_M \cdot P_A(t) \cdot (1 - P_x(t) \cdot (1 - f_{RDI} \cdot P_{RDI}(t))), \quad \text{Eq. (1)}$$

or as the extent of inactivation measured by a two-pulse protocol [1], assessed the fraction of peak calcium current remaining in the test-pulse relative to peak current in the absence of the pre-pulse.

$$I_{rel} = (I_{control} - I_{test}) / I_{control} \quad \text{Eq. (2)}$$

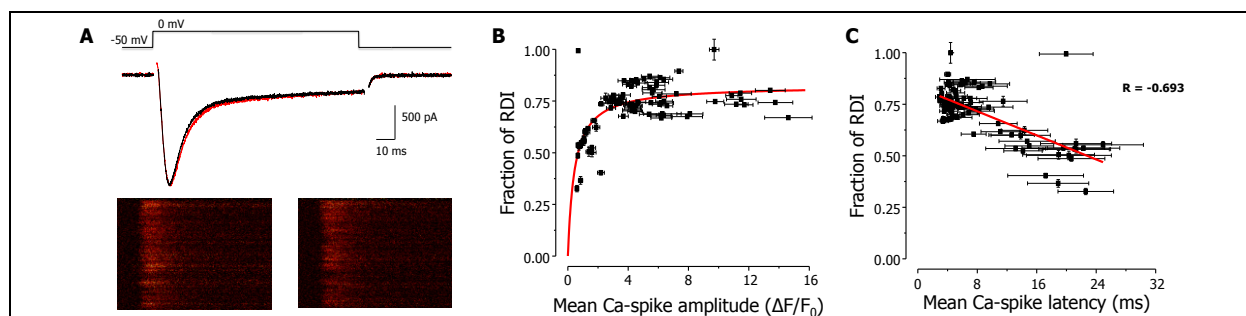
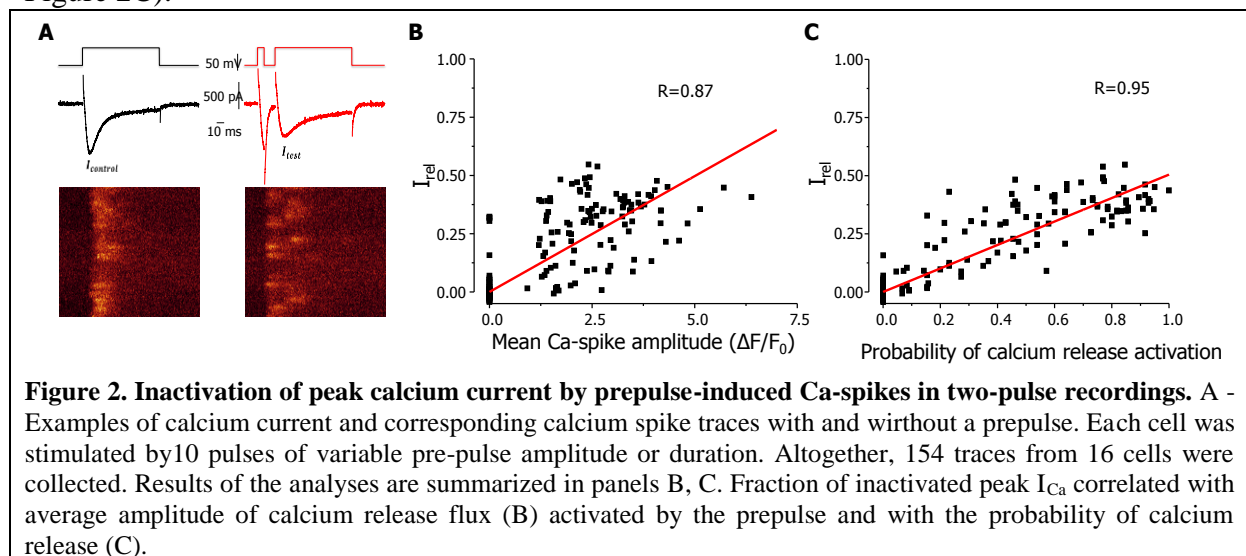


Figure 1. Inactivation of peak calcium current by prepulse-induced Ca-spikes in single-pulse recordings. A - Two examples of calcium current (black and red line) and the corresponding calcium spike traces. Typically, each cell was stimulated by 10 pulses with variable inter-pulse interval. Altogether, 109 traces from 8 cells were collected. Results of the analyses are summarized in panels B and C. B - Effect of Ca-spike amplitude on the fraction of calcium release dependent inactivation (f_{RDI}). Estimated amplitudes of individual Ca-spikes were averaged for every image. Fraction of RDI increases sigmoidally with calcium release flux. C - Effect of Ca-spike latency on f_{RDI} . Estimated latencies of individual Ca-spikes were averaged for every trace. Fraction of RDI decreases with Ca-spike latencies.

Local calcium release fluxes (calcium spikes) were measured by laser scanning fluorescence confocal microscopy using 0.1 mM fluo-3 and 1 mM EGTA in the patch-pipette solution. The parameters of local calcium release were obtained by fitting the time profiles of calcium spikes [3]. In this case, probability of calcium release activation (P_A) was calculated

as the fraction of activated calcium release sites and synchrony of calcium release was calculated as the inverse of the standard deviation of the latency.

The extent of RDI was affected by several parameters of local calcium release. It had a Hill-type dependence on the amplitude of calcium spikes within the pulse (Figure 1B) and showed a linear correlation with the amplitude of calcium spikes activated by a prepulse ($R = 0.87$; Figure 2B). Latency of calcium release negatively affected the fraction of Ca-current inactivated by RDI during a single pulse (Figure 1C). In two-pulse experiments, the extent of RDI showed a linear correlation with probability of Ca-release during the prepulse ($R = 0.95$; Figure 2C).



We conclude that the extent of calcium release dependent inactivation increases with the amplitude of local calcium release events and with the probability of their activation, while delayed calcium release activation decreases the fraction of calcium current inactivated by RDI. Thus, whole-cell release-dependent inactivation of L-type calcium currents results from the local character of calcium release.

Acknowledgement

This work was supported by research grants from the Slovak Grant Agency VEGA 2/0095/15, VEGA 2/0147/14 and VEGA 2/0148/14.

References

- [1] A Zahradníková, Z Kubalová, J Pavelková, S Györke and I Zahradník, *Am J Physiol Cell Physiol* 286 (2004) 330-341
- [2] A Zahradníková, J Pavelková, Z Kubalová and I Zahradník, in *Calcium Signaling*, M. Morad and P. Kostyuk (Eds.), IOS press, Amsterdam (2001), pp. 42 – 51.
- [3] R Janicek, M Hotka, A Zahradníková A Jr, A Zahradníková and I Zahradník, *PLoS One* 8 (2013) e64394.

Postnatal development of calcium signalling in rat ventricular cardiomyocytes

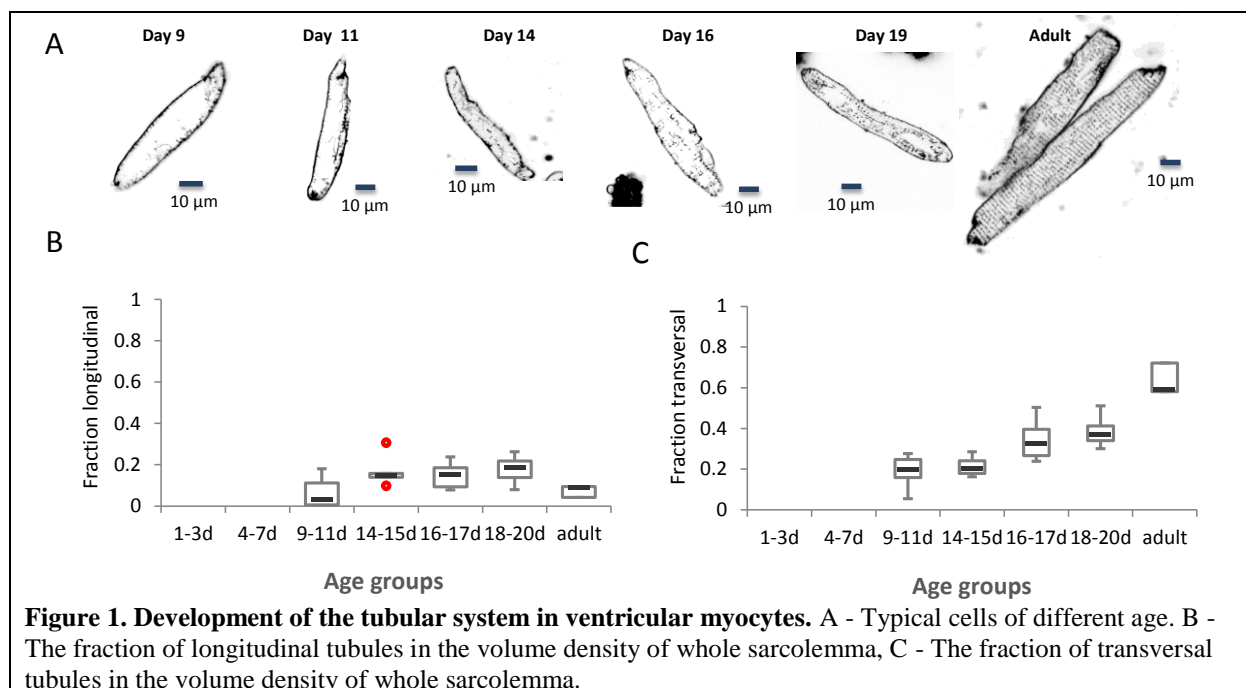
K. MACKOVÁ¹, M. HOŤKA¹, A. ZAHRADNÍKOVÁ¹, I. ZAHRADNÍK¹, AND A. ZAHRADNÍKOVÁ JR.¹

¹ Institute of Molecular Physiology and Genetics, Slovak Academy of Sciences, Bratislava, Slovakia
e-mail: katarina.mackova@savba.sk

During development, cardiac myocytes undergo rapid growth and structural remodelling. With increasing cell size, excitation-contraction coupling becomes increasingly dependent on calcium-induced calcium release taking place at dyads, the tubulo-reticular junctions. In this process, the t-tubules of plasmalemma form a network securing spreading of excitation into the whole volume of the cell. The aim of this study was to compare the postnatal development of t-tubules with the extent of calcium release using the fluorescent labelling of plasmalemma and the calcium release-dependent inactivation of calcium current. Cardiac myocytes and tissue were isolated from the left ventricle of new-born and young Wistar rats (n = 31, age 2 - 20 days and 90 days) as previously described [1] with the following modifications: With different age and weight of the animals, we optimized the amount of the anaesthetic, the volumes of solutions during retrograde perfusion and conditions of enzymatic treatment. L - type calcium currents were recorded in isolated ventricular myocytes (80 ms depolarization from -50 to 0 mV) using whole cell patch-clamp [1]. Kinetics of whole cell calcium currents we described by three processes: rapid activation, slow, voltage- and calcium current-dependent inactivation and fast, calcium release-dependent inactivation [2], according to the equation:

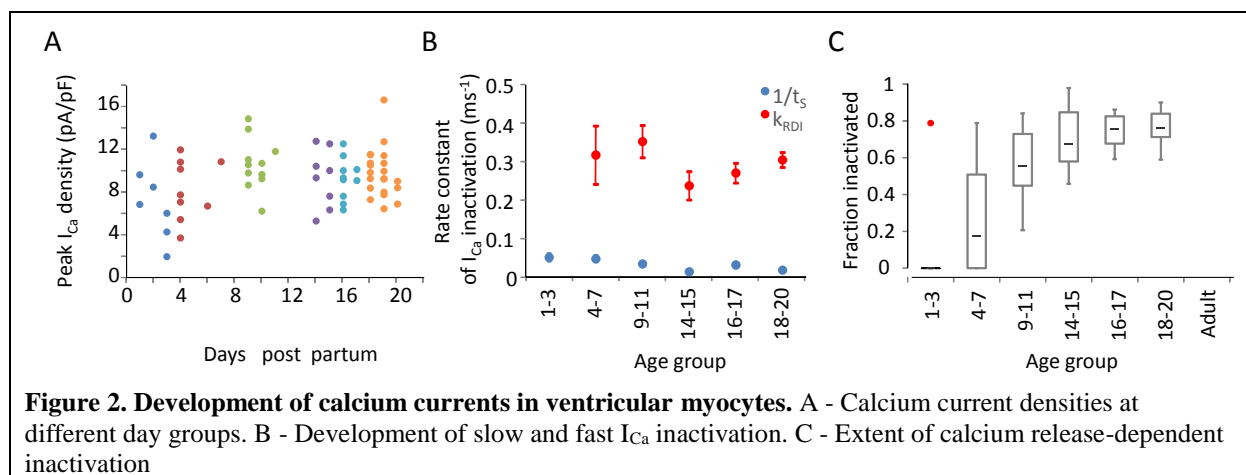
$$I_{Ca}(t) = I_M \cdot P_a(t) \cdot (1 - P_x(t)) \cdot (1 - f_{RDI} \cdot P_{RDI}(t))$$

The plasma membrane-specific fluorescent probe FM 4-64 was used to label plasma membrane and t-tubules of myocytes for observation by laser scanning confocal microscopy. The extent of tubular network was evaluated by the stereological method of vertical sections using the *Graphic Cell Analyzer* software [4].



Tubular network started to emerge around day 9 as short membrane invaginations that elongated around day 11, and then formed a loose network with profound participation of longitudinal elements around day 14, which after day 16 developed into a semi-regular tubular network. The contribution of longitudinal component was comparable to the transversal one around day 15 and then decreased, while that of transversal elements increased until adulthood (Figure 1).

During early development, calcium current density increased and saturated around day 9 (Figure 2A). The kinetics of voltage dependent inactivation as well as of the calcium release dependent inactivation did not change markedly during development (Figure 2B). The calcium release-dependent inactivation commenced on day 4 and after day 14 reached values typical for adult myocytes (Figure 2C). These data suggest that functional local calcium signalling is present already at D11, when the t-tubules only start to be discernible. This is supported especially by the dynamics of calcium current decay, which at D11 becomes as fast as in adult cardiac myocytes. It should be pointed out that the large scatter of data was not due to drawbacks in the method but due to heterogeneity in cell properties arising from the differences in the rate of their development.



In conclusion, the calcium release-dependent inactivation of calcium current appears earlier than the t-tubule system by several days, indicating participation of the surface sarcolemma in dyadic E-C coupling in the early postnatal period.

Acknowledgement

This work was supported by research grants from the Slovak Grant Agency VEGA 2/0095/15 and VEGA 2/0147/14.

References

- [1] A Zahradníková Jr., E Poláková, I Zahradník and A Zahradníková, *J Physiol* 578 (2007) 677-691.
- [2] A Zahradníková, J Pavelková, Z Kubalová and I Zahradník, in *Calcium Signaling*, M. Morad and P. Kostyuk (Eds.), IOS press, Amsterdam (2001), pp. 42 – 51.
- [3] J Parulek and I Zahradník, *Graphic Cell Analyzer*, unpublished software.

Fluorescence bioimaging in native 3D cell cultures

B. ČUNDERLÍKOVÁ^{1,2}, A. MATEAŠÍK¹

¹ International Laser Centre, Ilkovičova 3, 812 19 Bratislava, Slovakia

² Institute of Medical Physics, Biophysics, Informatics and Telemedicine, Faculty of Medicine, Comenius University, Sasinkova 2, 813 72 Bratislava, Slovakia

e-mail: beata@ilc.sk

Introduction. Cell behaviour in tissues depends on various factors that include extracellular matrix (ECM). Although originally considered to be merely structural support, ECM has been identified as a factor providing the cells with biochemical and biophysical cues affecting cellular processes, such as survival, differentiation, proliferation as well as treatment response (reviewed in [1]). Conventional assays to evaluate these processes have been developed for monolayer cell cultures and cannot be easily utilized with three-dimensional (3D) formats. We have sought to optimize methods of fluorescence bioimaging to enable visualisation of cell survival, morphogenesis, cellular biochemical activity (intracellular production of protoporphyrin IX (PpIX)) and response to external treatment (PpIX-induced photoinactivation) within native 3D collagen cultures.

Material and methods. 3D cell cultures were prepared from collagen type I and oesophageal cancer (Kyse 450, Kyse 70) or normal oesophageal immortalized (Het-1a) cell lines. The gels were formed by neutralization of mixtures of Human Collagen (CellSystems, Germany) and 10x DMEM (Sigma, Germany) on ice. Single cell suspensions were added to mixtures to a final density of 2×10^4 cells/ml. Collagen mixtures dropped on microscopy glasses were allowed to polymerize in a humidified incubator at 37°C. DMEM supplemented with 10% fetal bovine serum and antibiotics was added to gels for further incubation. To test the ability of cells in collagen gels to produce PpIX, aminolevulinic acid (ALA, Sigma, Germany) was added to samples from a 10 mM stock solution prepared in DMEM with 10% fetal bovine serum. The cultures were inspected 24 hours later. To induce PpIX-induced photoinactivation, 3D cell cultures incubated with ALA were irradiated by LED array system (UFPh-630-01-BIOSPEC, Russia) emitting light in red spectral region for 30 or 60 min. The samples were inspected 24 hours later. To visualize cells and intracellular organelles, the fluorescence dyes Acridine Orange (AO, Sigma, Germany) and Cell Mask Orange (CMO, Molecular Probes, USA) were used. Cell survival, morphogenesis and ALA-induced PpIX production were evaluated by using laser scanning confocal microscope Axiovert 200 laser scanning microscope 510 Meta (Zeiss, Germany). Laser lines of 488 nm (Argon ion laser) and 543 or 633 nm (He-Ne laser) were used to excite AO and CMO or PpIX fluorescence, respectively. To detect AO green and red fluorescence, BP 500-530 IR and BP 650-710 IR filters, respectively were used. For detection of CMO and PpIX fluorescence, BP 550-600IR and BP 650-710 IR filters, respectively, were chosen.

Results and discussion. All cell types used in the study survived 48 hours in collagen type I matrix as documented by AO and CMO fluorescence localizations in the cytoplasm/nucleus (green AO fluorescence) and acidic organelles (red AO fluorescence) [2] and in the cellular membranes (orange CMO fluorescence) [3] of single cells, respectively (Fig. 1a-c).

Incubation of single cells surrounded by collagen matrix with ALA resulted in PpIX accumulation, according to the typical PpIX fluorescence [4], in Kyse 450 cells only (Fig. 1f). Correspondingly, Kyse 450 single cells in 3D collagen cultures incubated with ALA could be photoinactivated after exposure to red light as judged from the fluorescence alterations compared to untreated controls (compare Fig. 1a, c with Fig. 1d,e) and from comparisons with cell-death positive samples (not shown).

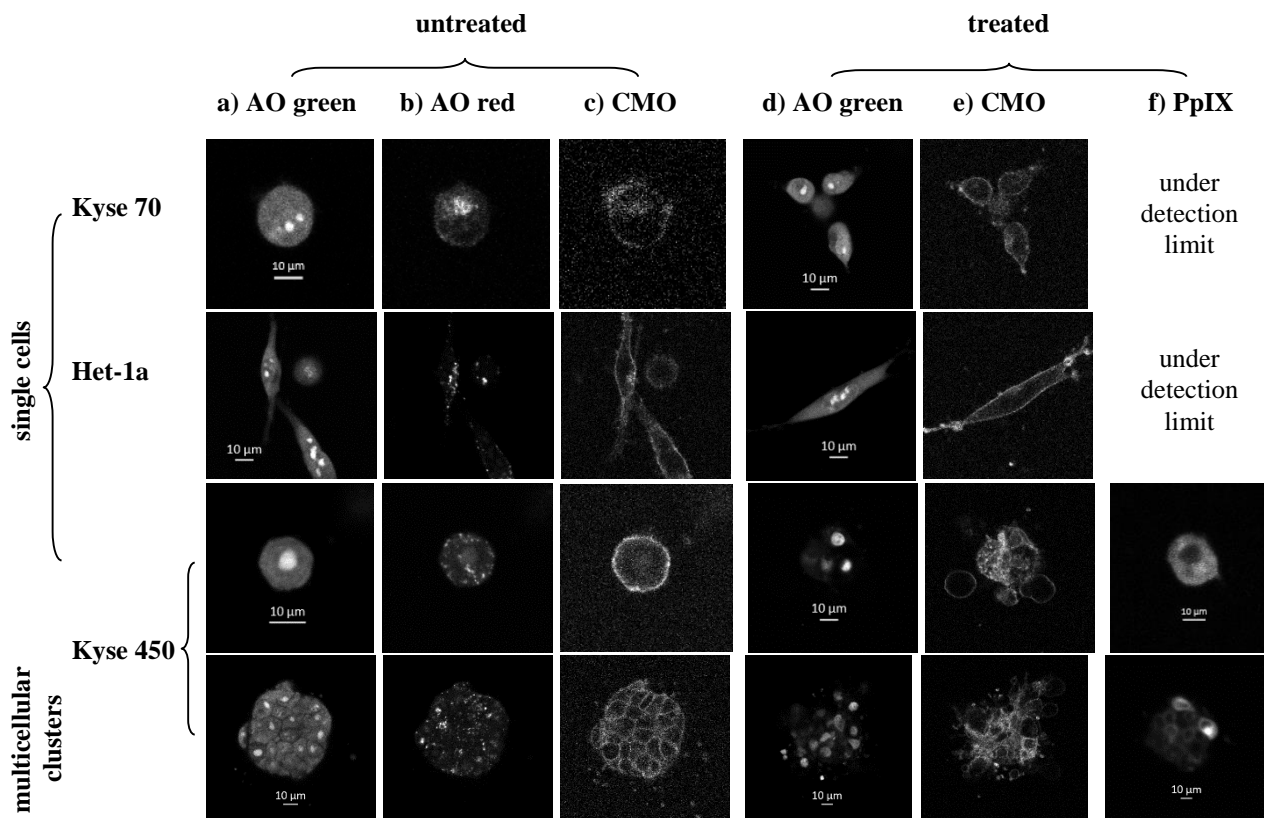


Fig. 1 Fluorescence images of single cells and multicellular clusters in 3D collagen matrices untreated (a-c) and 24 h after PpIX-induced photoinactivation (d,e). PpIX fluorescence from the cells incubated with ALA but untreated with light is shown in (f).

In the next step, we tested whether the cells naturally selforganizing into multicellular clusters in an ECM environment retain the cell-type dependent capability to produce PpIX and sensitivity to PpIX-induced photoinactivation. Following one week incubation, the cells underwent cell-type dependent morphogenesis. Similar to single cells, multicellular clusters of Kyse 450 cells produced bright PpIX fluorescence after incubation with ALA, while corresponding fluorescence was under detection limit in case of clusters of Kyse 70 and Het-1a cells. ALA-mediated photoinactivation could also be detected in multicellular clusters of Kyse 450 cells.

Conclusion. Fluorescence bioimaging can be used to evaluate different physiological cellular processes and cellular treatment response in native 3D collagen cell cultures.

Acknowledgement

This work was supported by The Integrated Initiative of the European Laser Infrastructures LASERLAB-EUROPE III and by the Slovak Research and Development Agency, project N. APVV-0242-11. Technical assistance of Dr. M. Ficková is highly acknowledged.

References

- [1] B. Čunderlíková, *Crit. Rev. Oncol. & Hematol.* 85(2013), 95-111.
- [2] K.H. Ahmed and B. Pelster, *J. Exp. Biol.* 211(Pt 20) (2008), 3306-3314.
- [3] Tracers for Membrane Labeling, in *Molecular Probes Handbook: A Guide to Fluorescent Probes and Labeling Technologies*, 11th Edition, Chapter 14, I. Johnson, M.T.Z. Spence (Eds.), Life Technologies (2010).
- [4] Q. Peng, T. Warloe, J. Moan, A. Godal, F. Apricena, K.E. Giercksky and J.M. Nesland, *Cancer Res.* 61(15) (2001), 5824-5832.

Heart rate variability during short-term exposure in teenage students

J. MISEK¹, D. SPIGUTHOVA¹, H. HABINAKOVA¹, M. VETERNIK¹, M. KOHAN¹, O. OSINA², AND J. JAKUS¹

¹ Department of Medical Biophysics, Jessenius Faculty of Medicine in Martin, Comenius Univ., Mala Hora 4, 036 01 Martin, Slovakia

² Clinic of Occupational Medicine and Toxicology, Jessenius Faculty of Medicine in Martin, Comenius Univ., Kollarova 2, 036 59 Martin, Slovakia

Introduction

The biological effects induced by mobile communication systems are very heterogeneous. Nowadays every adolescent student seems to be active user of mobile network that exploits every aspect of merging cellular phone (CP) into Internet. Thus, researches investigate for negative [1-4] (or positive[5]) impact on biological systems, especially during short-term calls. Non-thermal effects of CPs constitute effects that are not very well described.

In this study, group of 27 grammar school students were analyzed for heart rate variability (HRV) during short-time exposure to radiofrequency (RF) electromagnetic fields (EMF). HRV can reveal the gentle functional changes in sympathetic-parasympathetic autonomic nervous system (ANS) control.

Materials and methods

27 adolescent volunteers (in age 18.25 ± 0.37) were either exposed or sham-exposed to RF EMF (21 real-exposed and 6 sham-exposed) for 15 minutes. Measurements were performed during ortostatic test (transition movement of body from a stand to lay position). We conducted this blind protocol twice in well controlled conditions under control (sham-exposure) and trial (HR EMF exposure) conditions. Only probands with good health conditions, without acute or chronic diseases or any medications were included. They were not allowed to drink alcoholic and caffeine beverages and to smoke at least 12 hours before trial.

According to International Commission on Non-Ionizing Radiation Protection (ICNIRP [6]) safety standards, the maximum RMS (Root Mean Square) intensity of electric field (E) in 1800 MHz band is 58.34 V/m. Measurements were conducted by broadband meter Narda 550 (Narda Safety Test Solutions, Germany) which is certified for E measurements in a near field. Our exposure system comprises of functional signal generator Agilent N9310A (Agilent Technologies, USA) and 5 W amplifier 5S1G4 (Amplifier Research, USA) commonly used to produce 1788MHz sine wave with $E = 54 \pm 1.6$ V/m at the exposure position. We employed two loop antennas, one for stand position and one for lay position (where the head of person was located).

Results

Supine position was characterised by decrease in heart rate (HR) and rMSSD (root Mean Square Successive Difference – reflecting an increase in parasympathetic activity) in lying position after the RF EMF exposure (HR before exposure: 65.2 ± 5 , after exposure: 61.9 ± 5 , $p < 0.005$; rMSSD before exposure: 75.7 ± 57.4 , after exposure: 84.9 ± 58.7 , $p < 0.005$; mean \pm SD) in comparison to sham-exposure (HR before exposure: 61.2 ± 2.9 , after exposure: 60.0 ± 2.8 , $p = 0.5$; rMSSD before exposure: 67.7 ± 28.2 , after exposure: 59.7 ± 21.7 , $p = 0.3$; mean \pm SD). This result supports also frequency analysis of HRV, where increase in high frequency (HF) band spectral power also indicates increase in vagal activity (Power HF before exposure: 2311.7 ± 1101.0 , after exposure: 2717.4 ± 1419.0 , $p < 0.05$) comparing to sham-exposure (Power HF before exposure: 1689.6 ± 1450.1 , after exposure: $1322.5 \pm$

1174.9, $p = 0.5$). We did not detect any significant changes in LF (low frequency) component (which reflects mostly sympathetic activity) nor in stand position.

Conclusion

Our findings proved that short time exposure to generated RF EMF for 15 minutes was characterized by a comprehensive response of the cardiovascular system with increase in parasympathetic activity.

Acknowledgment

This study was supported (100%) by Slovak Research and Development Agency under the contract No. APVV-0189-11 (prof. Jakus).

References

- [1] J.C. Lin (ed.) Electromagnetic fields in biological systems. Boca Raton: CRC Press (2011).
- [2] V. Jakušová Ultrafialové žiarenie a mobilná komunikácia: fyzikálne vlastnosti, biologické účinky a ochrana zdravia. Bratislava: Samosato (2009).
- [3] L. Hardell, K.H. Mild, M. Carlberg Further aspects on cellular and cordless telephones and brain tumours. *Inter J Oncol* (2003) 22:399-407.
- [4] Belyaev I. Biophysical Mechanisms for Nonthermal Microwave Effects. In: M Markov (Ed.) *Electromagnetic Fields in Biology and Medicine*. Boca Raton: CRC Press (2015).
- [5] M.S. Markov Expanding use of pulsed electromagnetic field therapies. *Electromagn Biol Med.* (2007), 26(3):257-74.
- [6] ICNIRP guidelines for limiting exposure to time-varying electric, magnetic and electromagnetic fields (up to 300 GHz). (1998) ICNIRP, International Commission on Non-Ionizing Radiation Protection. *Health Phys* 74:494-522.

All-atoms versus „coarse-grained“ approaches for biomacromolecular and nanoparticle modeling

J. ULICNY¹, AND T. KOZAR²

¹ Department of Biophysics, P. J. Šafárik University, Jesenná 5, 041 54 Košice, Slovakia

² Centrum of Interdisciplinary Biosciences, P. J. Šafárik University, Jesenná 5, 041 54 Košice, Slovakia
e-mail: tiber.kozar@upjs.sk

Recent development in hardware and software resources (such as GPU *i.e.* *Graphics Processing Units* computing) influenced research activities in several fields including 3D biomacromolecular and nanoparticle visualization and modeling [1]. These are challenging field for both, model building and simulation methodologies.

New generation of coherent X-ray sources promises to obtain eventually sub-nm resolution images of single, non-repeatable biological objects, within few years. However, at the present state of knowledge and ability of experimental apparatus, whole cell imaging seems to be restricted to cells smaller than few μm . Larger cells and subcellular structures require fixed-target imaging where radiation damage limits resolution of biological objects to 10 nm at best [2]. Diffract-before-destroy experiments enabled by free-electron X-ray lasers are able to circumvent radiation damage, but still provide only 2D images instead of 3D information at the price of nontrivial data processing [3].

In recent years large attention was devoted to monolayer covered gold nanoparticles [4] due to their importance in biomedical research and life sciences, especially in biolabelling. Although several structures are reported every year, the field of molecularly precise noble metal nanoparticles, according Malola and Häkkinen [5] is still in a discovery phase.

There are several Internet resources available allowing on-line building of complex molecular systems. The majority of molecular visualizers (*e.g.* commercial programs like Maestro [6], Discovery Studio [7] or academic VMD [8] among them) allow detailed molecular modeling and simulations on atomistic level. On the other hand, „*in silico*“ building of complex systems, like liposome-based carriers for drug delivery systems in interaction with the particular drugs or complex monolayered nanoparticles having noble metal cores is still far from simplicity and needs diverse building methodologies in order to result in realistic molecular ensembles.

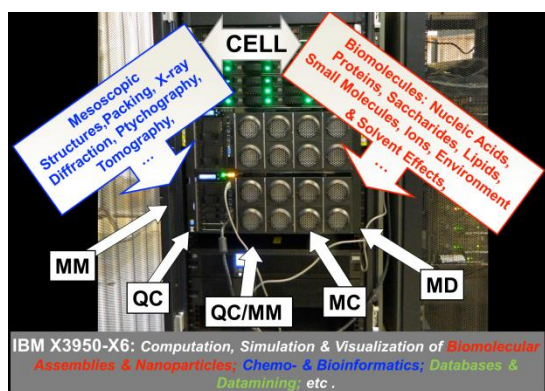


Figure 1: The 240 processors IBM system dedicated for biomodeling, drug and nanodesig

GROMACS, AMBER, NAMD, DESMOND and GALAMOST (the newest package for coarse-grained simulations).

We demonstrate here, that both, in-house hardware and „state of the art“ software resources together with our experience related to model building allow us to carry out comprehensive computations of complex macromolecular systems and nanoparticles of biological interest.

Figure 1 presents the high-end example for our hardware and software resources for modeling task mentioned above. In addition to academic/public domain programs we have access to several commercial packages, *e.g.* GAUSSIAN, SCHRODINGER and BIOVIA. From the comprehensive list of molecular dynamics software/packages we have access to

Multiscale modeling using coarse-grained methodology is very complex research topic applied to proteins [9], nucleosome [10], biomembranes [11] as well as addressing biomedicine-related issues like amyloid fibril nucleation [12]. The references above were selected from a large pool of published papers. Recent search of PUBMED using the Endnote program (‘All Fields’=’Coarse-grained’.and. ‘All Fields’=’molecular dynamics’ .and. ‘All Fields’=’simulation’) returned more than 1500 articles, illustrating that coarse-grained biomolecular modeling is a hot topic with significant research impact.

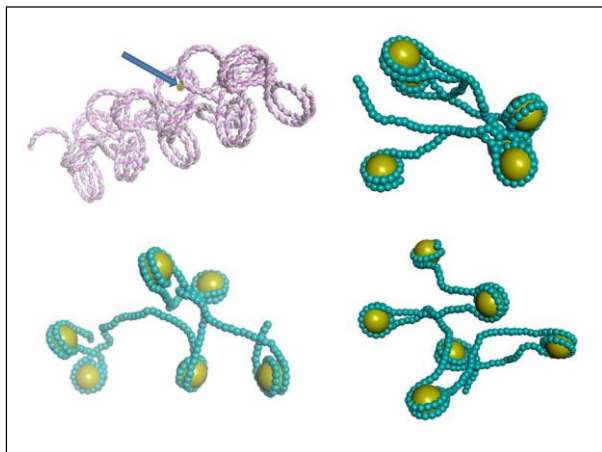


Figure 2: Generated coarse-grained chromatin models. Yellow spheres indicate the histone positions. All-atoms gold nanoparticle incorporated is shown on the upper left figure marked with arrow.

For atomistic simulations we downloaded the structure of nucleosome core particle resolved at 2.5 Å resolution (PDB code 1EQZ) [13]. The 1EQZ structure was “force-field updated” and then minimized. Gold nanoparticle was added to the nucleosome core structure. Figure 2 presents selected structures generated for coarse-grained simulations. The computer-aided modeling of chromosomes is indeed a very complex task due to the large size of these systems. In the case of *E. coli*, the contour length of the 4.6 Mb single circular chromosome is estimated to reach 1.5 mm [14]. For eukaryotic cells the total contour length of DNA is in the order of 1m [15]. Overall, taking into account our hardware and software resources, together our

experience in structure generation, we are ready to develop functionalized gold-marked structure in order to analyze/acquire data from/in free-electron X-ray experiments.

Acknowledgement

This work was supported by the EU 7FP grant CELIM 316310 and Development Agency APVV-0282-11.

References

- [1] T. Kozar, GPU Computing in Biomolecular Modeling and Nanodesign, in: G. Adam, J. Busa, M. Hnatic (Eds.) Lecture Notes in Computer Science: Mathematical Modeling and Computational Sciences, Springer Verlag, Heidelberg, Dordrecht, London, New York, 2012, pp. 276-283.
- [2] M.R. Howells, T. Beetz, H.N. Chapman, C. Cui, J.M. Holton, C.J. Jacobsen, J. Kirz, E. Lima, S. Marchesini, H. Miao, D. Sayre, D.A. Shapiro, J.C. Spence, D. Starodub, *J Electron Spectros Relat Phenomena*, 170 (2009) 4-12.
- [3] A.P. Mancuso, A. Aquila, G. Borchers, K. Giewekemeyer, N. Reimers, Scientific Instrument Single Particles, Clusters, and Biomolecules; (SPB), in, European X-Ray Free-Electron Laser Facility GmbH, 2013, pp. 1-232.
- [4] E. Pohjolainen, H. Häkkinen, A. Clayborne, *The Journal of Physical Chemistry C*, 119 (2015) 9587-9594.
- [5] S. Malola, H. Häkkinen, *Europhysics News*, 46 (2015) 23-26.
- [6] Maestro, version 10.1.012, in: Schrödinger Release 2015-1, Schrödinger, LLC, New York, NY, 2015.
- [7] K.M. Nakagawa, H. Noguchi, *Soft matter*, 11 (2015) 1403-1411.
- [8] W. Humphrey, A. Dalke, K. Schulten, *J. Mol. Graph.*, 14 (1996) 33-38, 27-38.
- [9] A. May, R. Pool, E. van Dijk, J. Bijlard, S. Abeln, J. Heringa, K.A. Feenstra, *Bioinformatics*, 30 (2014) 326-334.
- [10] A.P. Lyubartsev, N. Korolev, Y.P. Fan, L. Nordenskiöld, *J Phys-Condens Mat*, 27 (2015).
- [11] A. Farrotti, G. Bocchini, A. Pallechi, N. Rosato, E.S. Salnikov, N. Voievoda, B. Bechinger, L. Stella, *Bba-Biomembranes*, 1848 (2015) 581-592.
- [12] P. Nguyen, P. Derreumaux, *Accounts of chemical research*, 47 (2014) 603-611.
- [13] J.M. Harp, B.L. Hanson, D.E. Timm, G.J. Bunick, *Acta crystallographica. Section D, Biological crystallography*, 56 (2000) 1513-1534.
- [14] S. Jun, *Biophys J*, 108 (2015) 785-786.
- [15] V.A. Bloomfield, *Current opinion in structural biology*, 6 (1996) 334-341.

Reconstruction of diffractograms in X-ray imaging of biological objects using Bragg Magnifier Microscope

S. HRIVŇAK¹, L. MIKEŠ², J. ULIČNÝ¹, AND P. VAGOVIČ^{3,4}

¹ Department of Biophysics, Faculty of Science, P.J.Šafárik University, Jesenná 5, 041 54 Košice, Slovakia

² Department of Computer Science, Faculty of Science, P.J.Šafárik University, Jesenná 5, 041 54 Košice, Slovakia

³ Center for Free Electron Laser Science, DESY, Notkestrasse 85, 22 607 Hamburg, Germany

⁴ European XFEL, Albert Einstein Ring 19, 22 761 Hamburg, Germany

e-mail: stanislav.hrivnak@student.upjs.sk

Introduction

The in-line Bragg Magnifier Microscope (BMM) [1] is an imaging system composed of highly asymmetric germanium crystals, geometrically magnifying the X-ray beam in both the horizontal and the vertical direction. The sample of interest is placed in front of the BMM and the beam containing the information about the sample is then magnified by means of extreme asymmetric diffraction by germanium crystals. After the magnification, the propagated wavefront is detected by a single photon counting semiconductor detector (e.g. Medipix detector). The obtained image provides just the intensity measurement of the wavefront at the detector plane causing the loss of the phase information, which is also needed for straightforward back propagating of the wavefront to the plane of the original object. This is referred to as the phase problem. Many possible methods to solve this issue have been proposed [2,3], but still lacking generality. In this work, we have implemented propagator calculation and propose the improved iterative phase retrieval algorithm for imaging with BMM. Its performance is demonstrated on the experimentally measured holograms of well-defined samples and more complex objects.

Method

Let U_0 denote the wavefield right behind the sample, which we will refer to as an object plane and let U_D denote the wavefield at the detector plane. The relationship between U_0 and U_D is stated as convolution integral, which becomes multiplication in reciprocal space

$$\tilde{U}_D = H\tilde{U}_0$$

where \tilde{U}_D and \tilde{U}_0 are two dimensional Fourier transforms of U_D and U_0 with respect to the orthogonal coordinates perpendicular to the direction of the beam, respectively and quantity H is called propagator.

We performed the propagator calculation for BMM using the combination of Fresnel free space propagators and crystal functions, which describe the modification of the incoming wavefield reflected by a crystal. This is achieved by considering two beam dynamical theory of diffraction and its universal computational approach proposed by Huang et al. [4].

Secondly, we have developed iterative phase retrieval algorithm, which is the improved version of the algorithm published in [5]. At the beginning of it, the initial support function is defined, which describes the area where we expect the presence of the object. One iteration of the algorithm consists of forward propagating the actual guess of the wavefield U_0 , applying the constraints in the detector plane followed by the backward propagation of actual wavefield at the detector plane U_D and applying the constraints in the object plane. In the detector plane, the only applied constraint is the modulus constraint [2]. In the object plane, first we apply the unwrapping of the phase, then restrict the phases to nonpositive values, which is followed by the calculation of the support update performed by the shrink-

wrap algorithm [6] modified for phase objects. Finally we apply the support constraint and restrict the amplitudes to be not more than one.

Results

Number of testing measurements have been performed using the BMM setup in the last years. Fig.1 shows one of the measurement undertaken in Diamond Light Source Beamline I13 (UK) in July 2013. The sample was Siemens star X-50-30-20 and used energy 10.7 keV. The achieved magnification was determined to be 163.25 in the horizontal and 174.35 in the vertical direction. Middle figure shows the reconstruction using the proposed algorithm. Using the original design of the testing pattern shown in the right part of Fig. 1, the resolution of the imaging setup can be estimated to be around 400 nm in the horizontal and 700 nm in the vertical direction. The agreement between the known form and the reconstructed image is indisputable. After such a prove of concept, we are allowed to move on to the imaging of more complex objects. Fig. 2 shows the hologram and reconstruction of Tardigrada. Results confirm the potential of imaging of biological objects with BMM with the submicron resolution.

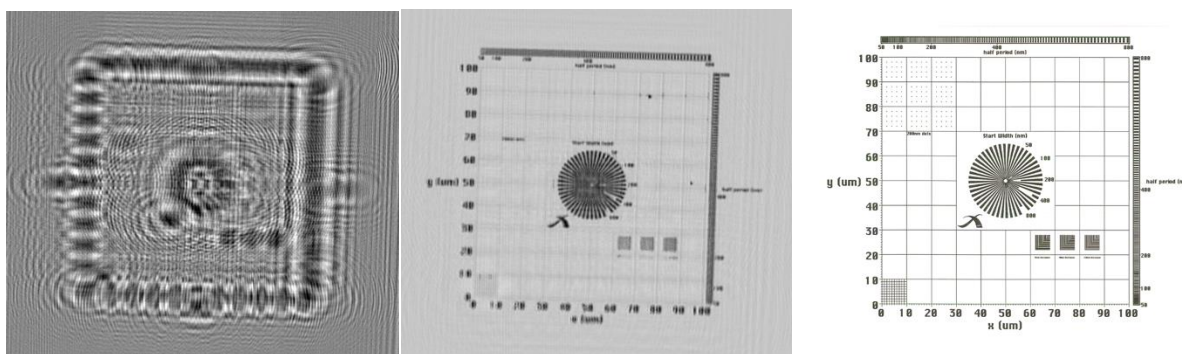


Figure 1. Siemens star X-50-30-20. Left image is the recorded hologram, middle image is the reconstructed image using the described algorithm and the right image shows the ideal design pattern.

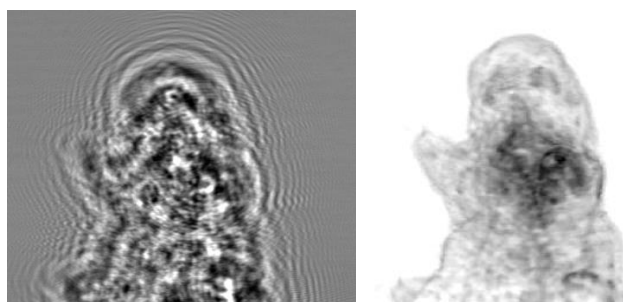


Figure 2. Recorded hologram (left) of Tardigrada and the reconstructed image (right) using the described algorithm.

Acknowledgement

This work was supported by the internal University research grant VVGS-PF-2015-470.

References

- [1] P.Vagovic et. al., *J. Synchrotron Radiat.*, 20 (2013), 153–159.
- [2] J.R.Fienup, *Appl. Opt.*, 21 (1982), 2758–2769.
- [3] A.Burvall et al., *Opt. Express*, 19 (2011), 10359.
- [4] X. Huang et al., *Acta Crystallographica A*, 59 (2003), 163-167.
- [5] P.Vagovic et. al., *Opt. Express*, 22 (2014), 21508–21520.
- [6] S. Marchesini et al., *Phys. Rev. B*, 68 (2003), 140101.





POSTERS
Contributions

Catalytic properties of trypsin and chymotrypsin in the presence of salts

E. DUŠEKOVÁ¹, K. GARAJOVÁ², R. YAVASER³, A. KAŇUKOVÁ², S. HAMADEJOVÁ², AND E. SEDLÁK^{2,4}

¹ Department of Biophysics, P. J. Šafárik University, Jesenná 5, 041 54 Košice, Slovakia

² Department of Biochemistry, P. J. Šafárik University, Moyzesova 11, 040 01 Košice, Slovakia

³ Department of Chemistry, Adnan Menderes University, 09010 Aydin, Turkey

⁴ Centre for Interdisciplinary Biosciences, P. J. Šafárik University, 040 01 Košice, Slovakia

e-mail: eva.dusekova@upjs.sk

Proteolytic enzymes, trypsin and chymotrypsin, are part of large class of enzymes called serine proteases. Serine proteases are widely distributed in nature and found in all kingdoms of cellular life as well as many viral genomes and participate in many important physiological processes, such as digestion, immune responses, blood coagulation, fibrinolysis and reproduction. This family name stems from nucleophilic Ser amino acid residue in the enzyme active site, which attacks the carbonyl moiety of the substrate peptide bond to form acyl-enzyme intermediate. Catalytic triad and oxyanion hole are important for enzyme activity [1–3]. Previous studies have shown that activity and specificity in these enzymes are influenced by residues directly involved in substrate recognition, especially in the primary specificity site and they have also demonstrated the critical role of the two loops outside the binding pocket in controlling the specificity of these two enzymes [1, 4]. Both proteases, trypsin and chymotrypsin, contain catalytic triad composed of Ser195, Asp102, and His57 located in active site between two six-stranded β -barrels. Catalytic mechanisms of these two proteases are similar but their substrate specificities are different. Specificity is usually determined by the residues at positions 189, 216 and 226 which formed S1 binding pocket. The S1 binding pocket in trypsin and chymotrypsin are almost identical in primary sequences and backbone structures. An important difference is that residue 189 is a negatively charged Asp in trypsin and a polar Ser in chymotrypsin. This fact is the reason why trypsin cleaves polypeptide chains after positively charged (Arg and Lys) residues and why chymotrypsin prefers large hydrophobic (Phe, Trp and Tyr) residues [1, 5, 6].

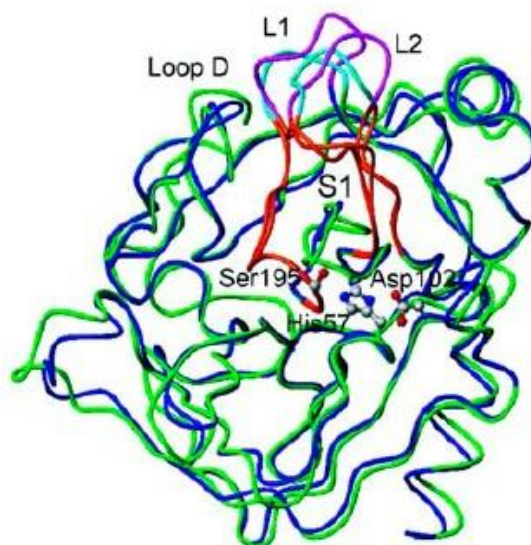


Figure 1. Superposition of trypsin and chymotrypsin. Trypsin is shown in green ribbon and chymotrypsin in blue. Loops of trypsin are shown in magenta; loops of chymotrypsin are shown in pale green. S1 binding pocket is shown in red [1].

It is well known that the Hofmeister effect of ions on biological systems is as ubiquitous as the presence of these ions across all forms of life. Ions influence biomolecular interactions, stability of proteins as well as solubility of proteins in living systems. The most intensively studied Hofmeister effect concerns how ions affect protein/enzyme properties [7]. The kosmotropes, which were believed to be “water structure makers”, are strongly hydrated and have stabilizing and salting-out effects on proteins and macromolecules. On the other hand, chaotropes (“water structure breakers”) are known to destabilize folded proteins and give rise to salting-in behaviour [8]. Previous studies revealed that the effect of ions on enzyme activity usually follows the Hofmeister series but despite the intensive studies, the Hofmeister effect of ions on catalytic properties is not well understood [7, 9]. Therefore, we decided to study stability and catalytic activity of trypsin and chymotrypsin in the presence of salts of the Hofmeister series, such as NaBr, NaCl, NaClO₄ and Na₂SO₄. We compared the effect of concentration of four anions on activity and thermal stability of bovine pancreas trypsin and alpha-chymotrypsin. The influence of studied anions on the stability of trypsin and chymotrypsin is in agreement with Hofmeister series, i.e. kosmotropic sulphate stabilizes enzymes, whereas chaotropic perchlorate destabilizes them. We observed analogous effect of anions on catalytic properties of these enzymes. Whereas the kosmotropic sulphate increases the activity of enzymes, chaotropic perchlorate and chloride, decrease the maximal velocity of the reaction. Analysis of the effect of anions on the enzymes indicates that anions effect can be compared to mixed inhibitors. The correlation between parameters characterizing catalytic properties with different anion properties, such as polarizability, charge density, viscosity B-coefficient, leads to the conclusion that the Hofmeister effect is determined mainly by charge density which is in agreement with the results of our previous experimental studies.

Acknowledgement

This work was supported by the research grant from VVGS-PF2015-478, VEGA 2/0062/14, VEGA 1/0423/16 and by a grant from CELIM (316310) funded by 7FP EU Programs REGPOT.

References

- [1] W. Ma, Ch. T. and L. Lai, *Biophysical Journal* 89 (2005), 1183-1193.
- [2] L. Polgár, *Cell. Mol. Life Sci.* 62 (2005), 2161-2172.
- [3] M. J. Page and E. Di Cera, *Cell. Mol. Life Sci.* (2008), 1220-1236.
- [4] E. R. Guinto, S. Caccia, T. Rose, K. Fütterer, G. Waksman and E. Di Cera, *Proc. Natl. Acad. Sci. USA* 96 (1999), 1852-1857.
- [5] L. Hedstrom, *Chem. Rev.* 102 (2002), 4501-4523
- [6] E. Di Cera, *IUBMB Life* 61 (2009), 510-515.
- [7] E. Sedlák, L. Stagg and P. Wittung-Stafshede, *Archives of Biochemistry and Biophysics* 479 (2009), 69-73.
- [8] Y. Zhang and P. S. Cremer, *Curr. Opin. Chem. Biol.* 10 (2006), 658-663.
- [9] Z. Yang, *Journal of Biotechnology* 144 (2009), 12-22.

On a quest to finding the most effective method for glucose oxidase deflavination

K. GARAJOVÁ¹, E. DUŠEKOVÁ², AND E. SEDLÁK^{1,3}

¹ Department of Biochemistry, P. J. Šafárik University, Moyzesova 11, 040 01 Košice, Slovakia

² Department of Biophysics, P. J. Šafárik University, Jesenná 5, 040 01 Košice, Slovakia

³ Centre for Interdisciplinary Biosciences, Jesenná 5, 040 01 Košice, Slovakia

email: katarina.garajova@student.upjs.sk

Glucose oxidase (GOX) is homodimeric glycoprotein, which contains one molecule of FAD cofactor noncovalently, but strongly bound to each subunit [2, 3]. The carbohydrate content (mainly D-mannose, D-galactose and D-glucosamine) of the enzyme differs in dependence on a source. It is usually 16-25% when isolated from its main sources, the bacteria and moulds (the main producers being genera *Penicillium*, for the former and *Aspergillus*, for the latter) [2]. It is also possible to isolate recombinant GOX cloned in yeasts,

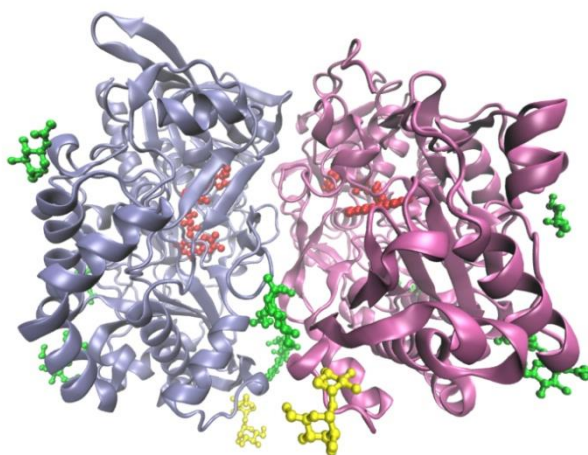


Figure 1 The representation of glucose oxidase (1GFE) [1] in its dimeric form, with 1 FAD molecule (red) bound to each subunit (blue and violet). The displayed carbohydrates on the protein surface are D-glucosamine (green) and D-mannose (yellow).

although it was reported that such GOX has significantly higher carbohydrate content (up to 60%) [4]. The primary role of GOX is oxidation of glucose, leading in last step towards hydrogen peroxide formation, with cofactor FAD playing the role of a redox carrier [2, 3]. The glucose biosensors which are used in medicine to determine the amount of glucose in the blood samples are based on this reaction. Even though, there are other proteins which use glucose as their substrate, each of them lacks some of the important properties for enzyme-based biosensor such as high stability, selectivity and turnover [2]. For example, glucose dehydrogenases require cofactor for activity, quinoprotein glucose dehydrogenases

is relatively unstable, and glucose-2-oxidases are not specific enough toward β -D-glucose [2]. Due to GOX-based biosensors high importance in medicinal practise, there is an ongoing tendency to improve their functions. For this to happen, it is important to understand how tightly-bound cofactor and covalently bound carbohydrates affect the enzyme properties. Here we methodically search for the best method of the preparation of apoform of GOX. Detailed study of thermodynamic properties of the apo-GOX and their comparison with the properties of the holoform of GOX enables us to assess the effect of the cofactor on stability and structure of the enzyme.

It is known, that the prolonged exposure of protein to non-native conditions, such as extreme pH and presence of denaturants can lead to its irreversible denaturation [5]. The main approach of any deflavination method is to modify conditions in solution to cause FAD dissociation without inducing irreversible changes in protein structure, thus allowing GOX to regain its function after refluination. All deflavination methods are based on either weakening of flavin binding or stabilization of apo-protein. Established strategies include low

pH, increased salt concentration, modification of different properties of solvent and combinations of these factors [5].

There are four basic methods for preparation of apo-GOX described in literature: (i) Akhtar et al. [6] used the presence of divalent cations, calcium and magnesium, (ii) Zlateva et al. [7] were able to prepare the apo-GOX by the effect of nucleophilic agents such as KCN, KOCN and KSCN, (iii) Massey et al. [8] used 3M KBr, and (iv) Swoboda [9], in which the author used the saturated ammonium sulphate at very acidic pH, pH 1.4, as deflavination agent.

In our project, all of the aforementioned methods have been tested including several modifications. In our hands, we were able to reproduce only the method developed by Swoboda [9]. The spectrum of apo-GOX prepared by this method showed that FAD molecules were completely dissociated from protein. CD spectra further indicated that the secondary structure of apo-GOX is not significantly affected in comparison with holo-GOX. Successful reconstitution of apo-GOX with FAD was demonstrated by cooperative thermal transition of the reconstituted GOX. However, this reconstitution is not ideal as only about 50% of apo-GOX reversibly bound the cofactor. Clearly, it is desirable to improve this deflavination method. In the future research we explore, in detailed manner, the synergic effects of low pH and the presence of denaturation agents such as urea and guanidium hydrochloride in variation with the original method, in which the denaturation agent was represented by ammonium sulphate.

Acknowledgement

This work was supported by the research grants VVGS-PF-2015-478, research grants from the Slovak Grant Agency VEGA no. 2/0062/14 and no. 1/0423/16 and by grant from CELIM (316310) funded by 7FP EU Programs REGPOT.

References

- [1] G. Wolfhart, S. Witt, J. Hendle, D. Schomburg, H. M. Kalisz and J. H. Hecht, *A. Crystallogr., sect. D*, 55 (1999), 969 - 977.
- [2] R. Wilson and A.P.F. Turner, *Biosens. Bioelektron.* 7 (1992), 165-185.
- [3] V. Leskovic, S. Trivić, G. Wohlfahrt, J. Kandrač and D. Peričin, *Int. J. Biochem. Cell B.* 37 (2005), 731-750.
- [4] A. Kohen, T. Jonsson and J.P. Klinman, *Biochemistry* 36 (1997), 2603-2611.
- [5] M.H. Hefti, J. Vervoort and W.J.H. van Berkel, *Eur. J. Biochem.* 270 (2003), 4227-4242.
- [6] S. Akhtar, A. Ahmad and V. Bhakuni, *Biochemistry* 41 (2002), 7142-7149.
- [7] T. Zlateva, R. Boteva, B. Fillippi, M. Veenhuis and I.J. van der Klein, *BBA* 1548 (2001), 213-219.
- [8] V. Massey and B. Curti, *JBC* 241 (1966), 3417-3423.
- [9] B.E.P. Swoboda, *BBA* 175 (1969), 365-379.

Correlation between perturbation of heme region and peroxidase-like activity of cytochrome *c*

N. TOMÁŠKOVÁ¹, R. VARHAČ¹, K. GARAJOVÁ¹, AND E. SEDLÁK^{1,2}

¹ Department of Biochemistry, Faculty of Sciences, P. J. Šafárik University, Moyzesova 11, 040 01 Košice, Slovakia

² Centre for interdisciplinary biosciences, Faculty of Sciences, P. J. Šafárik University, Jesenná 5, 041 54 Košice, Slovakia

e-mail: natasa.tomaskova@upjs.sk

Classical view on cytochrome *c* (cyt *c*) is that the protein is electron shuttle between respiratory complexes III and IV in mitochondria. But studies of last decades show other important roles of cyt *c* in cell, e.g. as a superoxide scavenger [1] and as a critical cell death factor for initiating the caspase cascade [2]. These important biological activities of cyt *c* are realized in its native structure. Moreover, Gebicka documented that unfolding of cyt *c*'s globule reveals a new function as peroxidase [3].

This small globular protein is often used as a good model for study local conformational changes in heme proteins. Native state of cyt *c* is a form when the sixth ligand of heme iron is occupied with Met80. Due to natural dynamics of the heme region, which includes residues 70-85 of the polypeptide chain, cyt *c* protein can switch between the native form (6-coordinated low spin Fe) and the so-called open form cyt *c* (6-coordinated and/or 5-coordinated high spin Fe). The rate of the dynamics and thus the fraction of the opened form of cyt *c* can be modified by denaturants such as urea or guanidium hydrochloride.

Our previous results suggest that the rate of interaction of heme iron with small external molecules (as CN⁻) is controlled by the polypeptide chain flexibility as a result of anion action on the water/protein arrangement [4, 5, 6]. In the present work, we show a correlation between binding of cyanide to heme iron with peroxidase-like activity monitored by guaiacol oxidation. The properties of heme region of cyt *c* are modified by increased urea concentration in the range from 0 to 6M at neutral and slightly acidic pH.

The conformational change of cyt *c* was monitored by absorption spectrometry at Soret region that reflects changes in the heme region and by fluorimetry that reflects changes in tertiary structure of protein.

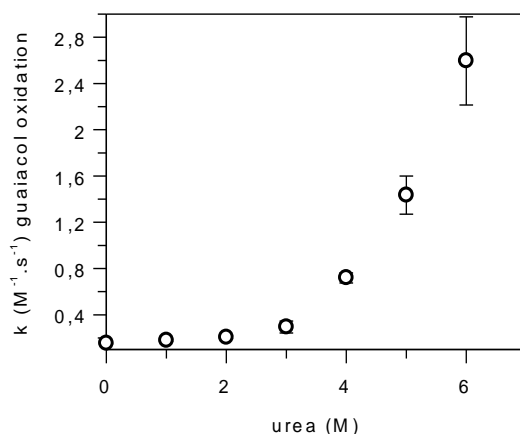


Figure 1 Comparison effect of urea concentration on *k* values of guaiacol oxidation and fluorescence intensity at 350nm of cyt *c*

Our results of urea effect on conformational properties of cyt *c*, its ability to bind cyanide as well as its peroxidase-like activity indicate that the peroxidase-like activity of cyt *c* is not accompanied by conformational change. On the other hand, the correlation between rate constant of cyanide binding and peroxidase-like activity of cyt *c* strongly indicates an involvement of dynamics in inducing of peroxidase-like activity in cyt *c*. Our results give a good illustration of cyt *c* properties at its physiological environment at the membrane interface.

Acknowledgement

This work was supported by the research grants from the Slovak grant agency VEGA no. 2/0062/14 and 1/0423/16 and the grant from CELIM (316310) funded by 7FP EU Programs REGPOT.

References

- [1] V. P. Skulachev, *FEBS Lett.* 423 (1998), 275-280.
- [2] X. Liu, C.N. Kim, J. Yang, R. Jemmerson, X. Wang, *Cell* 86 (1996), 147-157.
- [3] L. Gebicka, *Res. Chem. Intermed.* 27 (2001), 717-723.
- [4] R. Varhač, *BBA* 1834 (2013), 739-744.
- [5] R. Varhač, N. Tomášková, M. Fabián, E. Sedlák, *Biophys. Chem.* 144 (2009), 21-26.
- [6] N. Tomášková, R. Varhač, G. Žoldák, L. Olekšáková, D. Sedláková, E. Sedlák, *J. Biol. Inorg. Chem.* 12 (2007), 257-266.

Targeted mutagenesis of the gene *KCNJ2* for the potassium channel Kir 2.1

M. PETREŇÁKOVÁ

¹ Department of Biophysics, P. J. Šafárik University, Jesenná 5, 040 01 Košice, Slovakia

² Institute of molecular biology and biotechnology, Faculty of Pharmaceutics, VFU Brno
e-mail: martina.petrencakova@gmail.com

Gene *KCNJ2* codes inwardly rectifying potassium channel Kir 2.1. Kir 2.1 is an integral membrane protein responsible for cell excitability and resting membrane potential in skeletal muscles, heart and brain. Mutations in this gene cause different patho-physiological conditions such as Andersen-Tavil syndrome, short QT syndrome, familial atrial fibrillation [1,2,3].

The aim of this work was to design point mutations in gene *KCNJ2* and study the influence of this exchange on function of the channel. Plasmid *pcDNA3* containing this gene was provided by Dr. Marcel van der Heyden, Utrecht University, Netherlands. Two point mutations on nucleotide level G436C and T438C were chosen. On the level of amino acids these mutations are responsible for the consequent change of G146R. Mutation in this position are known to be responsible for Andersen Tavil syndrome [4] (Fig. 1). The change of function is supposed based on completely different properties (charge and size) of these two aminoacids.

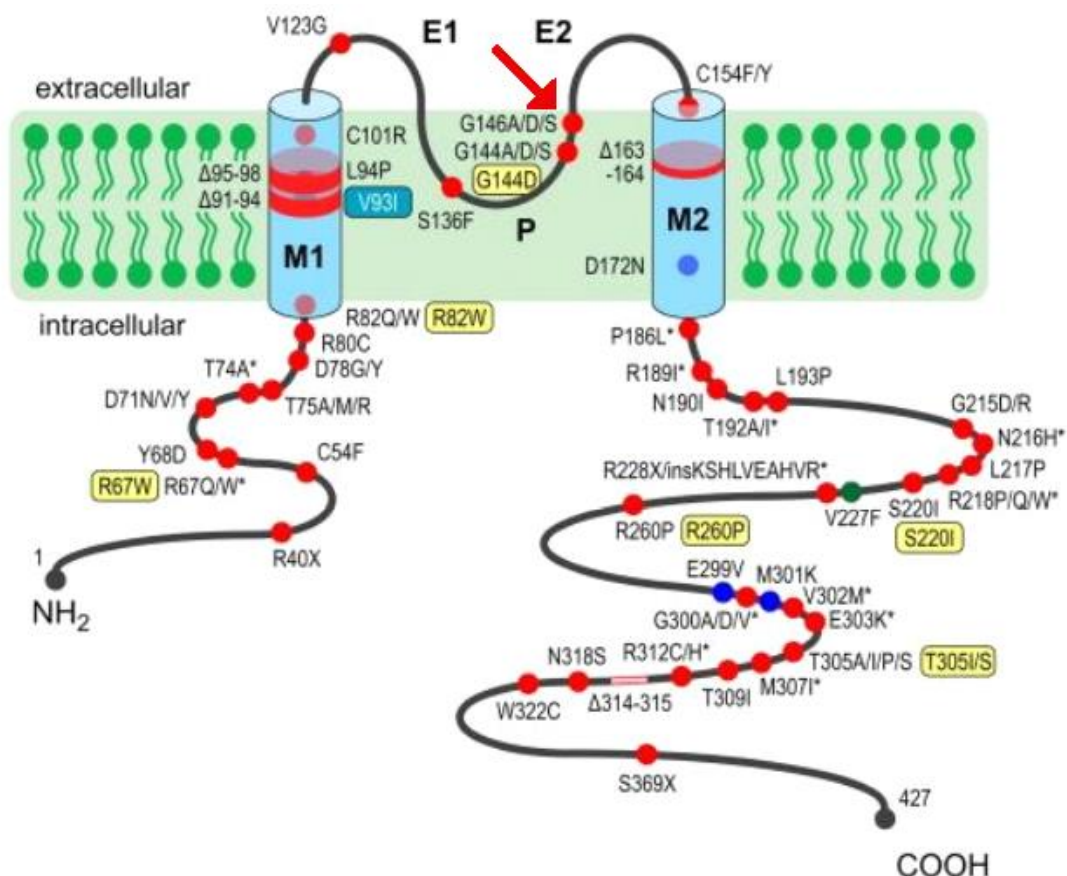


Figure 1. Previously studied mutations on Kir2.1 protein associated with channelopathies [4].

The mutation was completed *in vitro* with the set *QuickChange II XL Site-Directed Mutagenesis Kit* from the company Agilent Technologies. The results of mutagenesis were verified by the Sanger's sequencing method by the company GATC Biotech (Germany).

Successful point mutations and high efficiency transformation are good conditions for future expression and functional analysis of protein Kir 2.1 with mutation G146R with various methods for example *patch-clamp*.

References

- [1] NGUYEN, Hoai-Linh, Gerard H. PIPER, Ronald WILDERS. Andersen-Tawil syndrome: Clinical and molecular aspects. *International Journal of Cardiology*, 2013, 170, 1, 1-16.
- [2] PRIORI, Silvia G., Sandeep V. PANDIT, Ilaria RIVOLTA et al., A Novel Form of Short QT Syndrome (SQT3) is caused by a Mutation in the KCNJ2 gene. *Circulation research*, 2005, 96, 800-807.
- [3] XIA, Min, Qingfeng JIN, Saïd BENDAHHOU et al., A Kir 2.1 gain-of-function mutation underlies familial atrial fibrillation. *Biochemical and Biophysical Research communications*, 2005, 332, 4, 1012-1019.
- [4] KIM, June-Bum, Ki-Wha CHUNG. Novel de novo Mutation in the KCNJ2 Gene in a Patient with Andersen Tawil Syndrome. *Pediatric Neurology*, 2009, 41, 6, 464-466.

Kinetics of the interaction between intrinsically disordered protein tau and antibody Fab fragment against its C-terminus

O. CEHLÁR^{1,2}, M. JANUBOVÁ², R. ŠKRABANA^{1,2}, AND M. NOVÁK^{1,2}

¹ Institute of Neuroimmunology, Slovak Academy of Sciences, Dubravska cesta 9, 845 10 Bratislava, Slovakia

² Axon Neuroscience SE, Dvorakovo Nabrezie 10, 811 02 Bratislava, Slovakia

e-mail: ondrej.cehlar@savba.sk

The binding of prevalently rigid globular proteins tends to be limited by the diffusional approach toward their targets, and has been the subject of many experimental and computational studies. For flexible proteins, the binding mechanisms become much more complicated, presenting challenges to mechanistic interpretation of experimental observations [1]. The Alzheimer's disease-associated protein tau is a typical representative of flexible, disordered protein. Under physiological conditions, tau associates with microtubules and regulates their dynamics, whereas during the progression of neurodegeneration tau dissociates from microtubules, misfolds and deposits in brain tissue creating neurofibrillary tangles composed of paired helical filaments.

We have monitored the interaction of intrinsically disordered protein tau with antibody Fab fragment with epitope on the C-terminal part of tau molecule by surface plasmon resonance spectroscopy. All six human full length tau isoforms and tau variants truncated from N-terminus were used to study the binding kinetics with antibody Fab fragment (Figure 1). We have observed differences in values of rate constants for diverse tau variants, what suggests changed properties of tau conformational ensemble depending on tau primary structure, where the distant parts of tau molecule modulate the binding properties of its C-terminus.

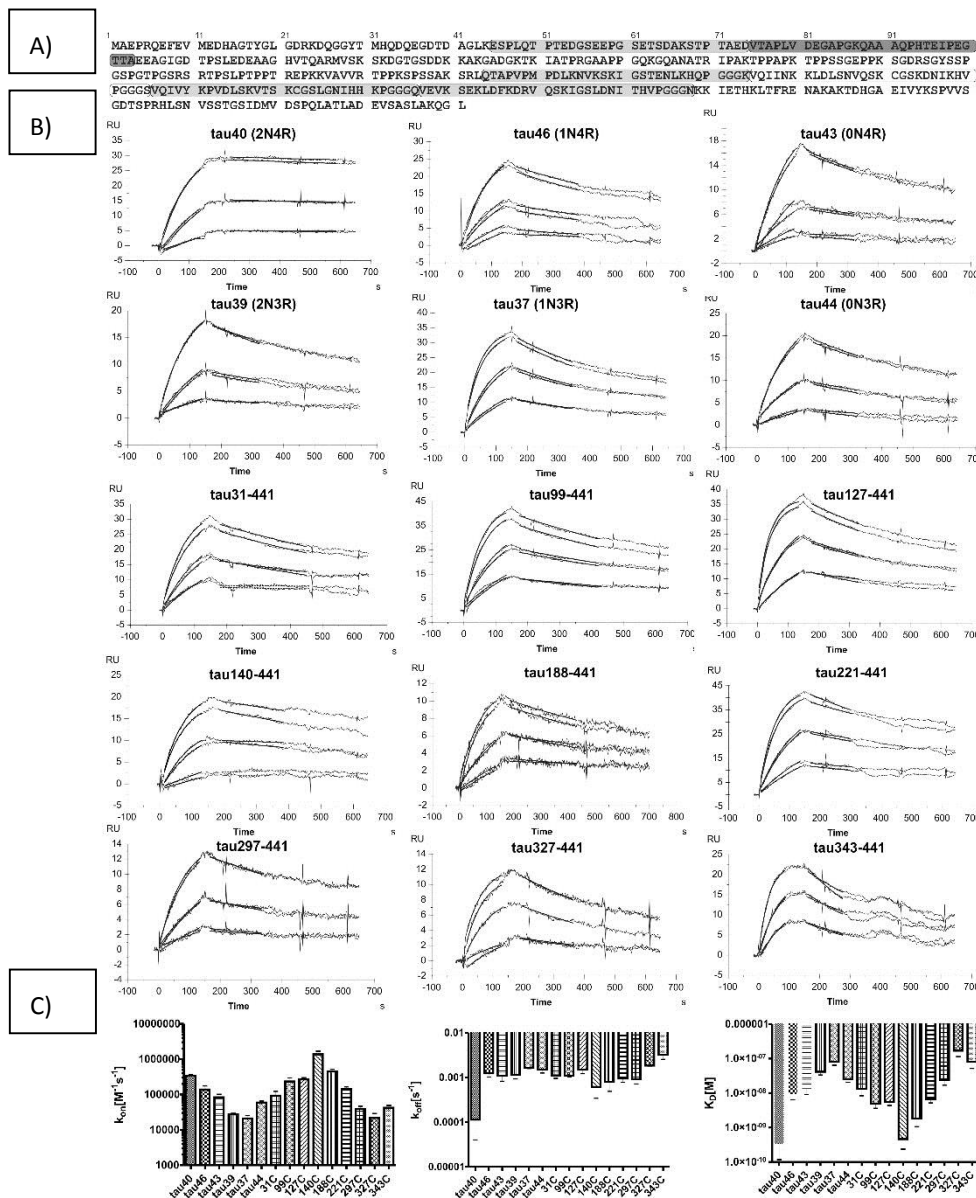


Figure 1 Kinetics of the binding of antibody with tau proteins. A Primary sequence of the longest human tau isoform (tau40-2N4R), the N-terminal inserts and microtubule binding repeats (MTBRs) are shown in boxes. The second MTBR that is not present in three repeat tau isoforms is shown in white box. **B** The sensorgrams of the interaction of DC39C antibody with various tau proteins. **C** The values of kinetic constants k_a , k_d and K_D shown in graphs.

Acknowledgement

This work was supported by the research grant from the Slovak Research and Development Agency under the contract No. APVV-0677-12 and the Slovak Grant Agency Vega No. 2/0177/15.

References

[1] H.X. Zhou, X.D. Pang, and C. Lu *Physical Chemistry Chemical Physics* 14 (2012), 10466-10476.

Influenza haemagglutinin fusion peptide: a story of three aminoacids that matter

A. FILIPEK, J. KRUPA, AND R. WORCH

Institute of Physics Polish Academy of Sciences, Al. Lotników 32/46, PL-02-668 Warsaw, Poland

Influenza virus is one of the most common viruses infecting people. The virus enters a cell by endocytosis and then has to pass membrane of endosome to enter cytoplasm. One of the proteins in viral membrane is haemagglutinin (HA). N-terminal part of haemagglutinin, fusion peptide anchors into endosomal membrane and participate in fusion between viral and endosomal membranes. The length of the haemagglutinin fusion peptide (HAfp) is not strictly defined. Most of the previous studies focus on 20 amino acids (aa) variant (HAfp20), which has boomerang-shape secondary structure. The next three aa (W₂₁Y₂₂G₂₃) are strictly conservative in all HA mutants. Recent studies unravel that addition of this three aa to HAfp20 changes its structure to hairpin (HAfp23) [1].

Knowing how important is correlation between structure and function for proteins and peptides, our studies have been focused on the differences between function of 20 and 23 aa HAfp. The Gibbs energy (ΔG) of association HAfp20 and HAfp23 with a membrane and their capability to enhance fusion between vesicles have been determined. Moreover, we have investigated the effect of cholesterol on HAfp function.

ΔG values were obtained using partition coefficients (K_x). K_x was determined by titration of HAfp with small unilamellar vesicles (SUV) and measuring fluorescence spectrum of tryptophan as described in [2]. The changes of tryptophan spectrum with increasing liposomes concentration allow to estimate the fraction of peptide in lipids and water environment.

To measure fusion capability of HAfp20 and HAfp23, two assays have been used. Both were based on FRET effect between NBD (donor) and rhodamine (acceptor). In first type of experiments, a small fraction of large unilamellar vesicles (LUV) were labelled with NBD and rhodamine, while the rest of LUV were unlabelled. After fusion caused by HAfp, labelled and unlabelled vesicles fused with each other resulting in an increase of the distance between dyes which leads to a decrease of rhodamine fluorescence intensity.

Second assay measured FRET between NBD-labelled giant unilamellar vesicles (GUV) and rhodamine labelled LUV. Fusion between vesicles was observed as decrease in fluorescence lifetime of the excited-state of NBD.

The obtained results show that at pH 5, ΔG of membrane-protein interaction is not significantly different for HAfp20 and HAfp23. Addition of cholesterol to DOPC membranes decreases the absolute value of ΔG . HAfp23 has higher fusion capability than HAfp20, and cholesterol increases fusion capability of both peptides. In cholesterol enriched membranes, phase separation have been observed only when HAfp23 was added.

In conclusion, the different structures of HAfp20 and HAfp23 affect their functionality and ΔG of the peptide-membrane interaction does not correspond with the fusion capability of the peptides.

References:

- [1] R. Worch, *Acta Biochemica Polonica*, Vol. 61, No.3, pp. 421-426, 2014
- [2] Ladokhin et al., *Analytical Biochemistry*, Vol. 285, pp. 235-245, 2000

The shape of mitochondria and its changes during oxidative stress

L. LENKAVSKA¹, A. FRAGOLA², F. SURREAU³, P. MISOVSKY^{4,5}, S. BONNEAU³, AND Z. NADOVA^{1,4}

¹ Department of Biophysics, P.J.Safarik University, Jesenna 5, 041 54 Kosice, Slovakia

² Laboratoire Physique et d'Etude de Matériaux, Université Pierre et Marie Curie, Paris, France

³ Laboratoire Jean Perrin, Université Pierre et Marie Curie, Place Jussieu 4, 752 52 Paris, France

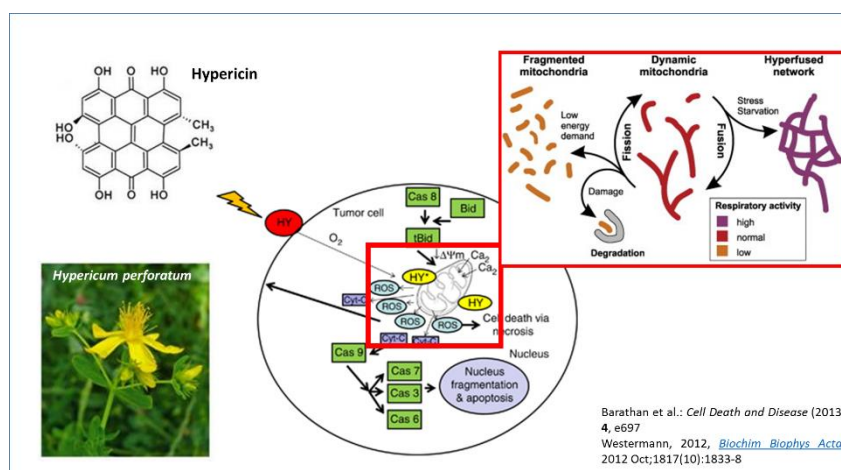
⁴ Center for Interdisciplinary Biosciences, P.J.Safarik University, Jesenna 5, 04001 Kosice, Slovakia

⁵ SAFTRA Photonics, Jesenna 5, 04001 Kosice, Slovakia

e-mail: lenka.lenkavska@gmail.com

Mitochondria play an important role in cellular processes associated with energy metabolism, ROS production and cell death. Oxidative stress is generally defined as an imbalance between the production of reactive oxygen species (ROS) and cellular antioxidant defense mechanisms. High unregulated level of ROS leads to oxidative stress, which is involved between signals inducing cell death/apoptosis. On the level of mitochondria, overproduction of ROS results in permeabilization of the mitochondrial membrane and the collapse of the mitochondrial network. This work is focused on raising the production of ROS after photoactivation of hypericin (HYP) in HeLa cells. Oxidative stress was induced after 1 hour incubation of cells with 5×10^{-9} M Hyp which were immediately irradiated with light ($\lambda=690\text{nm}$) dose 1 J/cm^2 vs 4 J/cm^2 .

We investigated the influence of ROS on the shape and structure of mitochondria using microscopic methods – fluorescence microscopy, 3D SIM and electron microscopy. Internal structure of mitochondria was observed by three-dimensional (3D) structured-illumination microscopy. Flow cytometry was used for assessment of cell survival and apoptosis, dissipation of mitochondrial membrane potential and for verifying of ROS production in HeLa cells.



Results

We show that ROS production in cells and/or mitochondria significantly depends on light dose used for Hyp photo-activation (Fig.1). Arising oxidative stress has a strong impact on mitochondrial organization in intracellular space. Network of tubular mitochondria is fragmented under oxidative stress (Fig. 1, inserted images). Observed fragmentation seems to be reversible process when cells are irradiated by lower light dose (1 J/cm^2). Serious oxidative stress induced by Hyp photo-activation by higher light dose (4 J/cm^2) leads to irreversible

changes in mitochondrial structure and function (dissipated mitochondrial membrane potential ($\Delta\psi_m$)).

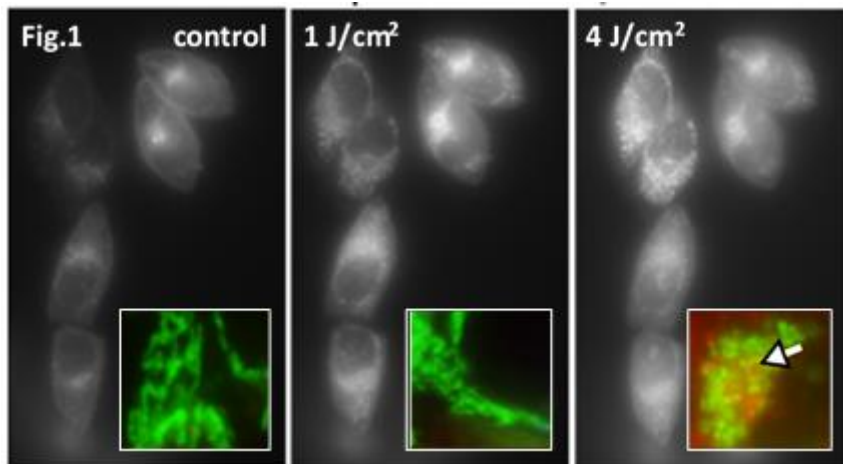


Fig. 1: Fluorescence images of O_2^- production in mitochondria after Hyp irradiation (light dose $1J/cm^2$ vs $4J/cm^2$) visualized by fluorescence microscopy after MitoSOX Red staining. Insert images: Mitochondria after MitoTracker Red staining

Tab.1 CELL SURVIVAL		live (%)	apoptosis (%)	dead (%)
	control	97,99	1,51	0,5
	Hyp control	96,38	3,41	0,21
1 J/cm²	immediately after irradiation	96,26	3,5	0,24
	1h after irradiation	96,77	3	0,23
	2h after irradiation	95,59	4,25	0,24
	3h after irradiation	93,64	5,79	0,57
4 J/cm²	immediately after irradiation	96,07	3,83	0,2
	1h after irradiation	85,2	13,48	0,82
	2h after irradiation	85,82	14,22	0,33
	3h after irradiation	80,81	18,82	0,37

Tab. 1: Percentage of viable, apoptotic and dead cells under oxidative stress was determined by flow cytometry (Annexin V-FITC/Propidium iodide staining)

Dissipation of $\Delta\psi_m$ represents the point of no return when cells start cell death program and undergo apoptosis (Tab.1). Observed changes in the shape, organization and functions of mitochondria under oxidative stress correlate with apoptotic program development.

Acknowledgement

This work was supported by the 7RP EU CELIM 316310 and SF Sofos ITMS 26110330088.

References

- [1] M. Ott, V. Gogvadze, S. Orrenius, B. Zhivotovski, Mitochondria, oxidative stress and cell death. In *Apoptosis*, 12:913–922 (2007).
- [2] M. Tim, Rapid colorimetric assays for cellular growth and survival: application to proliferation and cytotoxicity assays. In *Journal of Immunological Methods* 65 (1–2): 55–63 (1983).
- [3] L. Shao, et al.. Super-resolution 3D microscopy of live whole cells using structured illumination. In *Nature*. vol.8 doi:10.1038/nmeth.1734 (2011).
- [4] Barathan et al.: *Cell Death and Disease* (2013) 4, e697
- [5] Westermann, 2012, *Biochim Biophys Acta*. 2012 Oct; 1817 (10):1833-8

Activation and relocalization of Protein kinase C- α and Protein kinase C- δ in U-87MG glioma cells after hypericin treatment

M. MISUTH¹, Z. NADOVA^{1,2}, P. MISOVSKY^{1,2}, AND V. HUNTOSOVA^{1,2}

¹ Department of Biophysics, Faculty of Science, P.J. Safarik University (UPJS) in Kosice, Jesenna 5, 041 54 Kosice, Slovakia

² Center for Interdisciplinary Biosciences, Faculty of Science, P.J. Safarik University (UPJS) in Kosice, Jesenna 5, 041 54 Kosice, Slovakia

e-mail: matus.misuth@gmail.com

Protein kinase C is family of protein kinase enzymes that are involved in regulation of many cellular processes, cell survival and apoptosis among them. The correlation was found between apoptosis and expression of proapoptotic PKC- δ (PKC δ) and antiapoptotic PKC- α (PKC α) isoforms in glioma cells. One of the molecules which strongly influence PKCs activity is highly hydrophobic molecule hypericin. This may lead to significant decrease of cell viability through apoptosis.

The activity of both kinases in U-87MG cells after hypericin treatment was analyzed by western blotting. The most important phosphorylation sites are Ser645 (p(S645)PKC δ) at PKC δ and Thr638 (p(Thr638)PKC α) at PKC α . It was shown that 500 nM hypericin after photo-activation increased autophosphorylation of p(S645)PKC δ and catalytically competent form p(Thr638)PKC α . This effect is amplified with the time of hypericin incubation and the light dose applied.

The distribution of p(S645)PKC δ and p(Thr638)PKC α was observed by confocal fluorescence imaging. Hypericin treatment induced redistribution of p(S645)PKC δ mainly between Golgi apparatus and nucleus. Later after photo-activation p(S645)PKC δ is released into cytoplasm. In contrary localization of p(Thr638)PKC α was observed in cytoplasm and shortly after photo-activation it is relocalized toward the plasma membrane.

Taken all together, in the present work it was shown that hydrophobic hypericin causes activation of both PKC kinases in different cellular compartments. This could have important impact on cellular response to treatment and finally type of cell death.

Acknowledgement

This work was supported by: the FP7 EU project CELIM 316310, the project of the Slovak Res. And Dev. Agency APVV-0242-11 and by the grant of Faculty of Science at UPJS in Kosice: VVGS-PF-2015-475.

Singlet Oxygen Photosensitized by Hypericin in Dimethyl-Sulfoxide

J. VARCHOLA, K. ŽELONKOVÁ, D. JANCURA, P. MIŠKOVSKÝ, AND G. BÁNÓ

Department of Biophysics, P. J. Šafárik University, Jesenná 5, 041 54 Košice, Slovakia.
e-mail: jarovarchola@gmail.com

Hypericin (Hyp) is a photosensitizer studied intensively for its possible application in photodynamic therapy of cancer. Hyp is not soluble in water where it forms non-fluorescence aggregates. By contrast, Hyp is well soluble in dimethyl-sulfoxide (DMSO). Singlet oxygen ($O_2(^1\Delta_g)$) is produced when photo-excited (triplet state) Hyp monomers are quenched by molecular oxygen [1]. Published lifetime data of singlet oxygen in DMSO vary more than an order of magnitude. It was the main goal of this work to shed light on the singlet oxygen behavior in pure DMSO. Time-resolved singlet oxygen phosphorescence measurements were carried out with quasi-continuous excitation [2] using long laser pulses (35 μ s). This approach ensures low level of photo-bleaching still keeping the signal intensity high. Hypericin was excited at 532 nm and singlet oxygen phosphorescence was detected around its maximum at 1270 nm. The phosphorescence dynamics of $O_2(^1\Delta_g)$ was studied in DMSO using different oxygen and Hyp concentrations.

Acknowledgement

This work was supported by the APVV-0242-11 grant of the Slovak Ministry of Education and the FP7 EU projects: CELIM 316310 and LASERLAB-EUROPE 284464. This work was also supported by the projects SEPO-II (26220120039) and NanoBioSens (26220220107) of the Operation Programme Research and Development funded by the European Regional Development Fund.

References

- [1] P. R. Ogilby, *Chem. Soc. Rev.* 39 (2010), 3181-3209.
- [2] J. Varchola, V. Huntosova, D. Jancura, G. Wagnieres, P. Miskovsky, G. Bano, *Photochem Photobiol Sci.* 13 (2014), 1781-1787



Nuclear targeting *via* selective photo-activation and by regulation of P-glycoprotein

V. VEREBOVÁ¹, D. BELEJ², J. JONIOVÁ², Z. JURAŠEKOVÁ^{2,3}, P. MIŠKOVSKÝ^{2,3}, T. KOŽAR³, D. HORVÁTH³, J. STANIČOVÁ^{1,4}, AND V. HUNTOŠOVÁ³

¹ Institute of Biophysics, University of Veterinary Medicine and Pharmacy, Komenského 73, 041 81 Košice, Slovakia.

² Department of Biophysics, Faculty of Science, P.J. Šafárik University, Jesenná 5, 041 54 Košice, Slovakia

³ Center for Interdisciplinary Biosciences, Faculty of Science, P.J. Šafárik University, Jesenná 5, 041 54 Košice, Slovakia

⁴ Institute of Biophysics and Informatics, First Faculty of Medicine, Charles University in Prague, Salmovská 1, 120 00 Prague 2, Czech Republic

email: valeria.verebova@uvlf.sk

The successful anticancer treatment requests drugs that should be sufficiently hydrophobic to step into the lipid bilayer and they must be also capable to disengage from membranes [1]. For this reason drug hydrophobicity represents a central role in its distribution, metabolism and elimination from the body [2-3]. Very promising antiviral, anti-tumor and anti-inflammatory properties possess naturally occurring plant pigments with planar aromatic organic structure: emodin, hypericin and quinizarin [4-6]. They play important role as catalysts of redox reactions and participate in many processes, e.g. electron transport, photosynthesis or cellular respiration [7]. The impact of these molecules on cell death pathway was widely studied in dark condition as well after light-activation [8-10]. In this study emodin, hypericin and quinizarin were selected as the representative of moderately hydrophobic, highly hydrophobic and intercalator molecules that may be advantageously applied in cancer treatments. The main guardian that prevents the interaction of nuclear DNA with anticancer drugs is nuclear envelope. On the other hand there is the detoxification process accompanied with decreasing of drug concentration by active efflux of these drugs. In this process is involved the P-glycoprotein, a member of ABC transporter family [11]. The function of such proteins is to release chemically unrelated toxins [14]. Therefore one can regulate drug resistance by manipulation of P-glycoprotein activity as it was displayed across wide range of human cancer cells, including glioblastoma (U87 MG) [13]. Another approach how to avoid drug-resistance of the cancer cells could be photochemical activation in precisely defined point/organelle within the cells [12].

Two approaches mention above were studied in this work. By meaning of the first concept the P-glycoprotein of U87 MG cells was exposed to hypericin, emodin and quinizarin. It was observed that P-glycoprotein is mainly located in perinuclear area and on nuclear envelope site. The increase of P-glycoprotein expression was observed for all studied molecules. The molecular simulation methods identified hypericin as the strongest binder with P-glycoprotein among them. Further, the combination treatment with emodin and quinizarin or emodin and hypericin was performed. It was observed that quinizarin after emodin pretreatment passed through the nuclear envelope and it accumulated in the nucleus of U87 MG cells. This observation was not observed for quinizarin treatment only. Similarly, emodin pretreatment increases hypericin intracellular concentration, however hypericin intranuclear fluorescence was not observed. The increase of hypericin concentration caused morphological changes of cells that can activate one of the cell death pathways: apoptosis/necrosis [15]. In particularly this effect can be explained by high affinity of hypericin towards P-glycoprotein.

In the second approach the U87 MG cells were loaded by emodin or hypericin. The selective photo-activation was applied to allowing drugs passive diffusion into nucleus. In

both cases we were able to perform local irradiation in nuclear envelope, however only emodin was observed to pass into nucleus.

In conclusion we proposed two approaches how to overcome cellular hydrophobic drug defense.

Acknowledgement

This work was supported by the EU 7FP grant CELIM 316310 and by the Slovak Research and Development Agency APVV-0242-11 and VEGA 1-0425-15. The authors strongly appreciate this support.

References

- [1] H. Kubinyi, *Farmaco.edizionescientifica*34 (1979), 248-276.
- [2] D. Eisenberg and A. D. McLachlan, *Nature* 319 (1986), 199-203.
- [3] S. Miyamoto and P. A. Kollman, *P. Natl. Acad. Sci. USA*90 (1993), 8402-8406.
- [4] D. O. Andersen, N. D. Weber, S. G. Wood, B. G. Hughes, B. K. Murray and J. A. North, *Antivir. Res.*16 (1991), 185-196.
- [5] T. Ma, Q. H. Qi, W. X. Yang, J. Xu and Z. L. Dong, *World. J. Gastroentero.*9 (2003), 1804-1807.
- [6] L. Quinti, N. S. Allen, M. Edge, B. P. Murphy and A. Perotti, *J. Photoch. Photobio. A*155 (2003), 79-91.
- [7] A. Bogdanska, L. Chmurzynski, T. Ossowski, A. Liwo and D. Jeziorek, *Anal. Chim. Acta* 402 (1999), 339-343.
- [8] V. Huntosova, Z. Nadova, L. Dzurova, V. Jakusova, F. Sureau and P. Miskovsky, *Photoch. Photobio. Sci.* 11 (2012), 1428-1436.
- [9] L. Mikesova, J. Mikes, J. Koval, K. Gyuraszova, L. Culka, J. Vargova, B. Valekova and P. Fedorocko, *Photodiagn. Photodyn.*10 (2013), 470-483.
- [10] S. Rossi, C. Tabolacci, A. Lentini, B. Provenzano, F. Carlomosti, S. Frezzotti and S. Beninati, *Anticancer. Res.*30 (2010), 445-449.
- [11] M. M. Gottesman, T. Fojo and S. E. Bates, *Nat. Rev. Cancer.* 2 (2002), 48-58.
- [12] A. Weyergang, M. E. Berstad, B. Bull-Hansen, C. E. Olsen, P. K. Selbo and K. Berg, *Photochem. Photobiol. Sci.* 14 (2015), 1465-1475.
- [13] A. Regina, M. Demeule, A. Laplante, J. Jodoin, C. Dagenais, F. Berthelet, A. Moghrabi and R. Beliveau, *Cancer. Metast. Rev.*20 (2001), 13-25.
- [14] S. G. Aller, J. Yu, A. Ward, Y. Weng, S. Chittaboina, R. P. Zhuo, P. M. Harrell, Y. T. Trinh, Q. H. Zhang, I. L. Urbatsch and G. Chang, *Science*323 (2009), 1718-1722.
- [15] L. Dzurova, D. Petrovajova, Z. Nadova, V. Huntosova, P. Miskovsky and K. Stroffekova, *Photodiagn. Photodyn.* 11 (2014), 213-226.



***In vitro* regeneration system of selected *Hypericum* species**

Z. DIČÁKOVÁ^{1,2}, AND E. ČELLÁROVÁ²

¹ Department of Biophysics, P. J. Šafárik University, Jesenná 5, 041 54 Košice, Slovakia

² Department of Genetics, P. J. Šafárik University, Mánesova 23, 040 01 Košice, Slovakia
e-mail: zuzana.dicakova@student.upjs.sk

The aim of this work was to introduce seventeen taxons of the genus *Hypericum* into the *in vitro* culture and then to establish the most suitable nutrition conditions for the effective root and shoot regeneration of explants' cultures. There were roots, shoots and leaves explants cultivated on Murashige and Skoog agar medium supplemented with growth regulators auxins and cytokinins. Main focus was taken on the impact of different types of auxins and cytokinins as well as on their low and high concentration.

This study was designed to compare the regeneration potential of seventeen *Hypericum* species and to provide an overview of the results which revealed significant difference among all studied species. The highest regeneration response among all the representatives we obtained in *Hypericum annulatum* Moris. By application exogenous auxin indole-3-butyric acid (IBA) into the medium we induced rhizogenesis in *Hypericum annulatum* Moris, *Hypericum tomentosum* L., *Hypericum maculatum* Crantz, *Hypericum tetrapterum* Fries and *Hypericum pulchrum* L.. Between two examined cytokinins benzylamino purine (BA) and 6-(γ,γ -Dimethylallylamino)purine (2iP) we obtained the greatest biomass of differentiated shoots by application cytokinin benzylamino purine (BA) in *Hypericum tomentosum* L., *Hypericum annulatum* Moris, *Hypericum tetrapterum* Fries, *Hypericum humifusum*, *Hypericum monogynum* L. and *Hypericum maculatum* Crantz.

Genus *Hypericum* is extensive genus of family *Hypericaceae*, which contains more than 450 species. Although it has included only seventeen species, it was an extensive comparative study. Experiment was focused to gain qualitative characteristic and prepare material for next study of qualitative and quantitative observations.

Acknowledgement

This work was supported by the research grant from the Slovak Grant Agency Vega No. 1/0049/08 and APVV-0321-07.

Study of the NIR light induced effects on neuroblastoma N2A cells with Parkinson's-like feature

L. KOPTASIKOVA¹, V. HUNTOSOVA^{2,3}, E. GERELLI³, G. WAGNIERES³, AND K. STROFFEKOVA¹

¹ Department of Biophysics, PJ Safarik University, Kosice, Slovakia

² Center for Interdisciplinary Biosciences, PJ Safarik University, Kosice, Slovakia

³ Laboratory of Organometallic and Medical Chemistry, ISIC, EPFL, Lausanne, Switzerland

e-mail: l.koptasikova@gmail.com

Introduction

A new and interesting field of investigation is near-infrared (NIR) photobiostimulation (PBM) for the treatment of wounds, traumatic brain injuries and acute ischemic stroke. PBM accelerates wound healing, reduces inflammation, improves tissue repair, and it is a promising treatment for neurodegenerative conditions [1]. NIR has optimal penetration in biological tissues and can thus provide a minimally-invasive treatment. However, the mechanisms underlying the PBM effects, including an increase in ATP synthesis, modulation of reactive oxygen species, and induction of transcription factors [2] are not fully understood.

Parkinson's disease (PD) is an incurable neurodegenerative disorder associated with losses of dopaminergic neurons. The underlying cause is unknown. Recently, it was shown that NIR irradiation improves cellular functions of damaged neurons in *D.melanogaster* and mice [3-5], indicating that NIR irradiation may be a promising approach to slow down or even stop the neurodegenerative process involved in PD. Although the changes evoked by NIR irradiation are still not clearly defined, there is evidence [6] that NIR irradiation has the ability to stimulate cytochrome c-oxidase (complex IV.) activity in the mitochondrial electron transport chain (ETC).

The aim of our study was to elucidate NIR irradiation effects on the neuronal cells proliferation and their metabolism.

Methods

The model we chose was neuronal N2A cell line. We induced the PD-like neuron phenotype by moderate treatment of neurons with rotenone, the complex I. inhibitor that restricts electron flow in ETC.

We used a NIR laser at 808 nm with an irradiance of 50 mW/cm² and a light dose of 20 J/cm² applied twice a day every two days, with a four-hour rest time between treatments. Light was applied to the adherent neuronal N2A cells cultured *in vitro*. We compared the NIR effect between control and PD-like cells.

XF24 analyser (Seahorse) is a 24-well plate reader that simultaneously measures oxygen consumption rate (OCR) and extracellular acidification rate (ECAR) after injection of different compounds. It provides us with the information about metabolic characteristics of the cells in real time.

Results

Overall, we observed a significant stimulation of cell proliferation in control and rotenone-treated cells after PBM. This effect was accompanied by an increased oxygen consumption rate (OCR) by mitochondria and increased mitochondrial membrane potential. NIR irradiation shifted cellular metabolism in control and PD-like cells towards oxidative phosphorylation metabolism. Our further experiments will focus on the production of lactate, reactive oxygen species (ROS), and ATP by rotenone-treated and untreated N2A cells after

irradiation at 808 nm to better understand PBM-triggered metabolic changes inducing an enhanced cells proliferation.

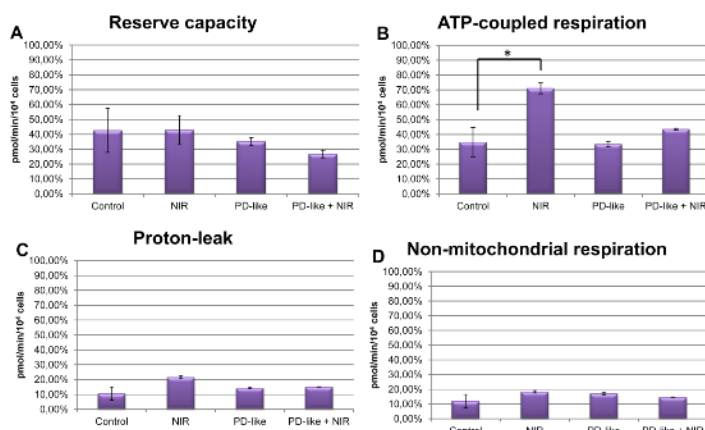


Fig.1 NIR irradiation increases ATP-coupled respiration of the treated cells. The contribution of each of the parameters (reserve capacity, ATP-coupled respiration, proton-leak, and non-mitochondrial respiration) to the maximal cellular oxygen consumption is depicted after normalization to 10,000 cells. Significance is shown: * $p < 0.001$.

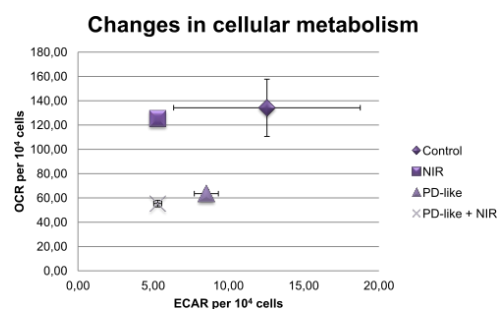


Fig.2 Changes in cellular metabolism after NIR irradiation. Results are plotted as OCR over ECAR of baseline conditions normalized to the cell count.

Conclusions

In summary, irradiation at 808 nm during 400s with an irradiance of 50mW/cm² resulted in increased cell proliferation, significantly increased ATP-linked respiration, and shift of cellular metabolism towards oxidative phosphorylation.

Acknowledgement

Study supported by the EU 7FP grants PIRG06-GA-2009-256580 and CELIM 316310; by the EU Structural Fund ITMS 26240120040; by the Slovak Grant Agency VEGA 1/0425/15; by the Slovak Research and Development Agency APVV-0242-11; by the PJ University Research Grant VVGS-PF-2015-489, and by the Swiss National Science Foundation, Project: CR32I3_159746.

References

- [1] S. Passarella and T. Karu, *Journal of Photochem and Photobiol B* 140 (2014) 344-358.
- [2] J. Tafur and P.J. Mills, *Photomed Laser Surg* 26 (2008) 323-328.
- [3] M. Vos, B. Lovisa, A. Geens et al., *PLoS One* 8 (2013) 1-9.
- [4] H.B. Liang, H.T. Whelan, J.T. Eells et al., *Neuroscience* 139 (2006) 639-649.
- [5] H.B. Liang, H.T. Whelan, J.T. Eells and M.T.T. Wong-Riley, *Neuroscience* 153 (2008) 963-974.
- [6] Karu, *Photomed Laser Surg* 31 (2013) 189-191.



Ability of nanoparticles coated with different types of dextran to inhibit amyloid aggregation of lysozyme

Z. BEDNARIKOVA^{1,2}, E. DEMJEN², S. DUTZ³, M. M. MOCANU⁴, K. ULICNA^{1,5}, P. KOPČANSKÝ², AND Z. GAZOVA^{2,6}

¹ Department of Biochemistry, Faculty of Sciences, P. J. Šafárik University, Šrobárova 2, 041 54 Košice, Slovakia

² Department of Biophysics, Institute of Experimental Physics, Slovak Academy of Sciences, Watsonova 47, 040 01 Košice, Slovakia

³ Institute of Biomedical Engineering and Informatics (BMTI), Technische Universität Ilmenau, Gustav-Kirchhoff-Straße 2, 98693 Ilmenau, Germany

⁴ Department of Biophysics, "Carol Davila" University of Medicine and Pharmacy, Bucharest, Romania

⁵ Institute of Biology and Ecology, Faculty of Science, Safarik University, Srobarova 2, 041 54 Kosice, Slovakia

⁶ Department of Medical and Clinical Biochemistry, Faculty of Medicine, Safarik University, Tr. SNP 1, Kosice, Slovakia

e-mail: bednarikova@saske.sk

The conversion of normally soluble protein into fibrillar aggregates is of central importance for several diseases, including Alzheimer's and Parkinson's diseases or diabetes mellitus. Hen egg-white lysozyme (HEWL) is one of the best known proteins with well-characterized molecular structure and physico-chemical properties; therefore it serves as model protein for study of protein amyloid aggregation *in vitro*. HEWL is homologous (40%) to human lysozyme whose mutant variants form massive amyloid deposits in the liver and kidneys of individuals affected by systemic lysozyme amyloidosis [1]. Several therapeutic approaches have been suggested so far to deal with amyloidogenic diseases. These approaches mainly include direct inhibition of the self-assembly processes [2] and in recent years the attention has been devoted to nanoparticles that inhibit amyloid fibril formation.

We have investigated the effect of magnetite nanoparticles coated with three different types of dextran on amyloid aggregation of HEWL using ThT assay, FTIR spectroscopy and AFM technique. Studied nanoparticles were composed of iron oxide (Fe₃O₄) core coated with carboxymethyl dextran (CMD), dextran (DEX) or diethylaminoethyl dextran (DEAE), respectively.

The data have shown that interference of nanoparticles with HEWL led to decrease of ThT fluorescence intensities with increasing nanoparticle concentration. The IC₅₀ values were determined in µg/ml range. The most effective inhibitory effect was obtained for negatively charged CMD and neutral dextran nanoparticles (DEX). The different extent of inhibition of HEWL fibrillization was confirmed by atomic force microscopy. Moreover, the kinetic profiles for HEWL fibrillization in presence of studied nanoparticles have shown that CMD and DEX nanoparticles prolong lag phase and decrease values for plateau phase. In order to assess the toxicity of nanoparticles we have measured their cytotoxic effect on SH-SY5Y cell line using WST-1 assay. The 24 h and 48 h exposure of cells to all types of nanoparticles caused no significant changes in viability relative to control at concentrations close to IC₅₀ values.

Our results indicate that all three types of nanoparticles are able to prevent the amyloid self-assembling of lysozyme, the extent of the inhibition depends on their physico-chemical properties. Moreover, they possess no cytotoxicity which is promising for further investigation of these nanoparticles as candidates for therapy of amyloid-related diseases.

Acknowledgement

This work was supported by the research grant from the Slovak Grant Agency Vega 02/181/13 and 2/0175/14.

References

- [1] M.R. Krebs, D.K. Wilkins, E.W. Chung, M.C. Pitkeathly, A.K. Chamberlain, J. Zurdo, C.V. Robinson, C.M. Dobson. *J Mol Biol* 300 (2000), 541–549.
- [2] C. Soto *FEBS Lett* 498 (2001), 204–207.

Destabilization and fibrillization of proteins in ionic liquids – anion vs. cation role

D. FEDUNOVÁ¹, Z. BEDNÁRIKOVÁ^{1,2}, E. DEMJÉN¹, J. MAREK¹, D. SEDLÁKOVÁ¹, AND Z. GAŽOVÁ¹

¹Institute of Experimental Physics, Slovak Academy of Sciences, Watsonova 47, Košice, Slovakia

²Department of Biochemistry, Institute of Chemistry, Faculty of Science, Moyzesova 11, 040 01, Košice, Slovakia
e-mail: fedunova@saske.sk

Amyloid aggregation has been in the centre of attention firstly due to a connection to amyloid-related diseases. The gradual increase in amount of proteins converted into amyloid fibrils *in vitro*, also those not connected to diseases, provided opportunities for better understanding the processes of amyloid aggregation. The formation and properties of amyloid aggregates are of interest now not only for searching efficient therapy but also as novel biomaterials or for protein biotechnology.

It is generally accepted that ability to form amyloid fibrils is general property of polypeptide chain and that the destabilization of native state is required for amyloid formation. Although the amyloidogenic proteins are not sequentially or functionally related, amyloid fibrils possess some common properties – such as core cross β -sheet structure or ability to specifically bound fluorescent probe Thioflavin T. However, obtained fibrils can be morphologically different (length, height, twisting, protofibril content) even within one particular protein type. The specific destabilizing conditions required for formation of amyloid fibrils *in vitro* are usually achieved by variation of elevated temperature, pH, denaturant content, stirring or solvent composition. Ionic liquids (ILs) are novel solvents recently used in many fields for their easily tunable properties. ILs are liquids (consisting of organic cations and anions) below 100°C and can be used as neat or dissolved in water (or other solvents).

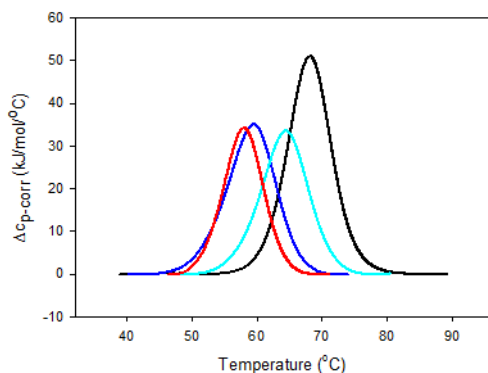


Fig. 1: DSC scans of lysozyme in 2 mM Glycine buffer, pH 2.7 (black) and at the presence of 300mM 1-butyl-3methyl imidazolium ILs with hydrogensulphate (cyan), chloride (blue) and acetate (red) as anions. Protein concentration 2mg/ml.

In this work we have studied the effect of 1-alkyl-3-methylimidazolium ionic liquids with butyl and ethyl groups as cations and chloride, acetate and hydrogensulfate as anions on stability and fibrillization of lysozyme at acidic pH by means of calorimetry, ThT fluorescence assay, AFM and image analysis. The efficiency of salts to affect the protein stability can be in some extent predicted by the position of ions in Hofmeister series, considering anions being more influential than cations. However, the effect of ions on fibrillization was found to be more complex than Hofmeister phenomenon [1]. Moreover, using complex organic anions and cations of ILs further contribute to complexity and unpredictability of the process. We have found that the stability of lysozyme is decreased in all studied ILs, following Hofmeister series in reversing order (from most stable) – hydrogensulfate > chloride > acetate

(Fig. 1) independent of used cation. The thermal denaturation is 2-state process as follows from ratio of van't Hoff and calorimetric enthalpies close to 1 as well as high reversibility of denaturation except for both ILs with hydrogensulphate as anion where the reversibility was only about 60%. Although the hydrogensulfate ion is considered to be chaotropic, it can dissociate in water to SO_4^{2-} anion with higher charge density leading to counteracting

stabilizing effect. Comparing the effect of cation in combination with the same anion, the transition temperature decreases about 2 °C for compounds with butyl group as larger cation.

The different behaviour of both ILs with hydrogensulfate as anion comparing with other studied ILs is also manifested in their effect on lysozyme fibrillization. Even though the conformational change leading to higher content of β -sheet structure in protein necessary for fibrillization was detected, from AFM follows that only large amorphous aggregates are present. At the used conditions (2 mM glycine buffer, pH 2.7, 65°C and shaking) lysozyme at 2 mg/ml concentrations doesn't form amyloid fibrils within the 50 hours interval. At the presence of all remaining ILs amyloid fibrils are formed within the 4 hour interval, depending on ILs concentration. From measurements of fibrillization kinetics is evident that fibril formation follow the nucleation-dependent model of fibrillization. At the presence of more destabilizing cation acetate the lag phase and half-time of fibrillization are lower than for chloride anion at the same ILs concentrations. The mature fibrils were morphologically analysed showing that both, not only anion but also cation type modulates the morphology of fibrils, whereas the destabilizing effect of anions on lysozyme thermal stability is much more prominent than that of cations.

Obtained results can be of importance for establishing conditions leading to morphologically defined fibrils with specific properties for biotechnological purposes as well as to better understanding the complex mechanism of amyloid fibrillization.

Acknowledgement

This work was supported by the research grant from the Slovak Grant Agency Vega No. 2/0176/14, 2/0175/14, 2/0181/13.

References

[1] J. S. Pedersen, J. M. Fink, D. Dikov and D. E. Otzen *Biophys J* 90 (2006), 4181-41942.

Lysozyme amyloid species and their influence on neural cell viability

E. BYSTRENOVA¹, Z. BEDNARIKOVA^{2,3}, M. BARBALINARDO¹, C. ALBONETTI¹, F. VALLE¹, AND Z. GAZOVA^{2,4}

¹ C.N.R. - I.S.M.N., via Gobetti, 101, 401 29 Bologna, Italy

² Department of Biophysics, Institute of Experimental Physics Slovak Academy of Sciences, Watsonova 47, 040 01 Košice, Slovakia.

³ Department of Biochemistry, Faculty of Sciences, P. J. Šafárik University, Šrobárova 2, 041 54 Košice, Slovakia

⁴ Department of Medical and Clinical Biochemistry, Faculty of Medicine, Safarik University, Tr. SNP 1, Kosice, Slovakia

e-mail: gazova@saske.sk

Identifying the cause of the cytotoxicity of aggregates forming during amyloid fibrillization is important for understanding the molecular basis of protein deposition diseases called amyloidosis. It has been shown that species forming in the early phases of *in vitro* aggregation of many different proteins are more cytotoxic than the corresponding mature amyloid fibrils [1].

We have examined different types of amyloid aggregates of hen egg white lysozyme by Thioflavin T fluorescence assay, circular dichroism (CD) and atomic force microscopy (AFM), and analyzed how they influence the neuroblastoma SH-SY5Y cells viability. We have prepared and characterized 3 different types of lysozyme aggregates: lysozyme amyloid fibrils, seeds (shorter fragments of fibrils) and native lysozyme. The kinetics of fibril formation were studied using ThT assay. The shape of fibrillization curves obtained for both fibrils formed from native lysozyme and fibrils formed in presence of seeds indicate that formation of fibrils underlie nucleation-elongation polymerization with typical lag phase followed by steep increase of fluorescence intensity corresponding to fibril formation. However, the data show differences in the length of lag phase. The addition of seeds to native lysozyme decreased the lag time significantly. The atomic force microscopy images showed in both cases the presence of linear unbranched fibrils. We investigated the differences in secondary structure of fibrils, seeds, seeds with native lysozyme and native lysozyme alone using circular dichroism. The CD spectra of native protein showed local minima at 208 and 222 nm corresponding to the high content of α -helixes. The minima detected for fibrils and seeds were at 218 nm and 213 nm, respectively which indicate higher content of β -sheet.

The effect of all studied species on neuroblastoma SH-SY5Y cell line was investigated using fluorescence microscopy. Incubation of cells with 10 μ M of aggregates for 24 h and 48 h decreased the number of cells. The most significant decrease was observed for cells in presence of seeds and seeds with native protein. The addition of native protein and fibrils did not cause any significant changes in cell proliferation. The obtained findings indicate that targeting seeds with amyloid inhibitors could be promising strategy for treatment of amyloid-related diseases.

Acknowledgement

This work was supported by the research grants from Slovak Grant Agency VEGA 2/0181/13 and CNR-SAS projekt „Amyloid aggregation of proteins in hybrid interfaces“.

References

[1] M. F. Mossuto et al., *J. Mol. Biol.* 402 (2010), 783-796.

Structure-activity relationship of acridine derivatives to amyloid aggregation of A β peptide

J. KUBACKOVÁ¹, K. ULIČNÁ^{1,2}, Z. BEDNÁRIKOVÁ^{1,3}, AND Z. GAŽOVÁ^{1,4}

¹ Department of Biophysics, Institute of Experimental Physics, Slovak Academy of Sciences, Watsonova 47, 040 01 Kosice, Slovakia

² Institute of Biology and Ecology, Faculty of Science, Pavol Jozef Safarik University, Srobarova 2, 041 54 Kosice, Slovakia

³ Department of Biochemistry, Faculty of Science, Pavol Jozef Safarik University, Srobarova 2, 041 54 Kosice

⁴ Department of Medical and Clinical Biochemistry, Faculty of Medicine, Pavol Jozef Safarik University, Trieda SNP 1, 040 11 Kosice, Slovakia

e-mail: kubackova@saske.sk

The presence of amyloid aggregates in different tissues has toxic consequence to various cell types leading to their dysfunction or death [1]. Nowadays, the precise mechanisms of toxicity are not fully elucidated; however, based on previous studies, the most promising therapeutic approaches seem to be targeting a protein stability and misfolding, direct inhibition of the self-assembly process or clearance of amyloid aggregates [2]. In the past few years, a range of low molecular weight compounds have been selected to actively inhibit amyloid aggregation and to promote the disaggregation of amyloid filaments in *in vitro* systems, including cell cultures. The advantage of the low molecular weight compounds is ability to cross the blood brain barrier easily, avoid immunological response, and they are more stable in biological fluids and tissues [3].

In the present work, we have investigated the ability of structurally distinct acridine derivatives to prevent the formation of A β amyloid aggregates *in vitro*. Studied acridines consist of the planar tricyclic core, aliphatic linker with different length terminated with side group.

Interference of acridine derivatives with A β peptide fibrils was monitored using Thioflavin T (ThT) assay and microscopic techniques. Fluorescence spectroscopy and atomic force microscopy have shown that impact of the studied small molecules on A β peptide amyloid fibrillization strongly depends on the structure of acridines. In case of tetrahydroaminoacridine no effect on the formation of the amyloid fibrils was observed. Binding of the oxygen group on the tricyclic acridine core led to partial inhibition of the fibrillization. However, the presence of the side group attached to the acridine core through linker caused significant increase in the inhibiting activity. Interestingly, the inhibition efficiency characterized by the half-maximal inhibition concentration IC₅₀ depended on the length of the linker. Derivates with short linker consisting of only two carbons and the longest linker (eight carbons) exhibited the lowest inhibitory activities.

Acknowledgement

This work was supported by the research grant VEGA 0181 and VEGA 0176.

References

- [1] I. Khlistunova, J.Y. Biernat, P. Wang, M. Pickhardt, M. von Bergen, Z. Gazova, E.M. Mandelkow, E. Mandelkow, *J. Biol. Chem.* 281 (2006) 1205-1214.
- [2] E.D. Roberson, K. Scarce-Levie, J.J. Palop, F. Yan, I.H. Cheng, T. Wu, H. Gerstein, G.Q. Yu, L. Mucke, *Science* 316 (2007) 750-754.
- [3] S.S.S. Wang, K.N. Liu, W.H. Lee, *Biophys. Chem.* 144 (2009) 78-87.

Fragments from human lysozyme affect lysozyme amyloid fibrillization

K. ULICNA^{1,2}, Z. BEDNARIKOVA^{1,3}, A. BHUNIA⁴, AND Z. GAZOVA^{1,5}

¹ Department of Biophysics, Institute of Experimental Physics, Slovak Academy of Sciences, Watsonova 47, 040 01 Kosice, Slovakia

² Institute of Biology and Ecology, Faculty of Science, Safarik University, Srobarova 2, 041 54 Kosice, Slovakia

³ Department of Biochemistry, Institute of Chemistry, Faculty of Science, Safarik University, Srobarova 2, 041 54 Kosice, Slovakia

⁴ Department of Biophysics, Bose Institute, P-1/12 CIT Scheme VII (M), Kolkata 700054, India

⁵ Department of Medical and Clinical Biochemistry Faculty of Medicine, Safarik University, Trieda SNP 1, 040 11 Kosice, Slovakia

Amyloid fibrillization of proteins includes complications like diabetes mellitus or Alzheimer's and prion diseases [1]. The molecular basis of these diseases is routed by the protein misfolding and formation of ordered β -sheet structures [2, 3]. Identification of the agents able to reduce the amount of amyloid aggregates represents one of the possible therapeutic strategies of amyloid-related diseases.

We have explored the potential of three peptide fragments (Lz-peptides) derived from human lysozyme, namely Lz peptide (sequence R¹⁰⁷-R¹¹⁵) and its two mutants LzK (A108K) and LzKW (A108K, A111W) to inhibit the amyloid fibrillization of human lysozyme using ThT fluorescence assay, circular dichroism (CD) and atomic force microscopy (AFM). The formation of human lysozyme fibrils achieved by incubation of the protein in acidic pH at high temperature and constant stirring was confirmed independently by ThT fluorescence assay and atomic force microscopy (AFM). Fluorescence intensity of ThT was enhanced in the presence of fibrils compared to the presence of native lysozyme.

The results obtained by ThT fluorescence assay suggest that all three Lz-peptides are able to influence the lysozyme fibrillization (10 μ M) in studied concentration range of Lz-peptides (from 10 pM to 1 mM). The highest decrease in fluorescence intensity was observed for LzK peptide, about 50 % of ThT fluorescence was detected compare to untreated lysozyme amyloid fibrillization. This corresponds to 50% inhibition of lysozyme self-assembly into amyloid fibrils. Slightly higher ThT intensities (~ 60%) were obtained for Lz peptide indicating about 40 % inhibiting activity. On the other hand, for LzKW peptide the fluorescence intensities were only slightly lower than fluorescence detected for lysozyme fibrillization indicating the lowest inhibitory activity, only about 10%.

Atomic force microscopy confirmed typical amyloid morphology of untreated lysozyme fibrils as long, unbranched fibrillar structures were observed (Fig. 1A). The presence of Lz or LzK peptides during lysozyme amyloid fibrillization leads to reduction in the amount and length of fibrillar aggregates (in Fig. 1B shown for LzK peptide). In case of LzKW peptide, the AFM image is similar to the image obtain for untreated amyloid fibrils.

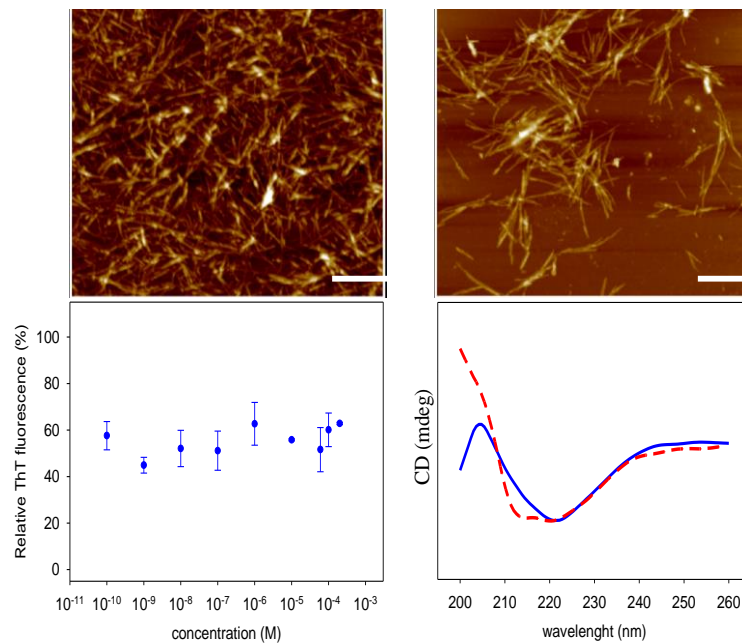


Figure.1 Representative AFM images obtained after amyloid fibrillization of human lysozyme alone (A) and in presence of 100 nM concentration of short peptide LzK (B). The fluorescence intensities detected after human lysozyme fibrillization using ThT assay in presence of increasing concentration of LzK peptide (C) and CD spectrum of human lysozyme after fibrillization alone (blue solid line) and in presence of 60 μ M (red dashed line) concentration of LzK peptide (D).

Changes in lysozyme secondary structure were estimated after protein fibrillization alone and in presence of Lz-peptides using far-UV CD spectroscopy. The spectra detected in presence of Lz and LzK peptides showed changes in shape of the spectra indicating lower content of β -sheets and higher content of α -helix compare to lysozyme fibrils. These changes were not observed in case of LzKW peptide. The obtained data corresponds to results obtained using ThT fluorescence assay.

The achieved results suggest that Lz and LzK peptides have a strong potential to bind with lysozyme and partially inhibit amyloid fibril formation. Hydrophobic interactions are the main driving force for mediating the binding of Lz-peptides to native lysozyme. The present study implicates that these peptides can be also tested against other amyloid-prone proteins to develop novel therapeutic agents.

Acknowledgement

This work was supported by research grant from the Slovak Grant Agency VEGA 2/0181/13.

References

- [1] T. P. Knowles, M. Vendruscolo and C.M. Dobson, *Nat. Rev. Mol. Cell. Biol.* 15 (6) (2014), 384-96.
- [2] C. Haass, D.J. Selkoe, *Nat. Rev. Mol. Cell. Biol.* 8 (2) (2007), 101-12.
- [3] R. S. Harrison, P. C. Sharpe, Y. Singh, D.P. Fairlie, *Rev. Physiol. Biochem. Pharmacol.* 159 (2007), 1-77.

Study of the thermal unfolding of human serum albumin

M. NEMERGUT¹, E. SEDLÁK², D. BELEJ¹, AND D. JANCURA¹

¹ Department of Biophysics, P. J. Šafárik University, Jesenná 5, 041 54 Košice, Slovakia

² Center for Interdisciplinary Biosciences, P. J. Šafárik University, Jesenná 5, 041 54 Košice, Slovakia

Human serum albumin (HSA) is one of the most abundant proteins in the blood where it is present at a high concentration ($\approx 600 \mu\text{M}$). HSA plays a special role in the transport of fatty acids, metabolites and drugs throughout the vascular system and also in maintaining the pH and osmotic pressure of plasma. For many drugs, reversible binding to serum albumin is a critical determinant of their distribution and pharmacokinetics. HSA is a single chain protein with 585 amino acids, with a molecular weight of $\sim 66.5 \text{ kDa}$. The structure of this molecule is composed from three homologous domains (I, II, and III) which are further divided into a pair of subdomains termed “A” and “B”. According to the conventional view based on Sudlow’s classification, drug ligands of HSA are accommodated at two main binding sites located in subdomain IIA (site IIA) and IIIA (site IIIA), respectively [1-3].

HSA is known to undergo different pH dependent conformational transitions, the N \leftrightarrow F transition between pH 5.0 and 3.5, the F \leftrightarrow E transition (acid expansion) below pH 3.5, and the N \leftrightarrow B transition between pH 7.0 and 9.0 [4]. It is increasingly recognized that the structure of non-native states of the proteins can provide significant insight into fundamental issues such as the relationship between the sequence of a protein and its three dimensional structure, the nature of protein folding pathways and the stability of proteins [5].

The mechanism by which proteins fold from a structure-free denatured state to their unique biologically active state is an intricate process. Human serum albumin is a multi-domain protein and its domains are capable of unfolding and refolding independently. Structural and functional aspects of HSA in response to chemical and thermal denaturation revealed the existence of intermediates in the unfolding pathway suggesting that there are structural parts in the molecule with different stabilities, which unfold in steps [6, 7].

In this work, we characterized conformational states as well as temperature-induced transitions of HSA (both with and without fatty acids) at different pHs using fluorescence, CD spectroscopy and differential scanning calorimetry (DSC). Our results indicate that the conformational states of HSA depends on pH value of solvents (Fig. 1). In fact, thermodynamic properties of HSA,

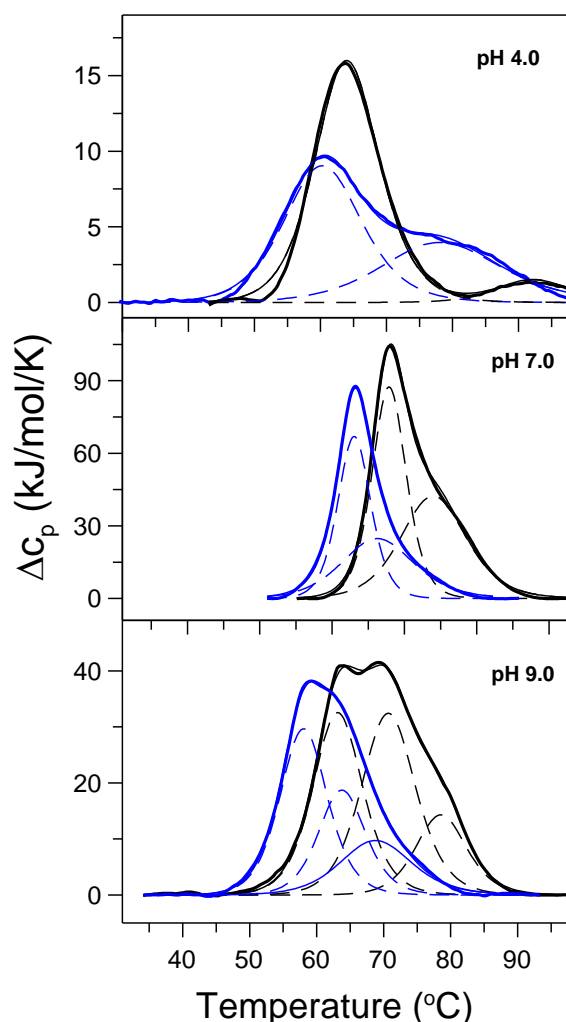


Figure 1. Representative DSC scans of HSA with fatty acids (black lines) and without fatty acids (blue lines) at pH 4.0, 7.0 and 9.0.

calorimetric and van't Hoff enthalpies, transition temperature as well as a number of intermediates, are strongly pH-dependent. Moreover, thermodynamic properties of HSA are also significantly affected by the presence of ligands such as fatty acids (the present work) as well as low-weight ligands such as warfarin, ibuprofen (data not shown).

Detailed knowledge of thermodynamic properties of HSA as well as its ability to bind different ligands on pH value of solvent has a strong implication for its utilization as a part of drug delivery vehicles.

Acknowledgement

This work was supported by the 7RP EU project CELIM 316310.

References

- [1] N. A. Kratochwil, W. Huber, F. Muller, *Biochem. Pharmacol.* 64 (2002), 1355–1374.
- [2] S. Curry, *Drug Metab. Pharmacokinet.* 24 (2009), 342–357.
- [3] D. C. Carter, Ho, J. X. *Adv. Protein Chem.* 45 (1994), 153–203.
- [4] T. Peters, *All About Albumin: Biochemistry, Genetics, and Medical Applications*, Academic Press, 1995.
- [5] B. Ahmad et al., *Int. J. Biol. Macromol* 75 (2015), 447-452.
- [6] P. L. Privalov, *Adv. Protein Chem.* 35 (1982), 1-104.
- [7] M.K. Santra, A. Banerjee, O. Rahaman, D. Panda, *Int. J. Biol. Macromol.* 37 (2005), 200– 204.

Kinetic Monte-Carlo simulation of hypericin aggregation in bilayer lipid membranes

M. REBIČ¹, J. JONIOVÁ¹, A. STREJČKOVÁ², V. HUNTOSOVA³, J. STANIČOVÁ², D. JANCURA^{1,3}, P. MISKOVSKÝ^{1,3}, AND G. BÁNÓ^{1,3}

¹ Department of Biophysics, P. J. Šafárik University, Jesenná 5, 041 54 Košice, Slovakia

² Department of Chemistry, Biochemistry and Biophysics, University of Veterinary Medicine and Pharmacy, Komenského 73, 04181 Košice, Slovakia

³ Center for Interdisciplinary Biosciences, P.J. Šafárik University, Jesenná 5, 041 01 Košice, Slovakia
e-mail: gregor.bano@upjs.sk

Hypericin (Hyp) is a naturally occurring photosensitizer that can be extracted from the plants of *Hypericum perforatum*. Hyp forms non-fluorescent aggregates in aqueous environment [1]. By contrast, it is well soluble in polar organic substances and is known to have high affinity to lipid structures. Previous theoretical studies showed preferential localization of Hyp in the densest regions of lipid bilayers close to the polar head groups of the membrane [2]. At higher Hyp concentrations aggregation and/or self-quenching of Hyp was observed inside of LDL particles [3] and in artificial bilayer membranes [4].

Our present experiments indicated extensive Hyp aggregation in giant unilamellar vesicles (GUV). After adding Hyp to the GUV surrounding the fluorescence signal of Hyp in the membrane first increased, reached a maximum and finally decayed towards late times. At the same time formation of large Hyp aggregates was observed on the GUV surface as viewed under a microscope.

It was the goal of the present work to build a theoretical model that can describe the formation of large Hyp aggregates (composed of thousands of Hyp molecules) in GUV membranes. The following processes were included in the model: diffusion of Hyp aggregates from the buffer solution to the GUV surface, further aggregation (fusion of smaller aggregates) and fragmentation (detachment of Hyp monomers) in the membrane. All the processes were characterized by appropriate rate constants and the evolution of Hyp aggregate size distribution was calculated by a kinetic Monte-Carlo code. Based on the simulation results the time-dependence of the expected fluorescence signal was calculated and compared with experiments.

Acknowledgement

This work was supported by the APVV-0242-11 grant of the Slovak Ministry of Education and the FP7 EU CELIM 316310 project. This work was also supported by the projects SEPO-II (26220120039) and NanoBioSens (26220220107, 50%) of the Operation Programme Research and Development funded by the European Regional Development Fund.

References

- [1] G. Bánó, J. Staničová, D. Jancura, J. Marek, M. Bánó, J. Uličný, A. Strejčková and P. Miškovský, *J. Phys. Chem. B* 115 (2011) 2417-2423.
- [2] E. Eriksson, S. E., D. J. V. A. dos Santos, R. C. Guedes, and L. A. Eriksson, *Journal of Chemical Theory and Computation* 5 (2009) 3139-3149.
- [3] Kascakova, S., M. Refregiers, D. Jancura, F. Sureau, J. C. Maurizot and P. Miskovsky. *Photochemistry and Photobiology* 81 (2005) 1395-1403.
- [4] A. Strejčková, J. Staničová, D. Jancura, P. Miškovský and G. Bánó, *J. Phys. Chem. B* 117 (2013) 1280-1286.

Transfer of lipophilic molecules into water solutions of the natural surfactant saponin

L. BLASCAKOVA¹, A. FILIPEK¹, K. KOPCOVA¹, D. JANCURA^{1,2}, AND M. FABIAN²

¹Department of Biophysics, Faculty of Science, Safarik University, Kosice

²Center for Interdisciplinary Biosciences, Faculty of Science, Safarik University, Kosice

Many commercial applications in cosmetics, food, pharmaceutical or agricultural industries are based on the solubilization and stabilization of lipophilic components in water solutions [1,2]. The barrier for lipophilic molecules to enter the hydrophilic solutions is often overcome by using some surfactants. The surfactants, possessing both the lipophilic and hydrophilic properties, are able to stabilize the lipophilic nano or micro droplets in water solution. Since most of the used surfactants are the artificial molecules, there is the increased tendency to replace them by natural compounds. One promising category of natural surfactants is group of saponins. Saponins, widely distributed in plant kingdom, include chemically very diverse group of compounds [3,4]. Even more important is, however, that saponins exhibit not only surface activity; they show the diverse biological activity, too [3,5]. Consequently, these two activities, surface and biological, open the prospect of synergistic effects in the formation of a potential drug delivery system.

In this study we search for the conditions appropriate to solubilize the lipophilic compounds (triglycerides, dye Nile red, hemin, hypericin, chlorophyll) by the mixture of neutral Quillaja bark saponins (QBS). It is shown that QBS can facilitate the transfer of lipophilic molecules from sunflower oil into the water solutions as particles with the diameter of ~35 nm. Data indicate that, independent on the chemical nature of lipophilic molecule, the transfer is effectively mediated by the monomeric forms of saponin in the buffer. The molecular mechanism of the extraction of hydrophobic compounds by the saponins from the oil into water is proposed.

Acknowledgement

This work was supported by FP7 EU project CELIM 316310. We would like to express our gratitude to Dr. V. Zavisova for the light scattering measurements.

References

- [1] D. J. McClements, *Soft Matter* 7 (2011), 2297-2316
- [2] D. J. McClements, *Soft Matter* 8 (2012,) 1719-1729
- [3] M. J. Augustin, V. Kuzina,, S. B. Andersen and S. Bak, *Phytochemistry* 72 (2011), 435-457
- [4] C. Y. Cheok, H. A. K. Salaman and R. Sulaiman *Food Research International* 59 (2014), 16-40
- [5] O. Gluclu-Ustundag and G. Mazza *Crit. Review, Food Chem. Nutrition* 47 (2007), 231-258



Aptamer conjugation of polymer based nanoparticles – a possible strategy for cancer treatment

Z. GARAIOVÁ¹, Y. MØRCH², C. DE LANGE DAVIES³, AND T. HIANIK¹

¹ Department of Nuclear Physics and Biophysics, Faculty of Mathematics, Physics and Informatics, Comenius University, Mlynska dolina F1, 842 48 Bratislava, Slovakia

² Department of Biotechnology and Nanomedicine, SINTEF Materials and Chemistry, Sem Sælandsvei 2A, 7024 Trondheim, Norway

³ Department of Physics, Norwegian University of Science and Technology, Høgskoleringen 5, 7491 Trondheim, Norway

e-mail: zuzana.garaiova@fmph.uniba.sk

DNA/RNA aptamers are becoming increasingly important in the field of early detection and treatment of cancer [1]. When conjugated to various nanomaterials such as polymeric nanoparticles, these systems can be used as highly effective cancer cell drug delivery targeting tools [1,2]. In this study, novel biodegradable polymeric nanoparticles developed by SINTEF Materials and Chemistry [3] were tested as nanopatform for conjugation of RNA aptamer specific towards $\alpha_v\beta_3$ integrins (Apt- $\alpha_v\beta_3$) [4]. Integrins $\alpha_v\beta_3$ are highly expressed receptors on activated endothelial cells, newly formed vessels and some tumor cells; but not present in most normal systems. This makes $\alpha_v\beta_3$ integrins suitable target for anti-angiogenic therapy. Apt- $\alpha_v\beta_3$ specifically binds to $\alpha_v\beta_3$ integrins on the surface of human umbilical vein endothelial cells (HUVECs) and it is also predicted to be a possible good anti-angiogenic drug candidate [4].

Conjugation of fluorescein labelled amino-modified Apt- $\alpha_v\beta_3$ on the surface of carboxylated polycyanoacrylate (PACA) nanoparticles was performed by means of covalent activation chemistry (EDC/NHS) [2] and non-covalent coupling. Starting concentrations of Apt- $\alpha_v\beta_3$ and PACA (considering theoretical amount of carboxyl groups on the surface) were chosen to be equimolar. Fluorescence intensity was determined at excitation wavelength 488 nm and emission wavelength 535 nm. Fluorescence study indicated Apt- $\alpha_v\beta_3$ being complexed with PACA for both covalent and non-covalent conjugation approaches as evidence of non-zero fluorescent signal after extensive dialysis. To be noted, in the case of EDC/NHS treated samples, quenching of fluorescence was observed. For this reason regulation of aptamer density was further studied only for non-covalently conjugated samples. Aptamer density was regulated by variation of aptamer concentration in the immobilization reaction mixture and thus variation of aptamer/nanoparticle ratio (APT/NP). Increasing the molar ratio of APT/NP led to decreased fluorescence. Equimolar amount of APT/NP (1/1) led to 25% of initial fluorescence intensity (fluorescence intensity of aptamer before conjugation). Increasing the molar amount of aptamer twice (2/1) decreased fluorescence to 9.4%. On the other hand at APT/NP ratio 1/2, the intensity of conjugated aptamer fluorescence was approx. 77% of the initial fluorescence.

The preliminary results point towards successful conjugation of aptamers to PACA nanoparticles and emphasize the potential for further optimization and investigations of studied polymeric nanoparticles as suitable targeted drug delivery vehicles.

Acknowledgement

This work was supported by Stipend program EEA Slovakia – institutional collaboration between high education institution EEA/EHP-SK06-IV-V-01/(project No. SK06-IV-01-005), by the Slovak Research and Development Agency under the contracts No. APVV-14-0267 and SK-AT-2015-0004 and and by Science Grant Agency VEGA (project No. 1/0152/15).

References

[1] A. Aravind, Y. Yoshida, T. Maekawa, D. S. Kumar, Drug delivery and transl. Res. 2 (2012), 418-436.

- [2] O.C.Farokhzad, S.Jon, A. Khademhsseini, T.N.Tran, D.A. Lavan, R. Langer, *Cancer Res.* 64(21) (2004), 7668-72.
- [3] Y. Mørch., R. Hansen, S. Berg, A. K. Aslund, W. R Glomm, S. Eggen, R. Schmid., H. Johnsen., S. Kubowicz, S. Snipstad., E. Sulheim, S. Hak, G. Singh, B. H. McDonagh, H. Blom, C. de Lange Davies, P. M., Stenstad, *Contr.med. & molec.imaging.* 10 (2015), 356-366.
- [4] J. Mi, X. Zhang, P. H. Giangrande, J. O. McNamara, S. M. Nimjee, S. Sarraf-Yazdi, B. A. Sullenger, B. M. Clary, *Biochem. and biophys. Res. comm.* 338 (2005), 956-963.

Polymeric nanoparticles as potential drug carriers for cancer treatment – a cytotoxicity study.

V. SUBJAKOVA¹, Y.MØRCH², Z. GARAIOVA¹, C.DE LANGE DAVIES³, AND T. HIANIK¹

¹ Department of Nuclear Physics and Biophysics, Faculty of Mathematics, Physics and Informatics, Comenius University, Mlynska Dolina F1, 842 48 Bratislava, Slovakia

² Department of Biotechnology and Nanomedicine, SINTEF Materials and Chemistry, Sem Sælandsvei 2A, 7024 Trondheim, Norway

³ Department of Physics, Norwegian University of Science and Technology, Høgskoleringen 5, 7491 Trondheim, Norway

e-mail: veronika.subjakova@fmph.uniba.sk

Cancer is one of the leading causes of death worldwide. Chemotherapy is widely used cancer treatment, which includes administration of cytotoxic drugs although it produces unwanted side effects for healthy cells and thereby greatly reduces the quality of life for the patients.

One of the possibilities to minimize side effects is targeted drug delivery using nanoparticles (NPs). Polymeric NPs can encapsulate cytotoxic drugs and deliver them to tumor tissue via the enhanced permeability and retention effect (EPR) [1].

In this study, cytotoxic effect of polymeric NPs namely polybutylcyanoacrylate (PBCA) developed by SINTEF Materials and Chemistry, Norway [2] was studied. PBCA were loaded with cabazitaxel (10 wt%). The effect of unloaded NPs as well as free cabazitaxel was also examined. Cytotoxicity was inspected using Alamar Blue cell viability assay [3] on breast cancer cell line (MDA-MB-231). The concentration range of NPs was from 0,01 ng/ml to 10µg/ml, and incubation times 24h, 48h and 72h.

Only the highest concentration (10µg/ml) of unloaded PBCA was toxic; the toxicity was depending on the incubation time. In the case of cabazitaxel-loaded PBCA NPs, the cell viability started to decrease from 50 ng/ml (24h) and 1ng/ml (72h). Free cabazitaxel had similar cytotoxic trend. However, the viability of cells upon the treatment with PBCA-encapsulated cabazitaxel was slightly higher.

The obtained results showed that PBCA NPs might serve as possible vehicles to encapsulate cytotoxic drugs with the potential for further clinical research.

Acknowledgement

This work was supported by Stipend program EEA Slovakia – institutional collaboration between high education institution EEA/EHP-SK06-IV-V-01/(project No. SK06-IV-01-005).by the Slovak Research and Development Agency under the contracts No. APVV-14-0267 and SK-AT-2015-0004 and and by Science Grant Agency VEGA (project No. 1/0152/15).

References

- [1] V.Torchilin, *Advanced Drug Delivery Reviews* 63 (2011) 131-135
- [2] Y. Morch,. R. Hansen, S. Berg, A. K. Aslund, W. R. Glomm, S. Eggen, R. Schmid,. H. Johnsen,. S. Kubowicz, S. Snipstad,. E. Sulheim, S. Hak, G. Singh, B. H. McDonagh, H. Blom, C. de Lange Davies, P. M.,Stenstad, *Contr.med. & molec.imaging.* 10 (2015), 356-366
- [3] J. Brien, I. Wilson, T. Orton, F. Pognan, *Eur. J. Biochem.*267(2000),5421-5426

Complex formation between photosensitizer hypericin and high-density lipoproteins (HDL)

A. JUTKOVÁ¹, Ľ. BLAŠČÁKOVÁ¹, D. JANCURA¹, P. MIŠKOVSKÝ^{1,2}, AND J. KRONEK³

¹ Department of Biophysics, P. J. Šafárik University, Jesenná 5, 041 54 Košice, Slovakia

² International Laser Center, Ilkovičova 3, 841 04 Bratislava 4, Slovakia

³ Polymer Institute of the Slovak Academy of the Sciences, Dúbravská cesta 9, 845 41 Bratislava 45, Slovakia

Cancer and other rapidly proliferating cells require cholesterol and other membrane components to achieve an increased rate of growth. It has been shown that high-density lipoproteins (HDL) are involved in cholesterol transport in some malignancies, including breast cancer, ovarian cancer, prostate cancer and adrenocortical tumors of the adrenal glands [1]. HDL molecules can be used as a delivery system for targeted drug biodistribution to the tumor cells, as they are biodegradable, do not trigger immune response and the incorporation of a drug into the HDL does not affect the drug stability [2]. The main task of the thesis was to construct a HDL-based nanodelivery system and to investigate properties of HDL complex with a photosensitizer hypericin (Hyp) by means of fluorescence spectroscopy. With the aim to increase the efficiency of Hyp transport, the HDL molecules were coated by dextran (Dex) and modified dextran (Dm). This coating should lead to prevention of the redistribution of Hyp molecules from the complex HDL/Dex and HDL/Dm to the free lipoprotein molecules. We have found that the coating of the HDL with modified dextran results in a 38 % reduction of Hyp redistribution from the complex HDL/Dm to free HDL molecules. We can conclude that HDL coating with dextran can effectively prevent the redistribution of incorporated molecules of drugs Hyp in HDL to other serum lipoproteins (Fig. 1). The thesis also shows that the presence of modified dextran leads to an increase of the capacity of HDL/Dm complex to accumulate a monomeric form of Hyp.

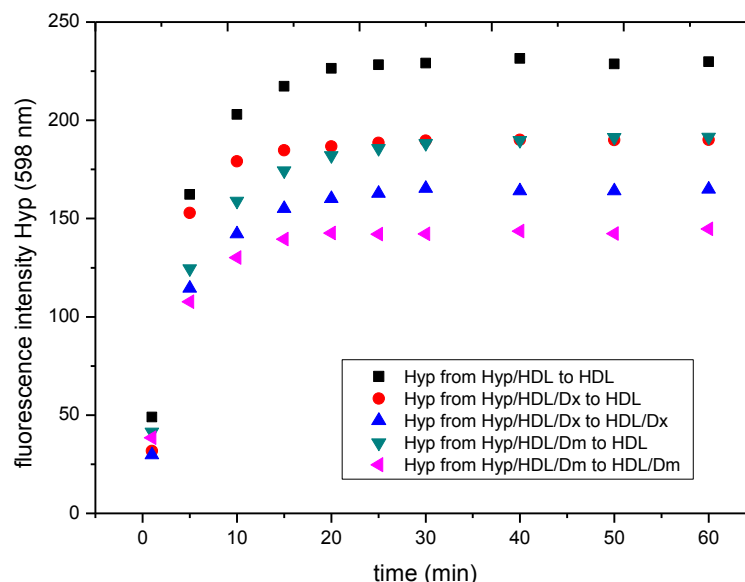


Figure 1: The kinetics of the redistribution of Hyp molecules from the complex Hyp/HDL, Hyp/HDL/Dex and Hyp/HDL/Dm to free HDL, HDL/Dex and HDL/Dm, $c(\text{Hyp}) = 700 \text{ nM}$, excitation wavelength 515 nm, fluorescence emission monitored at 598 nm.

Acknowledgement

This work was supported by the 7RP EU projekt CELIM 316310.

References

- [1] M. G. Damiano, R. K. Mutharasan, S. Tripathy, K. M. McMahon and C. S. Thaxton. Templated high density lipoprotein nanoparticles as potential therapies and for molecular delivery. *Adv. Drug Deliv. Rev.* 65 (2013), 649-662.
- [2] B. Lou, X. L. Liao, M. P. Wu, P. F. Cheng, C. Y. Yin and Z. Fei. High-density lipoprotein as a potential carrier for delivery of a lipophilic antitumoral drug into hepatoma cells. *World J. Gastroenterol.* 11 (2005), 954-9

Anionic liposomes in gene therapy

G. LISKAYOVÁ, L. HUBČÍK, A. BÚCSI, AND D. UHRÍKOVÁ

Faculty of Pharmacy, Comenius University in Bratislava, Odbojárov 10, 832 32 Bratislava, Slovakia
email: liskayova1@uniba.sk

Gene medicine can be described as the most potential strategy for the development of cures for inherited and acquired disorders with underlying genetic defects or malfunction. More than 1700 gene therapy protocols are under clinical investigation as potential treatment options for pathogenic and metabolic disorders including: cancer, cystic fibrosis, hemophilia, neuromuscular disorders and others [1]. Efficient delivery of plasmid DNA into cells is achieved via viral as well as nonviral vectors.

Viral vectors have high transfection efficiency, but on the other side experiments have shown that there are some limitations include their immunogenicity, toxicity towards host cells, problems with incorporation, transport of large therapeutic genes and high cost of production [2,3,4].

Consequently, nonviral transfection systems are preferred. Although their transfection efficiency is lower than that of viral vectors, they provoke lower inflammatory response, cost of production is lower and there is no limitation on DNA size [5]. Lipoplexes belong to the group of nonviral vectors. Many cationic lipoplexes have been found as relatively efficient in delivering DNA into cells, but they can be inactivated in the presence of serum, and are unstable upon storage. Moreover cationic lipoplexes were demonstrated to be cytotoxic agents both in vitro and in vivo. Anionic lipoplexes, composed of physiologically safe components, anionic lipids, plasmid DNA and divalent cations, have emerged to be a potential gene delivery vectors with low toxicity in comparison to cationic lipoplexes [6]. Divalent cations mediate complexation between DNA and the anionic lipids. Calcium has been shown to be superior [7]. It is very important to know the relationship between the physicochemical properties of lipoplexes, the structure, toxicity and transfection efficiency.

In the present study, anionic lipoplexes composed of unilamellar DPPC (1,2-dipalmitoyl-*sn*-glycero-3-phosphocholine) or DPPG:DPPC (1,2-dipalmitoyl-*sn*-glycero-3-phospho-glycerol:DPPC) liposomes and DNA in the presence of Ca^{2+} and Zn^{2+} cations were investigated. We have studied the effect of divalent cations and ionic strength of aqueous solution on DNA condensation process. Unilamellar liposomes were prepared from multilamellar liposomes by extrusion using polycarbonate filters with diameter 100 nm. The process of DNA condensation was followed using fluorescence spectroscopy. Changes in the emission intensity of fluorescent probe ethidium bromide have shown that the most effective DNA condensation is in presence of Ca^{2+} cations and 10 mM NaCl at 60°C when ~ 98 % DNA is bound into the aggregates (Fig.1). At high ionic strength (150 mM NaCl) we found 87 % DNA condensed between the lipid bilayer. The size of formed aggregates was followed using static light scattering (Fig. 2). Small angle X-ray scattering has shown structural changes in dependence on both the used cations and NaCl concentrations (Fig. 3). We observe a coexistence of two lamellar phases: phase L is a phase of lipid ($d \sim 6,3$ nm) and phase L^c is a phase of DNA between the lipid bilayers with irregular packing ($d_{LC} \sim 7,8$ nm). With increasing Ca^{2+} concentration we observe a condensed lamellar phase with DNA strand packed regularly between the lipid bilayer ($d_{DNA} \sim 5,7$ nm).

In conclusion, anionic liposomes with divalent cations mediate DNA condensation process and the structure of anionic lipoplexes is similar to that of cationic.

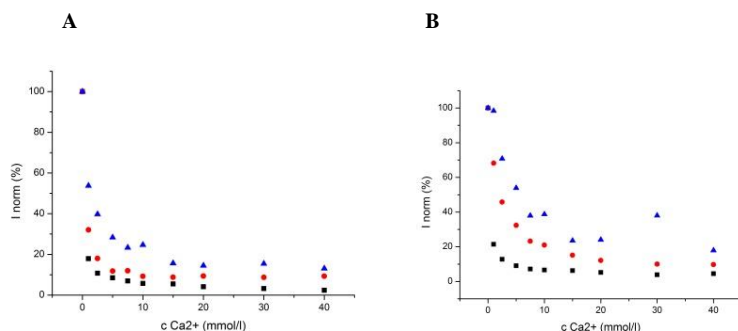


Figure 1: Dependence of the normalized fluorescence emission intensity of EtBr in the system A) DNA – DPPC – Ca^{2+} - EtBr B) DNA- DPPG:DPPC- Ca^{2+} - EtBr on the concentration of Ca^{2+} at molar ratios DNA:lipid= 1:5, DPPG:DPPC= 1:9 mol/mol at 60°, ionic strength: ■10 mM, ●100 mM, ▲150 mM.

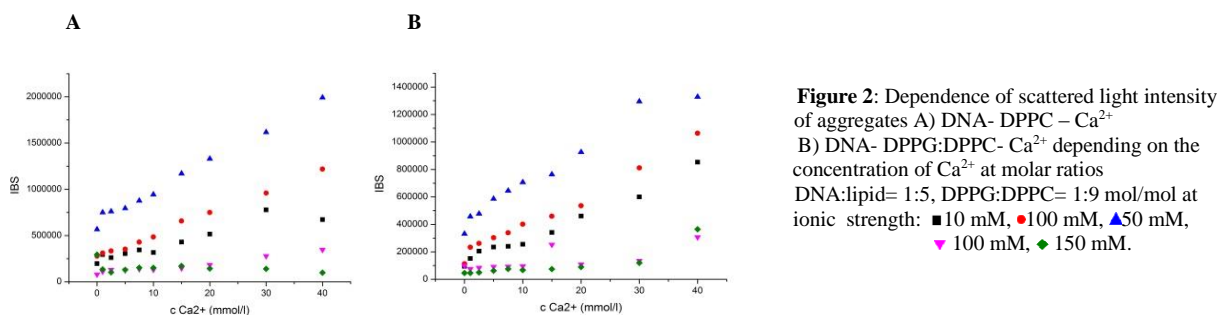


Figure 2: Dependence of scattered light intensity of aggregates A) DNA- DPPC – Ca^{2+} B) DNA- DPPG:DPPC- Ca^{2+} depending on the concentration of Ca^{2+} at molar ratios DNA:lipid= 1:5, DPPG:DPPC= 1:9 mol/mol at ionic strength: ■ 10 mM, ● 100 mM, ▲ 50 mM, ▼ 100 mM, ◆ 150 mM.

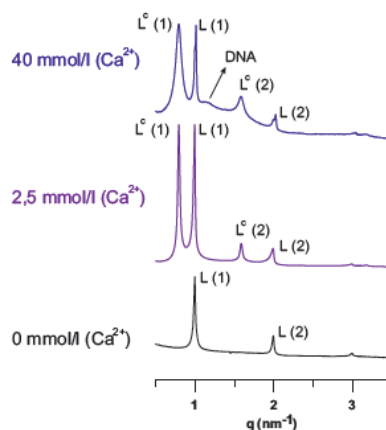


Figure 3: Diffractograms of fully hydrated DPPC and DNA - DPPC – Ca^{2+} aggregates at various Ca^{2+} concentrations at 20°C in 5 mM NaCl.

Acknowledgement: SAXS experiments were performed at BL11-NCD beamline at Alba Synchrotron with the collaboration of Alba staff and supported by BioStruct X/Calipso programme; experiments were supported by the JINR project 04-4-1121-2015/2017; grant VEGA 1/0916/16 and grant FaF UK/35/2015.

References

- [1] Srinivasan, C., Burgess, D.J., 2009. Optimization and characterization of anionic lipoplexes for gene delivery. *J. Control. Release Off. J. Control. Release Soc.* 136, 62–70.
- [2] Thomas, C.E., Ehrhardt, A., Kay, M.A., 2003. Progress and problems with the use of viral vectors for gene therapy. *Nat. Rev. Genet.* 4, 346–358.
- [3] Schmidt-Wolf, G.D., Schmidt-Wolf, I.G.H., 2003. Non-viral and hybrid vectors in human gene therapy: an update. *Trends Mol. Med.* 9, 67–72.
- [4] Woods, N.-B., Bottero, V., Schmidt, M., von Kalle, C., Verma, I.M., 2006. Gene therapy: therapeutic gene causing lymphoma. *Nature* 440, 1123.
- [5] Kogure, K., Akita, H., Harashima, H., 2007. Multifunctional envelope-type nano device for non-viral gene delivery: concept and application of Programmed Packaging. *J. Control. Release Off. J. Control. Release Soc.* 122, 246–251.
- [6] Patil, S.D., Rhodes, D.G., Burgess, D.J., 2005. Biophysical characterization of anionic lipoplexes. *Biochim. Biophys. Acta* 1711, 1–11.
- [7] Kulkarni, V.I., Shenoy, V.S., Dodiya, S.S., Rajyaguru, T.H., Murthy, R.R., 2006. Role of calcium in gene delivery. *Expert Opin. Drug Deliv.* 3, 235–245.



Formation of ABTS Radical Cation in the Presence of Silver Nanoparticles as Revealed by UV-visible and Raman spectroscopy

Z. JURAŠEKOVÁ^{1,2}, A. GARCÍA-LEIS³, S. SÁNCHEZ-CORTÉS³, AND D. JANCURA^{1,2}

¹ Department of Biophysics, P. J. Šafárik University, Jesenná 5, 041 54 Košice, Slovakia

² Center for Interdisciplinary Biosciences, P. J. Šafárik University, Jesenná 5, 041 54 Košice, Slovakia

³ Instituto de Estructura de la Materia, Serrano 121, 28006 Madrid, Spain

e-mail: zuzana.jurasekova@upjs.sk

ABTS (2,2'-azinobis(3-ethylbenzothiazoline-6-sulfonic acid) is a compound extensively employed to monitor the reaction kinetics of specific enzymes [1, 2] and to evaluate the free radical trapping capacity of antioxidant compounds and complex mixtures such as biological fluids, beverages or foods [3-5]. This evaluation is based on an assay where preformed ABTS radical cation (ABTS^{•+}) molecules are reduced in the presence of antioxidants. ABTS^{•+} is known to be a persistent radical species [6-8]. The formation of ABTS^{•+} is readily detected by electron paramagnetic resonance (EPR) spectroscopy and characteristic UV-visible absorption spectrum [7]. In aqueous solutions, ABTS^{•+} possess absorption maxima at 645, 734 and 815 nm as well as a very intense and thus commonly used maximum at 415 nm [3, 9, 10]. The addition of antioxidants to the preformed ABTS^{•+} reduces this molecule and the extent of the reduction corresponding to the antioxidant capacity of the studied molecule is evaluated by the decrease of specific ABTS^{•+} absorption bands, mostly of the 734 nm absorption maximum. This approach is commonly known as an ABTS decolourization assay.

Physicochemical properties of ABTS molecule as well as corresponding radical ion have been studied yet by various methods: UV-visible absorption spectroscopy [7, 11-13], fluorescence spectroscopy [13], EPR and nuclear magnetic resonance spectroscopy [13, 14], and X-ray crystallography [14, 15]. In addition, electrochemical parameters as redox potentials of the ABTS/ABTS^{•+} and ABTS^{•+}/ABTS²⁺ redox pairs, acid ionization constants, and electron exchange rates of ABTS have been also examined [7, 16, 17]. Up to our best knowledge, vibrational characteristics of ABTS and its oxidation products have not been thoroughly studied yet.

Raman spectroscopy is a useful technique which can provide important information about the vibrational properties and structure of studied molecules. Another technique used for elucidation of the vibrational properties of molecules at low concentrations is surface-enhanced Raman spectroscopy (SERS). This technique is based on the large local enhancement of the incident electromagnetic field in the proximity of the metal nanoparticles (NPs), as a consequence of localized surface plasmon resonance, which gives rise to large enhancements of the cross section for optical spectroscopies such as SERS [18]. Metal colloids have become the most commonly used nanostructures for SERS. In many instances, the nanostructured metal NPs or roughened SERS substrate can also function as a working electrode, which allows for the possibility of electrochemical SERS. In addition, a silver cluster shows efficient catalytic activity in a redox reaction because the cluster acts as the electron relay centre behaving alternatively as an acceptor and as a donor of electrons.

In the present work, we have applied optical spectroscopy techniques, UV-visible absorption, Raman and SERS spectroscopy, in order to characterize the ABTS redox behaviour in the presence of silver nanoparticles (Ag NPs). In addition, we have suggested mechanism by which ABTS is oxidized at or near silver surfaces.

This study was aimed at both the vibrational analysis of ABTS and the characterization of redox properties of plasmonic nanoparticles usually employed in the SERS spectroscopy. NPs are electron acceptors whose capability in redox reactions can be monitored here by using

ABTS. The consumption of the Ag NPs as a consequence of its interaction with the ABTS was proposed and confirmed by SEM images. In addition, characteristic Raman/SERS spectra of ABTS, ABTS^{•+} and ABTS²⁺ have been determined. All the processes undergone by ABTS on metal surfaces were monitored using different metallic nanoparticles, spherical and star-shaped (AgNS), and at different pH, in order to study the effect of pH on these processes. AgNS NPs demonstrated both higher reproducibility of the corresponding ABTS oxidation kinetics as well as higher stability of the produced radical cation in comparison to the spherical Ag NPs.

In conclusion, ABTS/Ag NPs-system has been proposed to be a reliable substrate to test the antioxidant capacity of various compounds, even at concentrations much lower than that usually used in spectrophotometric assays.

Acknowledgement

This work was supported by the Agency of the Ministry of Education of Slovak Republic for the Structural funds of the European Union, Operational program Research and Development (Contract: NanoBioSens, ITMS code: 26220220107) and the 7FP EU project CELIM 316310. This work has also been financially supported by MINECO (Project FIS2014-52212-R).

References

- [1] R. E Childs, W. G. Bardsley, *Biochemical Journal* 145 (1975), 93-103.
- [2] R. Bourbonnais, M. G. Paice, I. D. Reid, P. Lanthier, M. Yaguchi, *Applied and Environmental Microbiology* 61 (1995), 1876-1880.
- [3] N. J. Miller, C. Rice-Evans, M. J. Davies, V. Gopinathan, A. Milner, *Clin Sci (Lond)* 84 (1993), 407-412.
- [4] I. Gulcin, *Arch Toxicol* 86 (2012), 345-391.
- [5] R. Re, N. Pellegrini, A. Proteggente, A. Pannala, M. Yang, C. Rice-Evans, *Free Radic Biol Med* 26 (1999), 1231-1237.
- [6] C. Lee, M. Cho, J. Yoon, *Applied Chemistry* 9 (2005), 332-335.
- [7] S. L. Scott, W. J. Chen, A. Bakac, J. H. Espenson, *The Journal of Physical Chemistry* 97 (1993), 6710-6714.
- [8] K. J. Reszka, B. E. Britigan, *Archives of Biochemistry and Biophysics* 466 (2007), 164-171.
- [9] O. Erel, *Clin Biochem* 37 (2004), 277-285.
- [10] C. Rice-Evans, N. J. Miller, *Methods Enzymol.* 23 (1994), 279-293..
- [11] B. S. Wolfenden, R. L. Willson, *Journal of the Chemical Society, Perkin Transactions 2* (1982), 805-812
- [12] C. S. Johnson, J. B. Holz, *The Journal of Chemical Physics* 50 (1969), 4420-4424.
- [13] P. Maruthamuthu, D. K. Sharma, N. Serpone, *The Journal of Physical Chemistry* 99 (1995), 3636-3642.
- [14] C. Mousty, S. Therias, B. Aboab, P. Molinie, M. Queignec, P. Leone, C. Rossignol, P. Palvadeau, *New journal of chemistry* 21 (1997), 1321-1330.
- [15] A. Denis, K. Boubekour, P. Molinie, P. Leone, P. Palvadeau, *Journal of Molecular Structure* 689 (2004), 25-32.
- [16] R. Bourbonnais, D. Leech, M. G. Paice, *BBA - General Subjects* 1379 (1998), 381-390.
- [17] J. Janata, M. B. Williams, *The Journal of Physical Chemistry* 76 (1972), 1178-1183.
- [18] M. Moskovits, *Reviews of Modern Physics* 57 (1985), 783-826.

Development of biosensor for detection proteases activity by means of thickness shear mode transducer with immobilized casein

A. POTURNAYOVA^{1,2}, M. TATARKO¹, I. KARPISOVA¹, G. CASTILLO¹, Z. KERESZTES³, AND T. HIANIK¹

¹ Faculty of Mathematics, Physics and Informatics, Comenius University in Bratislava, Mlynska dolina F1, Bratislava 842 48, Slovakia

² Institute of Animal Biochemistry and Genetics, Slovak Academy of Sciences, 900 28 Ivanka pri Dunaji, Slovakia

³ Research Centre for Natural Sciences, Hungarian Academy of Sciences, Magyar tudosok korutja 2, 1117 Budapest, Hungary

e-mail: mtatarko1@gmail.com

Degradation of milk proteins plays a key role in flavour and consistency changes of milk and cheese. Control above desirable cheese ripening, undesirable gelation or bitterness after ultra high temperature (UHT) casein breakdown is important goal for food industry. Serine protease plasmin has been always connected with milk proteolysis thanks to its abundant transfer from blood circulation into bovine milk. Main goal of our work was to study mechanism of a degradation of β -casein by plasmin and trypsin proteases. Thickness shear mode method (TSM) allowed us analyzing changes in frequency and in motional resistance of casein layer caused by proteases cleavage. After enzymatic reaction with plasmin, short fragments of casein were cleaved by protease causing increase in resonance frequency of TSM transducer. Plasmin detection was performed in the range of concentration 1-20 nM, which corresponding to protease concentration causing changes of milk quality. The casein layer has been substantially affected also by trypsin. Detection limit of TSM transducer for plasmin was found to be 0,65 nM. As opposed to plasmin and trypsin, thrombin, which doesn't cleave casein, caused only small decrease in frequency and increase in motional resistance. This is an evidence of weak nonspecific adsorption of thrombin on casein layer. Topography of casein layers and its changes following plasmin cleavage was also studied by atomic force microscopy.

Acknowledgment

This work has been performed thanks to the funding from the European Union's Horizon 2020 research and innovation programme under the Marie Skłodowska-Curie grant agreement No 690898.



AUTHOR INDEX



Albonetti C.	PO15	Hořka M.	SC9, SC11
Babelova L.	SC5	Hrivňák S.	SC15
Balgavý P.	SC4	Hubčík L.	PO24
Bánó G.	PO9, PO19	Huntošová V.	PL2, PL3, PO8, PO10, PO12, PO19
Barbalinardo M.	PO15	Jakuš J.	SC13
Bednáriková Z.	PO13, PO14, PO15, PO16, PO17	Jancura D.	PO9, PO18, PO19, PO20, PO23, PO25
Belej D.	PO10, PO18	Janubová M.	PO5
Berényiová A.	SC7	Joniová J.	PO10, PO19
Bhunja A.	PO17	Jurašková Z.	PO10, PO25
Bizik J.	SC5	Jutková A.	PO23
Blaščáková Ľ.	PO20, PO23	Kamma-Lorger CH.	SC4
Bonneau S.	PO7	Kaňuková A.	PO1
Búcsi A.	PO24	Karmažínová M.	SC8
Burikova M.	SC5	Karpisová I.	SC5, PO26
Bystrenová E.	PO15	Keresztes Z.	PO26
Castillo G.	PO26	Klacsová M.	SC4
Cechlár O.	PO5	Kohan M.	SC13
Cortese-Krott M. M.	SC7	Kopčanský P.	PO13
Čačanyiová S.	SC7	Kopčová K.	SC6, PO20
Čellárová E.	PO11	Koptašíková L.	PL2, PO12
Čunderlíková B.	SC12	Kožár T.	PL2, SC14, PO10
Demjen E.	PO13, PO14	Kronek J.	PO23
Dičáková Z.	PO11	Krupa J.	PO6
Dušeková E.	PO1, PO2	Kubacková J.	PO16
Dutz S.	PO13	Lacinová Ľ.	SC8
Ebner A.	SC5	de Lange Davies C.	PO21, PO22
Fabian M.	SC6, PO20	Leitner M.	SC5
Faltinová A.	PL1	Lenkavská L.	PO7
Feelish M.	SC7	Liskayová G.	PO24
Fedunová D.	PO14	Macková K.	SC11
Filipek A.	PO6, PO20	Marek J.	PO14
Fragola A.	PO7	Martínez J. C.	SC4
Gaburjáková J.	SC1, SC2	Mateášik A.	SC12
Gaburjáková M.	SC1, SC2	Mikeš L.	SC15
Garaiová Z.	PO21, PO22	Míšek J.	SC13
Garajová K.	PO1, PO2, PO3	Miškovský P.	PO7, PO8, PO9, PO10, PO19, PO23
García-Leis A.	PO25	Mišuth M.	PO8
Gažová Z.	PO13, PO14, PO15, PO16, PO17	Mocanu M. M.	PO13
Gerelli E.	PO12	Mørch Y.	PO21, PO22
Grman M.	SC7	Nadřová Z.	PO7, PO8
Habinakova H.	SC13	Nagy P.	SC7
Hamadejová S.	PO1	Nemergut M.	PO18
Hianik T.	SC5, PO21, PO22, PO26	Nichtova Z.	PL2
Hoffmannová B.	SC10	Novák M.	PO5
Horváth D.	PO10	Novotova M.	PL2



Ondáčová K.	SC8
Ondriaš K.	SC7
Osina O.	SC13
Perez-Reyes E.	SC8
Petrenčáková M.	PO4
Poláková E.	SC10
Poturnayová A.	SC4, PO26
Rebič M.	PO19
Sánchez-Cortés S.	PO25
Sedlák E.	PO1, PO2, PO3, PO18
Sedláková D.	PO14
Sevčík J.	PL1
Snejdarkova M.	SC5
Spiguthova D.	SC13
Staničová J.	PO10, PO19
Strejčková A.	PO19
Subjaková V.	PO22
Sureau F.	PO7
Škrabana R.	PO5
Štroffeková K.	PL2, PO12
Tatarko M.	PO26
Tomášková N.	PO3
Uhríková D.	SC4, PO24
Uličná K.	PO13, PO16, PO17
Uličný J.	PL4, SC14, SC15
Urbániková E.	SC3
Vagovič P.	SC15
Valle F.	PO15
Varchola J.	PO9
Varhač R.	PO3
Verebová V.	PO10
Veternik M.	SC13
Wagnieres G.	PO12
Worch R.	PO6
Yavaser R.	PO1
Zahradník I.	SC9, SC10, SC11
Zahradníková A.	PL1, SC10, SC11
Zahradníková A., Jr.	SC9, SC10, SC11
Želonková K.	PO9





LIST OF PARTICIPANTS



1. **Bánó Gregor** Department of Biophysics, P. J. Šafárik University in Košice, Jesenná 5, 041 54 Košice, Slovakia
2. **Bednáriková Zuzana** Department of Biophysics, Institute of Experimental Physics, Slovak Academy of Sciences, Watsonova 47, 040 01 Košice, Slovakia
3. **Blaščáková Ľudmila** Department of Biophysics, P. J. Šafárik University in Košice, Jesenná 5, 041 54 Košice, Slovakia
4. **Cechlár Ondrej** Institute of Neuroimmunology, Slovak Academy of Sciences, Dubravská cesta 9, 845 10 Bratislava, Slovakia
5. **Čunderlíková Beata** International Laser Centre, Ilkovičova 3, 812 19 Bratislava, Slovakia
Institute of Medical Physics, Biophysics, Informatics and Telemedicine, Faculty of Medicine, Comenius University, Sasinkova 2, 813 72 Bratislava, Slovakia
6. **Demjen Erna** Department of Biophysics, Institute of Experimental Physics, Slovak Academy of Sciences, Watsonova 47, 040 01 Košice, Slovakia
7. **Dičáková Zuzana** Department of Biophysics, P. J. Šafárik University in Košice, Jesenná 5, 041 54 Košice, Slovakia
8. **Dušeková Eva** Department of Biophysics, P. J. Šafárik University in Košice, Jesenná 5, 041 54 Košice, Slovakia
9. **Fabian Marián** Center for Interdisciplinary Biosciences, P. J. Šafárik University in Košice, Jesenná 5, 04001 Košice, Slovakia
10. **Fabriciová Gabriela** Department of Biophysics, P. J. Šafárik University in Košice, Jesenná 5, 041 54 Košice, Slovakia
11. **Fedunová Diana** Department of Biophysics, Institute of Experimental Physics, Slovak Academy of Sciences, Watsonova 47, 040 01 Košice, Slovakia
12. **Filipek Alicja** Institute of Physics Polish Academy of Sciences, AL. Lotników 32/46, PL-02-668 Warsaw, Poland
Center for Interdisciplinary Biosciences, P. J. Šafárik University in Košice, Jesenná 5, 04001 Košice, Slovakia
13. **Gaburjáková Jana** Institute of Molecular Physiology and Genetics, Slovak Academy of Sciences, Dúbravská cesta 9, 840 05 Bratislava, Slovakia



14. **Gaburjaková Marta** Institute of Molecular Physiology and Genetics, Slovak Academy of Sciences, Dúbravská cesta 9, 840 05 Bratislava, Slovakia
15. **Garaiová Zuzana** Department of Nuclear Physics and Biophysics, Faculty of Mathematics, Physics and Informatics, Comenius University, Mlynska Dolina F1, 842 48 Bratislava, Slovakia
16. **Garajová Katarína** Department of Biochemistry, Faculty of Sciences, P. J. Šafárik University in Košice, Moyzesova 11, 040 01 Košice, Slovakia
17. **Gažová Zuzana** Department of Biophysics, Institute of Experimental Physics, Slovak Academy of Sciences, Watsonova 47, 040 01 Košice, Slovakia
18. **Grman Marián** Institute of Clinical and Translational Research, Biomedical Research Center, Slovak Academy of Sciences, Dúbravská cesta 9, 845 05 Bratislava 4, Slovakia
19. **Hoffmannová Barbora** Faculty of Mathematics, Physics and Informatics, Comenius University, Bratislava, Slovakia
20. **Hrivňak Stanislav** Department of Biophysics, P. J. Šafárik University in Košice, Jesenná 5, 041 54 Košice, Slovakia
21. **Huntošová Veronika** Center for Interdisciplinary Biosciences, P. J. Šafárik University in Košice, Jesenná 5, 04001 Košice, Slovakia
22. **Jakuš Ján** Department of Medical Biophysics, Jessenius Faculty of Medicine in Martin, Comenius University, Mala Hora 4, 036 01 Martin, Slovakia
23. **Jancura Daniel** Department of Biophysics, P. J. Šafárik University in Košice, Jesenná 5, 041 54 Košice, Slovakia
Center for Interdisciplinary Biosciences, P. J. Šafárik University in Košice, Jesenná 5, 04001 Košice, Slovakia
24. **Jurašková Zuzana** Department of Biophysics, P. J. Šafárik University in Košice, Jesenná 5, 041 54 Košice, Slovakia
Center for Interdisciplinary Biosciences, P. J. Šafárik University in Košice, Jesenná 5, 04001 Košice, Slovakia
25. **Jutková Annamária** Department of Biophysics, P. J. Šafárik University in Košice, Jesenná 5, 041 54 Košice, Slovakia
26. **Klacsová Mária** Department of Physical Chemistry of Drugs, Faculty of Pharmacy, Comenius University in Bratislava, Odbojárov 10, 832 32 Bratislava, Slovakia



27. **Kohan Miroslav** Department of Medical Biophysics, Jessenius Faculty of Medicine in Martin, Comenius University, Mala Hora 4, 036 01 Martin, Slovakia
28. **Kopčová Katarína** Department of Biophysics, P. J. Šafárik University in Košice, Jesenná 5, 041 54 Košice, Slovakia
29. **Koptašiková Lenka** Department of Biophysics, P. J. Šafárik University in Košice, Jesenná 5, 041 54 Košice, Slovakia
30. **Kožár Tibor** Center for Interdisciplinary Biosciences, P. J. Šafárik University in Košice, Jesenná 5, 04001 Košice, Slovakia
31. **Kubacková Jana** Department of Biophysics, Institute of Experimental Physics, Slovak Academy of Sciences, Watsonova 47, 040 01 Košice, Slovakia
32. **Lacinová Ľubica** Institute of Molecular Physiology and Genetics, Slovak Academy of Sciences, Dúbravská cesta 9, 840 05 Bratislava, Slovakia
33. **Lenkavská Lenka** Department of Biophysics, P. J. Šafárik University in Košice, Jesenná 5, 041 54 Košice, Slovakia
34. **Liskayová Gilda** Faculty of Pharmacy, Comenius University in Bratislava, Odbojárov 10, 832 32 Bratislava, Slovakia
35. **Macková Katarína** Institute of Molecular Physiology and Genetics, Slovak Academy of Sciences, Dúbravská cesta 9, 840 05 Bratislava, Slovakia
36. **Míšek Jakub** Department of Medical Biophysics, Jessenius Faculty of Medicine in Martin, Comenius University, Mala Hora 4, 036 01 Martin, Slovakia
37. **Miškovský Pavol** Center for Interdisciplinary Biosciences, P. J. Šafárik University in Košice, Jesenná 5, 04001 Košice, Slovakia
Department of Biophysics, P. J. Šafárik University in Košice, Jesenná 5, 041 54 Košice, Slovakia
38. **Mišuth Matúš** Department of Biophysics, P. J. Šafárik University in Košice, Jesenná 5, 041 54 Košice, Slovakia
39. **Nemergut Michal** Department of Biophysics, P. J. Šafárik University in Košice, Jesenná 5, 041 54 Košice, Slovakia
40. **Ondriaš Karol** Institute of Clinical and Translational Research, Biomedical Research Center, Slovak Academy of Sciences, Dúbravská cesta 9, 845 05 Bratislava 4, Slovakia



41. **Petrenčáková Martina** Department of Biophysics, P. J. Šafárik University in Košice, Jesenná 5, 041 54 Košice, Slovakia
42. **Poturnayová Alexandra** Institute of Animal Biochemistry and Genetics, Slovak Academy of Sciences, Moyzesova 61, 900 28 Ivanka pri Dunaji, Slovakia
43. **Štroffeková Katarína** Department of Biophysics, P. J. Šafárik University in Košice, Jesenná 5, 041 54 Košice, Slovakia
44. **Tatarko Marek** Faculty of Mathematics, Physics and Informatics, Comenius University in Bratislava, Mlynska dolina F1, Bratislava 842 48, Slovakia
45. **Uličná Katarína** Department of Biophysics, Institute of Experimental Physics, Slovak Academy of Sciences, Watsonova 47, 040 01 Košice, Slovakia
46. **Uličný Jozef** Department of Biophysics, P. J. Šafárik University in Košice, Jesenná 5, 041 54 Košice, Slovakia
Center for Interdisciplinary Biosciences, P. J. Šafárik University in Košice, Jesenná 5, 04001 Košice, Slovakia
47. **Urbániková Ľubica** Institute of Molecular Biology, Slovak Academy of Sciences, Dúbravská cesta 21, 845 51 Bratislava, Slovakia
48. **Varchola Jaroslav** Department of Biophysics, P. J. Šafárik University in Košice, Jesenná 5, 041 54 Košice, Slovakia
49. **Verebová Valéria** Institute of Biophysics, University of Veterinary Medicine and Pharmacy, Komenského 73, 041 81 Košice, Slovakia
50. **Zahradník Ivan** Institute of Molecular Physiology and Genetics, Slovak Academy of Sciences, Dúbravská cesta 9, 840 05 Bratislava, Slovakia
51. **Zahradníková Alexandra** Institute of Molecular Physiology and Genetics, Slovak Academy of Sciences, Dúbravská cesta 9, 840 05 Bratislava, Slovakia

Book of Contributions, 7th Slovak Biophysical Symposium, April 6-8, 2016, Nový Smokovec, Slovakia

Editors: D. Jancura, G. Fabriciová

Reviewers: M. Fabian, A. Musatov

Published: Department of Biophysics, Institute of Physics, Faculty of Science, P. J. Šafárik University in Košice, Košice, Slovakia

Printed: Equilibria, s.r.o., Košice

First edition, Košice, 2016

Number of pages: 106

ISBN: 978-80-972284-0-8

EAN: 9788097228408